

3 Detector description

Introduction

This Chapter is composed of two parts. The first part is dedicated to the design and construction of a HMPID module, including all the prototyping and technical work carried out for proto-2 on the main elements of the CsI RICH system, such as the photodetector, photocathode, radiator vessel, C₆F₁₄ circulation, electronics and CsI evaporation system. Some specific procedures to produce and assemble them will be described here, as well as the calculations and test results on which their designs were based, optimized and validated.

In the second part, the system aspects of the HMPID detector are described.

3.1 Module production and final prototype

3.1.1 The photodetector

The detector is constructed by stacking a series of independent metallic frames which are designed in such a way that simple machining ensures:

- the parallelism and a controlled thickness of the two anode-to-cathode gaps of the MWPC,
- the parallelism between the radiator trays and the photodetector.

Peralumin is used as the raw material for the frame to guarantee optimum surface quality (porosity, polishing) and flatness during machining. The sealing between the frames is achieved by machining standard grooves for the Viton O-ring joints. In order to minimize the outgassing, care was taken to avoid using composite, organic material and gluing, in favour of metallic components. We shall first describe the production of the pad cathode panel, then the sequence of the frames and the related assembly procedures.

The main representations of the detector are shown in Fig. 3.1 as a cross-section and in Fig. 3.2 as an axonometric projection. In Fig. 3.2, the final HMPID module is represented, based on six apertures for pad panels and three radiator trays. Proto-2 was built according to the same design but reduced to four apertures and two radiator trays, keeping the same dimensions in the other direction (see Fig. 2.26).

3.1.1.1 The pad cathode panel

Besides acting as a substrate coated by the CsI film, the pad-PCB also has to be designed in such a way that all the pads are electrically connected to the external Front End Electronics (FEE), ensuring optimum sealing with respect to the chamber gas.

The first pad-PCBs were designed to solve the FEE implementation, using standard two-layer circuit technology. Pads and traces were etched on a copper-clad G10 foil and protected with a chemical deposit of gold of 0.5 μm thickness. The open ‘through-holes’, traversing the PCB to carry the signal from each pad to the external traces were filled with tin soldering. As shown in Section 2.1.1.5, the CsI films were of poor quality and not efficient.

In order to avoid unwanted contact between the CsI film and copper substrate, it was decided to cover the copper with a 7 μm thick nickel layer which is known to be sufficiently dense. In addition, more care was devoted to surface preparation by using different kinds of polishing.

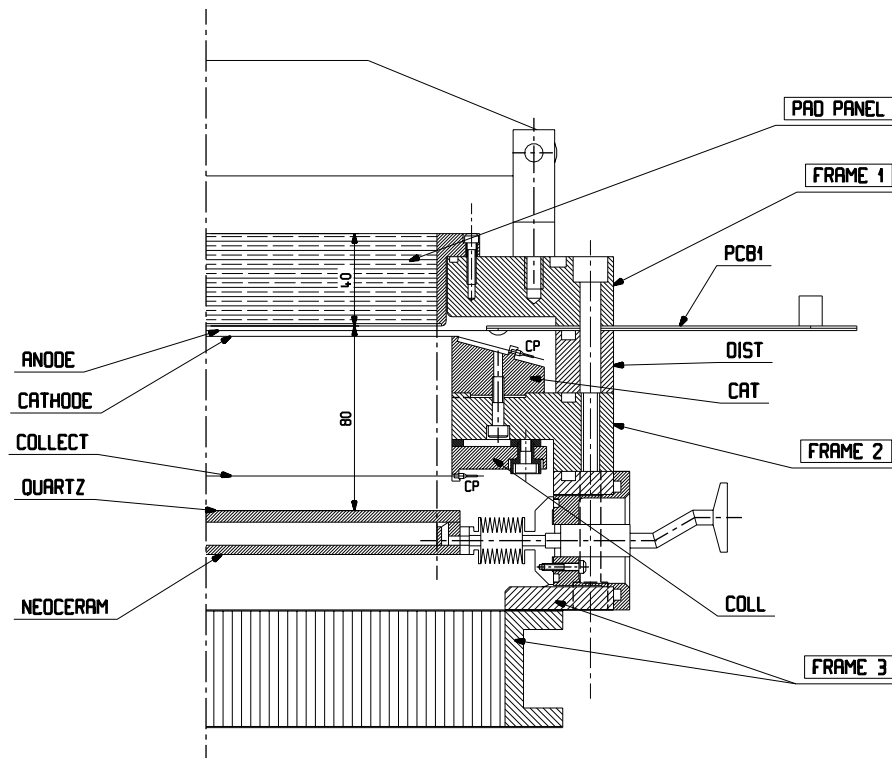


Figure 3.1: Cross-section of a HMPID module in a plane parallel to the anode wires.

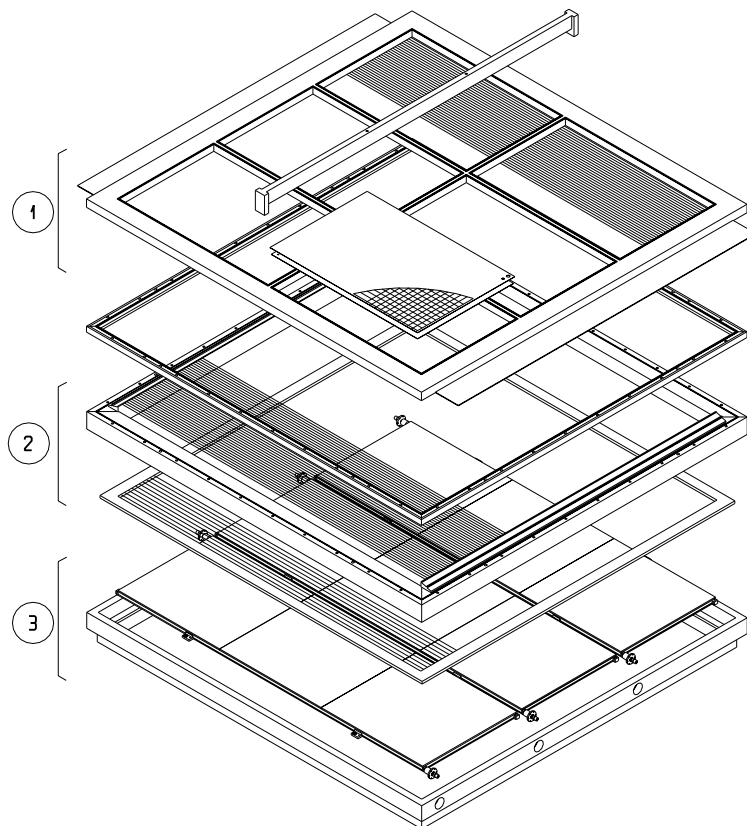


Figure 3.2: Axonometric view of a HMPID module. (1), (2), (3) are the elements described as Frame-1, Frame-2, Frame-3, respectively.

Two main lines of procedure are still under consideration, using two- or three-layer circuits, as shown in Fig. 3.3. Since they may also have several options, we refer to Ref. [1] where details are given and describe here only the main characteristics.

The solution based on three layers avoids having ‘through-holes’ and provides a perfectly gas-tight circuit, but uses more expensive technology (see Fig. 3.3a). First, on a two-sided copper-clad G10 foil, 0.5 mm thick, the pads are etched on one side and connected to traces on the other side by metallized holes. Then, a second circuit one-sided copper-clad G10 foil, 0.2 mm thick, where traces needed for electronic connections have been etched, is glued to the first one in such a way that by blind hole drilling and further metallization, the electrical connections are created between the two circuits. Mechanical and chemical polishing on the pad side are then performed on the circuit. Finally, the nickel and gold layers are deposited either by chemical or electrolytical processes. According to the technology in use, the structure and chemical composition of these layers are quite different and are expected to influence the germination and growth of the CsI film evaporated on them. Microstructural studies are used to characterize these layers. The solution based on two-layer circuits (see Fig. 3.3b) has electrical connections made by open ‘through-holes’ which are filled by glue insertion and protected by a new metallic layer necessary to mask each hole and achieve a smooth surface on the side where the pads are. The rest of the process follows the same steps as mentioned above. Comparable QE performance is at present obtained with both solutions. Given the large number of operations involved in this procedure, the final choice will be made on the basis of the one ensuring the best reliability in the mass PCB production. Further developments will be pursued with a VUV scanning set-up, as described in Section 3.1.5.2.

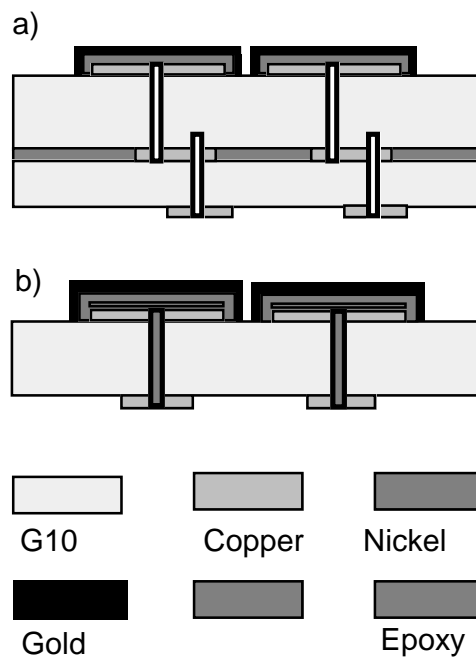


Figure 3.3: Schematic cross-sections of the pad PCB: a) version without through holes; b) version with through holes.

In order to minimize the length of connections between the pads and FE channels and their dispersion, groups of 48 pad channels are made corresponding to a pattern of 8×6 pads in the X and Y coordinates, respectively. This modularity in fact fits to three FE chips and available SMD connectors. The connection is established by soldering flexible Kapton foils on the back of the pad-PCB (see Fig. 3.4a,b). At the other end of the pad-PCB there is an SMD flat connector (ERNI-004863) with 50 contacts, which will be plugged into the FE board to ensure easy dismounting of the FE electronics (see Fig. 3.4b,c).

The last operation is a test that all pads are electrically connected to the SMD connectors.

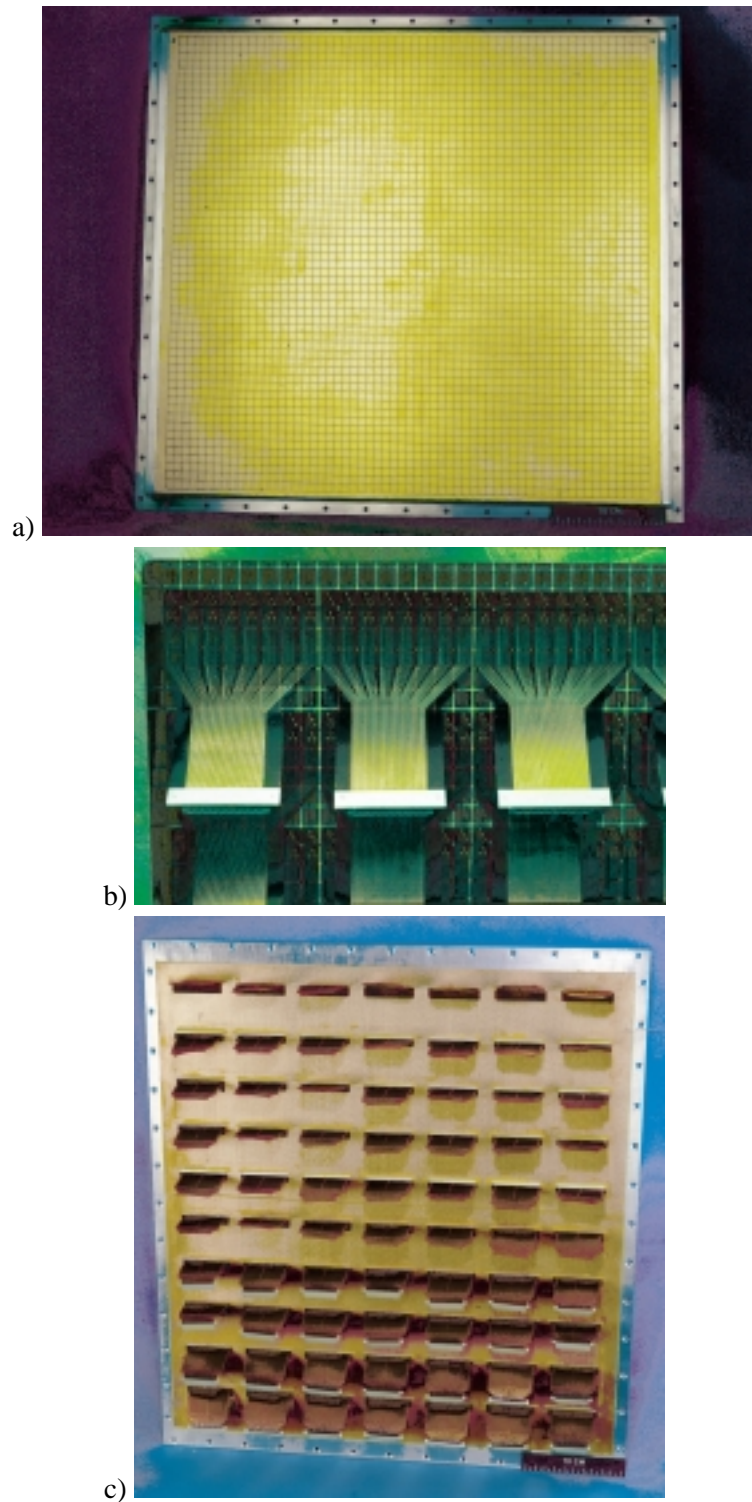


Figure 3.4: a) Pad panel viewed from the side of the pad PCB. The size is of 60×56 pads of $8 \times 8 \text{ mm}^2$ each. One sees the aluminium frame used to tighten the pad panel on the detector.
 b) Close-up view of the back of the pad PCB, where Kapton circuits (carrying by groups of 48 the pad signals to the FEE) are soldered.
 c) Pad panel viewed from the side of the FE electronics showing the Kapton circuits sticking out of the sandwich panel. Some of the circuits hold the flat connector (48 channels) to be plugged into the GASSIPLEX boards.

Assembly of the pad panel

Since no drastic requirements are imposed with respect to the detector dead zone, the pad panel is assembled as a sandwich composite structure inserted in a metallic frame (see Fig. 3.4a). This technology was selected in order to provide a stiff structure with a minimum of material and efficient gas sealing of the pad panels. The panel structure is schematically shown in Fig. 3.5.

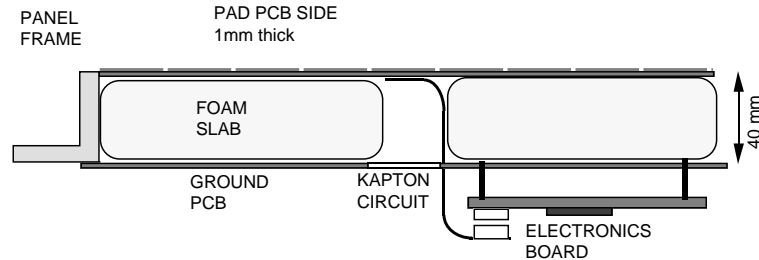


Figure 3.5: Schematic cross-section of the pad panel. The foam is Rohacel-51-HF, 52 g/l. The glue in use is Araldite epoxy AW106-HV 953-4.

The composite structure is made of the pad-PCB and Kapton circuits spaced by a 40 mm thick foam plate from another circuit referred to as the ground-PCB. The Kapton foils are soldered on the pad-PCB in rows, leaving a free space of about 30 mm between them for placing foam strips of that width (see Fig. 3.4b). The grooves thus formed allow the Kapton foils to come out through apertures created in the ground-PCB. The pad-PCB is first glued to the frame on a granite table and the necessary ground connections made with conductive glue. Then, the elements are stacked and glued together under proper load, keeping the pad-PCB in contact with the granite table.

A flatness of $\pm 50 \mu\text{m}$ is achieved over an area of $64 \times 40 \text{ cm}^2$. The ground-PCB makes good grounded electromagnetic shielding. The pins necessary for plugging the FEE boards are implemented last.

3.1.1.2 Frames

Frame-1

As shown in Fig. 3.1 and Fig. 3.2, Frame-1 holds the elements forming half of the wire chamber, i.e. the pad cathode and the anode wire plane. A design is described which allows the gap value and the parallelism of the two planes to be controlled within $\pm 50 \mu\text{m}$, allowing the pad cathode to be removed with a simple procedure. For this purpose, Frame-1 consists of a plate with six openings in which six pad cathode panels are mounted from the outside, tightened with screws and sealed with O-rings.

The anode wire plane: installation and HV supply

On the opposite side to the pad panel, the anode wires are stretched between two PCBs glued on opposite edges of the frame (PCB1 in Fig. 3.1). The wires are $20 \mu\text{m}$ diameter, tungsten rhenium gold plated, 861/60, grade L, quality 4.

As the two PCBs are glued in grooves, further machining is necessary to adjust them to the same level as the frame and ensure a flat surface for the O-ring to run over. As the cathode pads are held at ground potential, the high voltage must be applied to the anode wires. The PCBs are designed such that they act as a high-voltage feedthrough for every wire by using a three-layer configuration.

As shown in Fig. 3.6, $20 \mu\text{m}$ wires are soldered to pads etched at one edge of the circuits. Then, in order to pass over the frame region, the trace is enclosed between two G10 foils of 1 mm thickness ensuring HV insulation. Another advantage is that the O-ring is in contact with a perfectly smooth surface of the PCB whilst running over all the wires put under HV. Outside the chamber and at each end of the anodic wires, traces are pulled in groups of eight to a well-insulated flat connector. On one side of the chamber, a PCB is used to make the HV distribution. Each wire is fed through a $1 \text{ M}\Omega$ resistance implemented on

small cards grouping eight resistors. All these cards can, in turn, be fed by a single trace linked to the HV supply. All these external components, which are put under HV, are enclosed in a housing that can be flushed with a dry gas (nitrogen) in order to eliminate any external surface-leakage current caused by moisture.

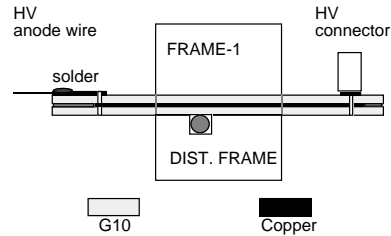


Figure 3.6: Schematic cross-section of the anode wire circuit.

It has been checked that in the case of possible sustained discharges, one or several wires could be disconnected from the HV source without affecting the operation of the remainder of the wire plane. It is therefore foreseen to study a scheme where each group of eight wires is fed by an independent HV line that can be interrupted by a remote-controlled HV switch in case of severe defects. This would allow the chamber to still be operated, losing only a 32 mm wide slice.

The connectors available on the opposite PCB may be used for implementing electronics for reading out fast wire signals, after convenient decoupling by HV capacitances. This facility was used locally during the test period and makes it possible to check that every wire is actually under voltage and to supply a current for controlling the wire stretching (see below).

Support line for anode wires

Given the length of the anode wires of 120 cm, a support line structure is needed to ensure the stability of the wires against the electrostatic force. For assembly reasons, this element can only be implemented between the pad cathode and the wire plane as the second cathode also consists of wires. As shown in Fig. 3.7, the support line is attached along the rod traversing Frame-1 through the middle, perpendicular to the anode wires, permitting the pad panels and the second wired cathode to be removed. This region is, in any case, a nonactive area of the pad cathode, making the inefficiency created by the support line of no importance. The sagitta and the stability of the wire under the electrical field have been studied with a full-length mock-up [2]. The safest solution is to make the gap anode-to-pad slightly smaller than the opposite one in order to have a constant resultant force directed towards the pad cathode, such that the anode wires are pressed against the support line.

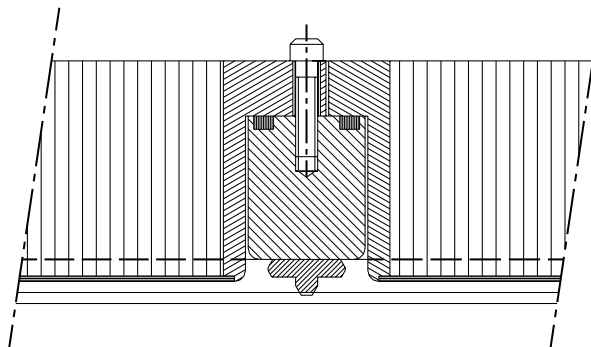


Figure 3.7: Cross-section of Frame-1 showing the implementation of the anode wire support structure. To achieve the necessary electrical insulation, the material in use is a machinable ceramic, Macor.

Soldering of the anode wires

The anodic plane is in fact divided into three parts by the dead zones created by the 30 mm wide aluminium transverse rods of Frame-1. Each part has 96 wires and is terminated at both edges by two field degrading wires of 50 and 100 μm , in such a way that the 20 μm wires overlap the full pad sensitive area. To give the correct spacing the wires are positioned using a comb, stretched by a weight of 40 g and held to the PCB by tin soldering. A flux is used to help the solder to run easily and at the end of the wiring, alcohol is used to remove the flux.

The wires are located in thin triangle-shaped grooves, 0.2 mm deep, machined at the surface of the Macor support line. For optimum safety (against vibrations, etc.), a very small amount of glue (AV144-2/HV 997) was added thus fixing the wires in these grooves.

The wire tensions are measured using CAEN instrument SY502. The tension is obtained by measuring the frequency of each wire fed with a known DC under a known magnetic field.

Adjustment of the anode/pad gap thickness

Once the anode plane has been soldered, the distance between this plane and the upper side of Frame-1 is measured at several points all around the frame. The thickness of each pad panel is also measured at several points between the pad surface and the inner side of its frame. After averaging and adjustments, the difference between these two measurements must be made equal to the nominal distance anode-to-pads, i.e. 2 mm. This is possible by machining, if necessary, the inner side of the pad-frame in the final adjustment.

Frame-2

Frame-2 holds two wire planes and its thickness contributes to the depth of the proximity gap of the RICH (see Figs. 3.1 and 3.2).

One of the wired planes is the second cathode of the photodetector MWPC that is kept at ground potential. It is made of 100 μm diameter gold plated Cu/Be wire, spaced by 2 mm. The wire specification is CuBe₂, hard, flash Ni, gold 1 μm . This spacing ensures 95% transparency to the incident Cherenkov photons and acts as an electric screen between the proximity and MWPC gaps. In order to avoid having a new PCB for holding these wires, crimping pins were used to support the stretching tension, fixed at 200 g/wire. Two independent machined bars are used to position and plug in the metallic crimping pins, allowing thus simpler drilling than would be the case of the large frame itself. The reason these bars have an oblique side (see Fig. 3.1) is to create a shape surrounding the edge of the PCB where the 20 μm wires at HV are soldered, such that the distances are much larger than the 2 mm gap. In this zone, the electrical field is kept at a low level, thus avoiding any breakdown from the anodes to surrounding grounds. The PCB is also long enough to avoid any leakage current along the circuit surface.

Once the cathode is wired, the distance between the wire plane and the upper side of Frame-2 is measured all around the frame. Then, the gap between the wired cathode and the anode planes can be adjusted to its nominal value by machining the distance frame, interleaved between Frame-1 and Frame-2, to the necessary thickness.

The second wire plane is the collection electrode which creates a small electric field in the proximity gap in order to drain primary ionization, deposited by the relativistic particles, instead of drifting into the MWPC gap. This electrode is fixed to Frame-2 by means of an independent frame. It is made of the same 100 μm diameter gold plated Cu/Be wire spaced by 5 mm also using crimping pins. It is raised to about 300 V. The gap between the collection electrode and the radiator tray should be kept to a minimum since primary ions created in that interval are repelled against the insulated radiator window and might create deposit.

Frame-3

A light composite panel is fixed on Frame-3 to close the detector (see Figs. 3.1 and 3.2). The three radiator trays are held by locating parts attached to the panel. Details are given in the next section which is

devoted to the radiator array. It should be mentioned that the depth of the proximity gap can be increased by inserting a distance frame between Frame-2 and Frame-3.

A photograph of proto-2, installed at the SPS test beam, is shown in colour Fig. 3.i.

3.1.2 The radiator array

This section is dedicated to prototype studies of the large radiator tray to be used in a HMPID module. Smaller devices used at the test beam were described in Section 2.3.1.1.

3.1.2.1 Introduction

The rather high C_6F_{14} and SiO_2 densities, 1.68 g/cm^3 and 2.1 g/cm^3 , respectively, and the need to minimize the total amount of material traversed by the incoming particles, required a careful investigation and optimization of the radiator vessel mechanical structure. In addition, since the HMPID performance depends strongly on transparency in the UV spectral range 160–220 nm and long-term stability of the perfluorohexane radiator, the emphasis was put on the choice of material. Indeed, in the definition of the structural mechanical design of the radiator vessel, we benefited from the long-term operational experience of DELPHI and SLD who employed C_6F_{14} in their RICH system [3].

3.1.2.2 Radiator description

The liquid radiator container consists of a tray made of a glass-ceramic material called Neoceram, closed by a UV-grade fused silica plate, as shown in Figs. 3.8 and 3.9.

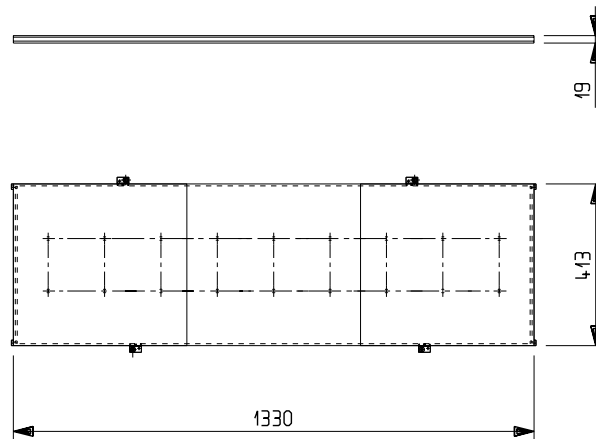


Figure 3.8: Schematic views of a radiator tray. The upper window is assembled by gluing three quartz plates together.

Neoceram, with its thermal coefficient of $0.5 \times 10^{-6} \text{ }^\circ\text{C}^{-1}$, ensures that no mechanical stress is induced on the vessel by temperature gradients. The limited size of commercially available fused silica plates and the need to keep the hydrostatic load within reasonable levels determined the thickness and size of the radiator vessel elements: in the current geometry, the quartz window is 5 mm thick, whilst the Neoceram base plate is 4 mm thick. The vessel elements are glued together with Araldite AW106. The liquid radiator inlet and outlet are obtained by gluing two stainless-steel pipes on the opposite sides of the Neoceram tray, the outlet always being at the highest location.

To withstand the hydrostatic pressure, 24 cylindrical spacers are glued to the bottom plate on one side and the quartz window on the other side. Spacers consist of fused silica rods with a diameter of 10 mm placed in two rows of 12 equidistant elements.

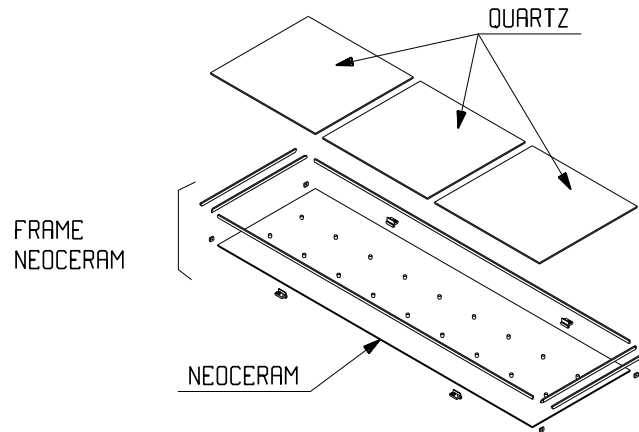


Figure 3.9: Axonometric view of the elements composing a radiator tray. Four carbon fibre feet are used to locate the tray in the detector back plane (Frame-3).

Each HMPID module has three independent radiator trays $1330 \times 413 \text{ mm}^2$, supported by a stiff composite panel made by sandwiching 50 mm of an aramide-fibre epoxy honeycomb material between two 0.5 mm thin layers of aluminium (Fig. 3.10). The radiator vessel and the fluid dominate the bulk of the detector material, estimated to be 17% X_0 (Table 3.1).

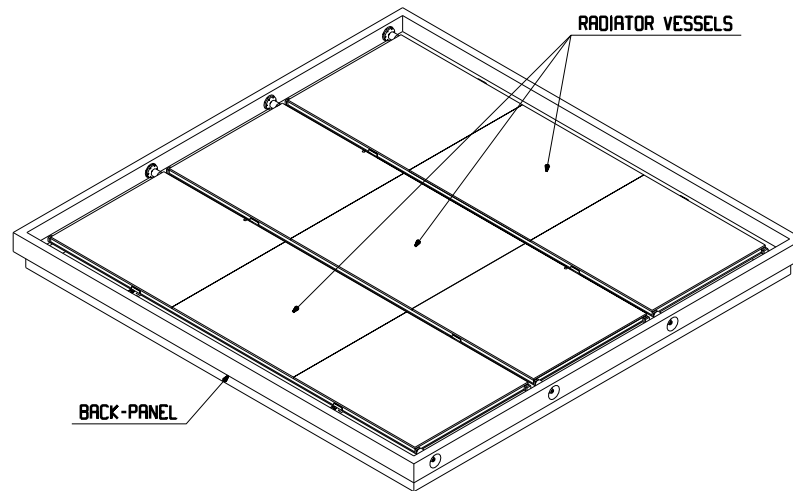


Figure 3.10: Perspective view of the HMPID back panel with the three radiator trays and feedthroughs for the liquid circulation.

Table 3.1: Material budget

	Material thickness [mm]	X/X_0
Honeycomb back panel	50	0.02
Neoceram plate	4	0.03
Quartz window	5	0.05
C_6F_{14}	10	0.05
PC panel + FEE	1	0.02

3.1.2.3 Assembly of a radiator tray

The long-term tightness of the radiator vessels depends critically on the quality of the assembly procedure. After delivery, the Neoceram elements and quartz windows are first visually inspected by looking for unwanted scratches on the surfaces or broken edges. A control of the dimensions and face parallelism is then performed to check that each part has been machined according to the specifications. Quartz windows are also inspected by measuring their UV transmission curve. Damaged or inaccurately machined pieces are rejected. Whilst the quartz plates used in the prototyping phase were always delivered within the specifications, the Neoceram parts needed a specific treatment, since suppliers only deliver large plates.

The procedure adopted for the Neoceram part is as follows:

- a diamond saw cut to almost the final size, within a tolerance of 0.5 mm;
- an accurate finish on a lathe provided a dimensional accuracy better than 0.05 mm.

Before gluing, all elements must be carefully cleaned to remove any trace of pollutants on the surfaces. The following steps are therefore performed:

- liquid soap (ph 5.5) and bi-distilled water washing;
- cerium oxide powder (the smallest size grain for a weak abrasive power) gently moved on the entire surface in order to remove more resistant chemical pollutants that might still be present;
- bi-distilled water washing to remove the cerium oxide powder;
- pure ethyl alcohol washing and drying with nitrogen gas flow.

The radiator is assembled by gluing the Neoceram pieces to the quartz windows in a dust-free room kept at 35°C constant temperature with a relative humidity of less than 50%. An optical table is used for assembly to ensure the right flatness over the whole surface of the radiator.

The lower Neoceram plate is at first glued to the thin Neoceram side walls by using a home-made tool that distributes the Araldite AW-106 at a constant rate to ensure that the glue thickness is 0.15 mm everywhere. On the assembly table there are fiducial marks that allow the surveyors to position the Neoceram pieces before gluing them.

In parallel, the final quartz window is obtained by gluing the three constituent plates using a specially built tool to guarantee a final flatness of the resulting plate (better than 0.05 mm).

Once the Neoceram box is ready, the same assembly table is employed to glue the quartz window on the Neoceram side walls. Finally, each radiator vessel is finished by installing the liquid Freon connections.

The following tests must be performed at the end of the radiator vessel assembly phase in order to ensure that each part works properly.

He leak test

The radiator vessel is mounted in a supporting structure and is flushed for several hours with pure He (flow rate = 10 l/h, 6 mbar overpressure due to an oil bubbler in the outlet line). The tightness test is performed by using a He sniffer with a sensitivity level of $(10 \times 10^{-7} \text{ atm} \times \text{cm}^3/\text{s})$. The entire set of glue joints as well as the inlet and outlet Freon fittings must be completely scanned. A satisfactory result is obtained when no appreciable leak is detected above $3 \times 10^{-7} \text{ atm} \times \text{cm}^3/\text{s}$.

He diffusion rate through the vessel quartz plates

This measurement is performed by keeping the radiator vessel in a sealed box flushed with pure nitrogen (at 50 l/h). The radiator vessel is flushed with He at a rate of 10 l/h. Helium diffuses through the quartz windows. Its content in nitrogen is measured with a He sniffer at the outlet of the nitrogen circulation circuit. If the radiator is He tight, the He content must be below ~ 0.36 ppm.

C₆F₁₄ circulation test

The vessel is tested during C₆F₁₄ filling and evacuation operations. A visual inspection ensures that the inlet and outlet fittings are free.

Pressurization test

The quartz vessel is filled with C₆F₁₄ and left for three days under a hydrostatic load of 103 mbar corresponding to an additional C₆F₁₄ liquid column of 20 cm.

3.1.2.4 Full-scale prototype mechanical test

A full-scale prototype of the liquid radiator vessel was made completely in Neoceram, with 16 equidistant spacers, and tested in several hydrostatic loading conditions. Strain, stress and deflection states of the two base plates measured in the test were compared with the Finite Element Analysis (FEA) by means of the IDEAS package, installed on a HP C180 workstation. In Table 3.2, we report the relevant material characteristics employed in the FEA. The adhesive joints were considered to have a minimum thickness of 0.150 mm.

Table 3.2: Material parameters of the radiator vessel components

Material	Young Modulus (N/mm ²)	Poisson coeff.	Density (g/cm ³)
Neoceram	80 000	0.24	2.51
Quartz	70 000	0.17	2.20
Araldite AW106	3700	0.39	1.75
C ₆ F ₁₄	–	–	1.68

An analysis with quadratic SOLID elements was necessary to achieve an accurate evaluation of the effective radiator stress and deformation states, particularly with respect to the plate joints to spacers and ribs.

The study was first performed on the radiator placed vertically in order to limit the computational cost and time by taking advantage of geometric and load symmetries.

The refined mesh adopted for the whole radiator finite element model consists of 22 016 quadratic SOLID elements for a total number of 108 050 nodes. Each plate and the edges, coupled to the shorter side of the radiator, were modelled with two layers of elements. A finer mesh refinement of the glued regions, by means of submodelling, was necessary to improve the analysis of the adhesive behaviour. However, this further mesh refinement has to be related to the effective adhesive film which would otherwise result in an overestimated stress state evaluation of the adhesive joints. The study was then extended to the radiator vessel prototype tilted in the most critical load condition in the ALICE HMPID structure (Chapter 1) in order to analyse stresses and deformations and to obtain the necessary information for the design of the radiator vessel in its final configuration.

3.1.2.5 The ALICE HMPID radiator vessel prototype loading

The analysis of the prototype, accomplished with the Finite-Element Method (FEM), was verified using a hydrostatic loading test executed on the radiator placed both vertically and in the most critical load condition.

The test data acquisition was performed by using the BEAM software installed on a personal computer and the UPM100 data logger unit. Two types of strain gauges were used to measure the stress and deformation states: rectangular rosettes were attached to the upper plate at the location of the supports and also close to the edges. The orthogonal strain gages were positioned between the spacers parallel to

the radiator sides. Two comparators on both sides of the geometrical centre of the upper and lower plates were used for the deformation measurements.

Tests were executed by overloading the ALICE HMPID radiator vessel prototype, filled with C_6F_{14} , with an extra 200 mm of liquid column corresponding to a maximum pressure of 103 mbar for the vertical position and 131 mbar for the most critical orientation. In addition, stress and deformation data were recorded by overloading the radiator vessel with 100 mm of liquid column. Other measurements were collected during filling and draining operations to check whether the equipment operates properly.

The stress value calculated in the region where the strain gauges localized the largest stress and the plate deflection measured by the comparators are reported in Table 3.3. Their respective FEA predictions are also reported for a comparison.

Table 3.3: Comparison between the test measurements and the FEA evaluation

	Measurement	Finite-element method
Maximum stress σ	12.5 N/mm ²	12.7 N/mm ²
Plate deflection	0.081 mm	0.079 mm

Since the strain gauge measurements confirmed the overall accuracy of the FEA, the FEM has been applied to evaluate the optimal number of spacers in the final radiator tray structure.

Results achieved on each radiator constituent with a tray containing 24(18) spacers are shown in Table 3.4.

Table 3.4: Maximum principal stress (N/mm²) versus C_6F_{14} hydrostatic pressure in the radiator tray with 24(18) spacers ($h = 0$ corresponds to the full radiator, while $h = 100$ corresponds to an additional liquid column 100 mm high, that takes into account the anticipated overpressures due to the liquid circulation system)

Radiator tray element	$h = 0$	$h = 50$	$h = 100$
Quartz plate	8.31(11.16)	9.00(12.26)	9.68(13.36)
Neoceram plate	11.6(16.93)	12.72(18.63)	13.84(20.33)
Quartz spacers	7.36(10.91)	8.12(12.06)	8.88(13.20)
Neoceram frame	4.10(4.33)	4.47(4.73)	4.84(5.13)

The safety coefficients for a brittle material have to be evaluated in the frame of the maximum stress criteria. In our case, the bending strength concerns the quartz and Neoceram plates (67 N/mm² and 100 N/mm², respectively), while the quartz tensile strength must be used for the spacers. The ratio between such quantities and the relevant maximum stress represents the ultimate safety coefficient allowed for brittle material in absence of significant flaws and defects.

By considering that flaws and defects could affect the plate and the spacers, and more significantly differences in spacer and rib dimensional tolerances could cause an initial curvature and an unwanted prestress state of the plates, it is prudent to adopt a minimum safety coefficient as large as 7 for both Neoceram and quartz.

As a consequence of the constraints imposed on the plate thickness, a spacer configuration with at least 24 elements is required. A photograph of two radiator trays mounted in a back plane is shown in colour Fig. 3.ii.

3.1.3 The C₆F₁₄ circulation system

3.1.3.1 Introduction

A liquid recirculation system was designed and built at CERN for the tests of the prototype at the SPS test beam during 1997 and 1998. The system was required to purify, fill, recirculate and empty two liquid C₆F₁₄ radiators independently, remotely and safely.

Movements of the prototype of up to ± 0.6 m horizontally and ± 0.4 m vertically had to be accommodated without interference to the circulation of liquid.

The reference pressure for the circuit was maintained constant and slightly positive with respect to atmosphere. Key pressures in the circuit were monitored electronically. Deviations from nominal conditions automatically interlocked the system into a safe stand-by state.

The liquid distribution to and from the radiators was based on a gravity flow principle — similar to that implemented by the CRID group at SLD [4]. The principle was considered a potential solution for the final ALICE system by virtue of its simple, passive and safe nature. These are important features in view of the inaccessibility of the detector and sub-systems, and the fragility of the liquid radiators.

The prototype system incorporated most of the essential features of a final system, including large volumes, to gain experience with the behaviour of the system and the technology of cleaning relatively large quantities of liquid¹.

3.1.3.2 Liquid and construction materials

Large C₆F₁₄ liquid radiator systems have been built and successfully operated for many years by the RICH group at DELPHI [5, 6] and the CRID group at SLD [4]. These groups have great experience in cleaning techniques, compatibility of materials and long-term operation with this liquid. We fully used that knowledge to avoid the pitfalls associated with this chemical.

C₆F₁₄ is not available in a high-purity research grade form with a guaranteed UV transparency. It comes in the form of proprietary branded products, which contain a large fraction of C₆F₁₄. The liquid is presently available from several manufacturers (3M, BNFL) but only the 3M product has been used to date.

Two forms are available from 3M: Performance Fluid PF-5060DL and Fluorinert FC-72. Both are manufactured by the same process but the FC-72 is purer as it is refiltered at the final stage until it satisfies more stringent specifications than PF-5060DL (Table 3.5). Note that the C₆F₁₄ content could be as low as 90%. FC-72 is promoted as the liquid to use for more demanding applications, whereas PF-5060DL is recommended for use in heat exchangers and as a solvent. For UV applications, it is always necessary to clean the raw liquid (FC-72 or PF-5060DL) since the liquid is filled into drums and stored in contact with air. The liquid chosen for the HMPID system was PF-5060DL — since it is cheaper, and the DELPHI and SLD experience has shown that PF-5060DL can be successfully cleaned with conventional filters. Since the liquid impurities can and do vary from batch to batch, it has been customary to order a sizeable quantity from the same production batch to ensure uniformity and predictability in its response to cleaning procedures.

Physical properties

The characteristics of PF-5060DL are shown in Table 3.6. Note the high density, volatility and the high solubility of air and water. These characteristics influence the circuit design. The high density causes considerable hydrostatic loading on fragile optical windows, the volatility implies high evaporation losses, which must be recovered; the high solubility of air and water vapour results in over 100 000 vpm oxygen and about 10 000 vpm water vapour in the raw material. Since both of these gases are strongly absorbent in the UV they must be reduced to trace levels to ensure high optical transparency in our application.

¹The circuit was designed together with the CERN DELPHI Gas Group, who later constructed the racks. The HMPID group greatly benefited from the help, advice and facilities of the CERN DELPHI RICH fluid team and the CERN EST/SM group.

Table 3.5: Specifications for 3M fluids

Test	FC-72	PF-5060DL	PF-5060DL 1997 Lot 30097	PF-5060DL 1998 Lot 30184
			Drums: 85 87 91 92 95	Drums: 13 16 18
Distillation range (50–60°C)	90% min.	90% min.	98%	96%
Viscosity @ 25°C (cSt)	0.42 ± 0.05	0.42 ± 0.05	0.40	0.40
Density@ 25°C (g/ml)	1.68 ± 0.02	1.68 ± 0.02	1.691	1.684
Dielectric strength	35 kV min.			
Pour point	< –60°C			
Residue (µg/ml)	10 max.			
Cost (CHF/kg)	132 (for 90 kg)	57 (for 100 kg)		

Table 3.6: Physical properties of PF-5060DL

ODP (ozone depletion potential)	0
Average molecular weight	338
Boiling point °C	56
Liquid density (g/ml @ 25°C)	1.68
Liquid viscosity (cSt @ 25°C)	0.40
Vapour pressure (mbar @ 25°C)	309
Solubility of H ₂ O (ppm by weight @ 25°C)	10
Solubility of air [ml gas/100 ml liquid (FC-72)]	48
Solubility of oxygen [ml gas/100 ml liquid (FC-72)]	65
Thermal expansion coefficient @ 25°C (ml/ml °C × 10 ³)	1.6
Refractive index (ND) @ 25°C (FC72)	1.251

Construction materials

The choice of materials to be used in the circuit (including the liquid radiators themselves) is an important issue. Long-term degradation of certain materials in contact with C₆F₁₄ has been observed by the DELPHI group [3]. The circuit was constructed using wherever possible metal (stainless steel, aluminium, copper) and glass. All-metal instruments are expensive and often difficult to find. Joints in contact with liquid were metal-metal except where an elastomer joint was unavoidable, in this case Viton was used. Chemical sealants were not used in order to avoid the liquid leaching away components from the compound.

During the construction phase, all welded stainless-steel components were subjected to a standard CERN surface-treatment. The stainless-steel pipe-work installed in the zone had already been chemically cleaned in situ. It was found necessary to pump down these lines via a LN₂ cold trap to remove all vestiges of water vapour. The remaining pipe-work was cleaned with ethyl alcohol and purged dry with nitrogen.

3.1.3.3 Circulation system

The circulation system was divided into a circulation rack, a control rack (outside the test zone) and a distribution rack (in the test zone and fixed to the detector). A schematic diagram is shown in Fig. 3.11.

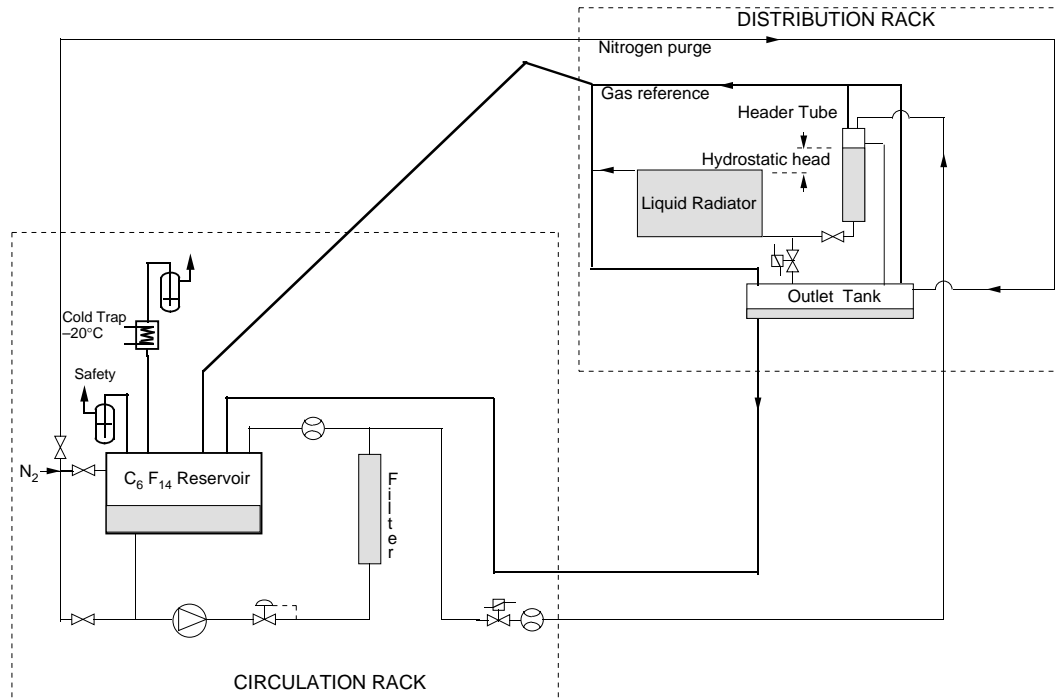


Figure 3.11: Schematic of the circulation system.

Gas reference system

The circuit contains a reservoir partially filled with liquid, the gas volume above the liquid forms the reference pressure for the system. A constant positive pressure is maintained by an oil bubbler purged by a flow of nitrogen gas. The nitrogen is introduced at the most distant part of the circuit at the distribution rack. The distribution rack is connected to the circulation rack by a large-diameter aerial line (without siphons) which acts as the purge gas return. The gas purge maintains all gas pipe-work at the same reference pressure and evacuates impurities out-gassed from the liquid and the materials in the system.

Liquid recirculation, gravity flow

The liquid from the reservoir is pumped via cleaning filters towards each radiator. The liquid first enters a header tube located above the radiator. The top of the tube is connected to the gas reference system; the bottom is connected via a valve to the low point of the radiator. The tube acts as a hydrostatic gravity feed for the radiator. It contains a large-diameter overflow pipe to limit the hydrostatic head (height difference between the overflow and the outlet at the top of the radiator). This head is set to produce the required flow through the filled radiator, taking into account the impedance of the filling line and the radiator. The header tube also traps gas bubbles in the input stream before they pass through the radiator.

Liquid from the radiator outlet falls unimpeded into a large-diameter outlet tube, connected upward towards the gas reference network and downwards toward a large-volume liquid outlet tank. The outlet tube was constructed to eliminate any siphons.

The circulation cycle starts with the progressive filling of the header tube, which in turn generates flow to the radiator. The level in the tube reaches overflow and then remains constant. The radiator filling continues until the radiator overflows into the outlet line and down to the outlet tank. At this point the gravity feed and the flow through the radiator become constant.

From the bottom of the outlet tank the liquid falls into a large diameter return line and back to the system reservoir. The outlet tank must always be above the level of the system reservoir to ensure return flow by gravity. The top of the outlet tank is connected to the gas reference network by lines without siphons.

When the flow to the radiators is stopped, the hydrostatic head drains via the radiator. The radiator then remains full until circulation is restarted.

Safety

The gravity flow system contains passive security to prevent an over-pressurization of the liquid radiator windows. The radiator is decoupled from the high-pressure part of the circuit by a header tube at the input and by a reference gas-filled collector pipe at the outlet. (It is, of course, essential that the reference pressure remains close to the atmospheric one and that the overflow can never be blocked or overloaded.)

In normal operation, the maximum pressure in the radiator is the sum of the reference plus hydrostatic pressure of the liquid column in the radiator itself. In the extreme case that the radiator output becomes blocked, the hydrostatic head is also added. Of course, the aim is to minimize this hydrostatic head.

3.1.3.4 Circulation rack

The circulation rack (Fig. 3.12) was based on the DELPHI RICH circulation system [6]. The system gas reference pressure (P1) was defined by the operational bubbler at +3 mbar. The reservoir volume of 100 litres was typically filled with 35 litres of liquid, which fed a pump (IWAKI MDGM2S220). The liquid height in the reservoir was measured by the hydrostatic pressure at P2 and was used as an interlock to prevent the pump from running dry.

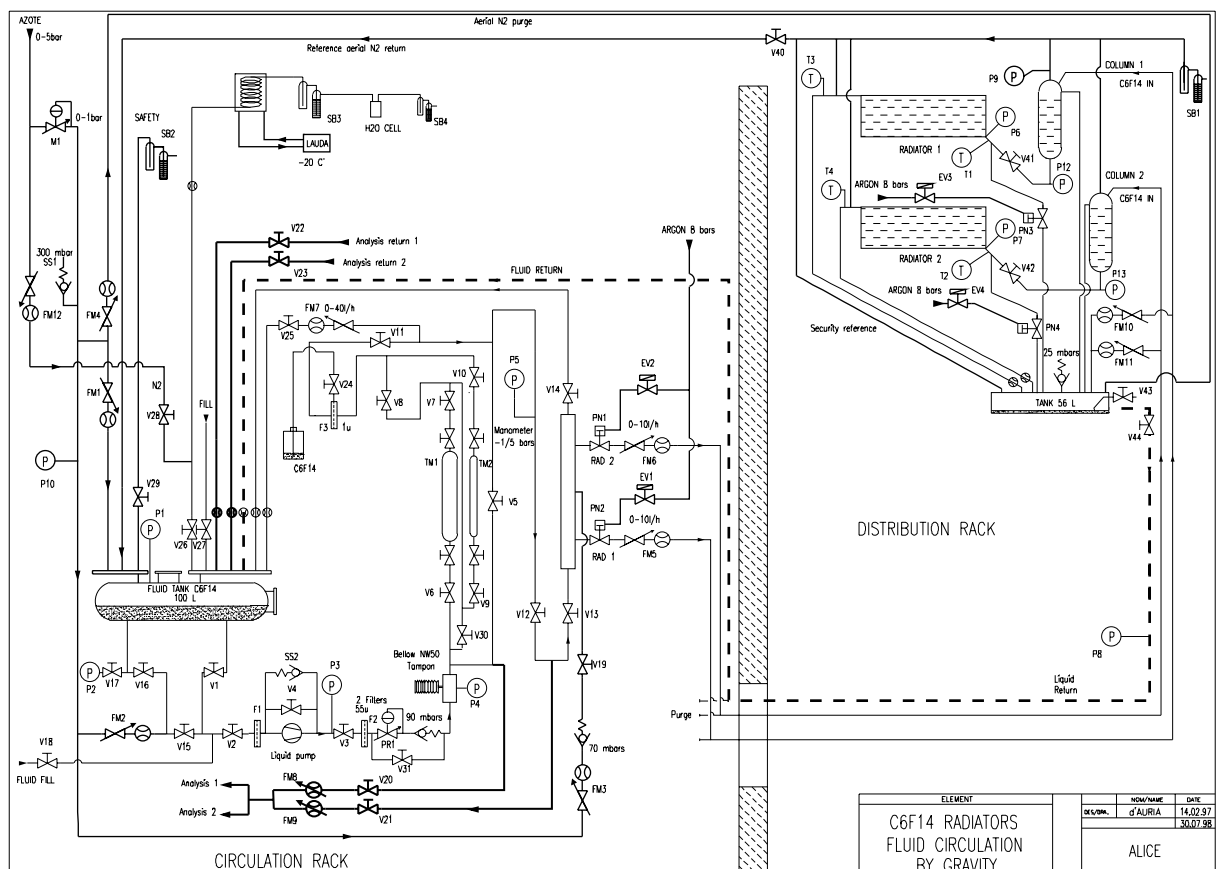


Figure 3.12: Circuit diagram of the recirculation system.

The pump pressure of about 2 bar was regulated down to 1.2 bar before entering the cleaning system (P4). The system was designed to hold two types of filter cartridges: molecular sieve (13X- standard DELPHI) and activated copper (small EST/SM). The cartridges could be used individually, or in series.

All liquid from the filters passed through a mechanical filter (ULTRAFILTER-1 micron). Mechanical filtering was essential to eliminate punch-through dust particles from the filter cartridge.

The filtered liquid at a pressure of 0.6 bar (P5) was divided into a closed-circuit flow back to the reservoir (30 l/h) and an external flow to the two radiators (12 l/h). In this way, the liquid volume was filtered at least once per hour and also the flow to the radiators could be interrupted without significantly altering the operation of the pump. The liquid quality was monitored via analysis lines (before or after the filters). The method used to date was to fill, purge, then seal a valved sample cell which was then disconnected and taken to be measured in a dedicated laboratory UV transparency measurement system.

A flow of 6 l/h to each liquid radiator was set by a manual flow-meter instrumented with an electrical low-flow alarm pick-up. A pneumatic valve (NC) enabled/disabled the flow. Pneumatic valves were used instead of electromagnetic valves in the liquid input and emptying lines to prevent local heating (bubble formation) by the valve body.

After passing through the radiator, the return liquid flow to the circulation rack fell unimpeded into the reservoir via a liquid manifold. The purge gas flow of 20 l/h was exhausted from the circuit via the same manifold. The C_6F_{14} vapour-laden gas passed via a cold trap provisionally cooled to -20°C by a thermostatically controlled bath. The condensate dropped into the liquid manifold and the purge gas and impurities exited the system via the operational bubbler.

Great care was taken, at start-up and after introducing large quantities of raw liquid, to ensure that the water vapour level was well below the dew point at the temperature of the cold trap. As a safety precaution, the coolant temperature was always raised in these circumstances. The water vapour level was monitored provisionally by inserting a hygrometer downstream of the operational bubbler.

As a final security, a safety bubbler (+5 mbar) was located upstream of the cold trap in case of blockage. The liquid loss in the 1997 run was typically 1.0 liquid litres/week. Figure 3.13 shows the variation of the liquid level in the reservoir versus time for the run Table 3.7. The losses were consistent with the losses expected from uncondensed vapour escaping from the system. A recovery system operating at -40°C is at present under study and should reduce the loss by a factor of 4.

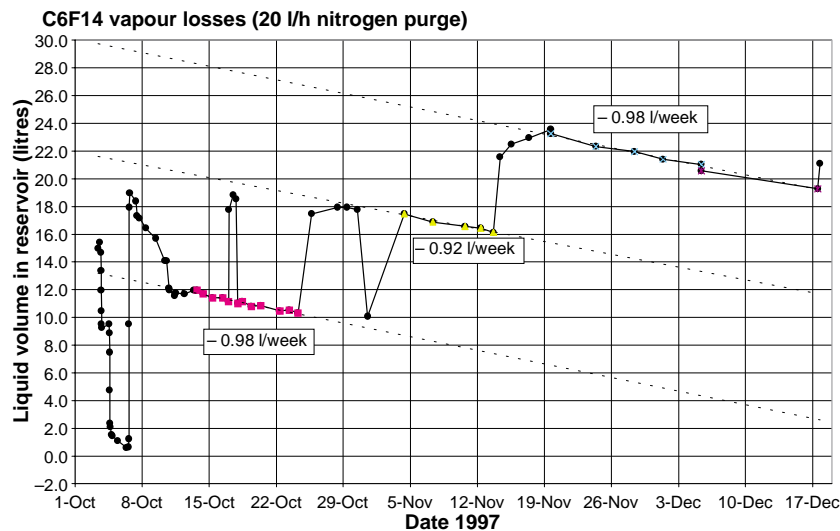


Figure 3.13: Variation of the liquid level in the reservoir versus time.

3.1.3.5 Distribution rack, mini-rack

The distribution rack (Fig. 3.12) was fixed to the detector to ensure that the correct hydrostatic heights were maintained during the detector movements in the test beam. The rack contained the header tubes with the overflow pipe at 12 cm above the radiator outlet corresponding to some 20 mbar hydrostatic head. This was estimated as a realistic minimum value for the final ALICE system.

The height of the liquid column in the tube was monitored by pressure gauges (P12, P13). The input flow to each tube was 6 l/h, the valves (V41, V42) were calibrated before the run to provide 3.5 l/h to a full radiator when the header tube was in overflow. The flow to the tubes could drop by 40% before the radiator flow changed, resulting in very stable running conditions. Note that a flow measurement in the input line is very difficult due to the inevitable pressure drop within the instrument. The pressure at the input to each radiator was monitored (P6, P7). The pressures observed corresponded to the sum of the reference pressure and of the hydrostatic height of liquid in the radiator plus several millibar of dynamical pressure generated by the flow at the input and outlet of the radiator.

The radiator outlet and header overflow pipes were inclined continuously downwards toward the outlet tank and were successfully tested at five times the nominal flow rate. The tank was chosen large (56 litres) for safety reasons — as planned for the final system. The tank had the capacity to contain all liquid in the system without the risk of backing-up into the liquid radiator outlet lines should the return line become blocked. In normal operation the tank contained a shallow layer of liquid. The tank was purged by nitrogen. The gas could rise via several large-diameter lines directly to a gas reference manifold on top of the rack, sweeping away any gaseous impurities liberated from the liquid. The manifold was protected by a safety bubbler (+5 mbar). The pressure at the manifold was measured at P9.

If circulation was stopped for an appreciable time, the shallow layer of liquid in the outlet tank evaporated away. On restarting circulation, liquid entering the ‘dry’ tank generated a large transitory gas flow by displacing part of the nitrogen atmosphere with C_6F_{14} vapour (Section 3.1.3.7).

The radiators were emptied by closing the input valves (PN1, PN2) and opening the valves (PN3, PN4) which linked the radiator filling lines to the outlet tank.

Scanning the detector by remote control necessitated that all lines connecting the rack to the circulation rack were flexible over the first five metres. A pressure probe (P8) was installed in the liquid return line to monitor the return liquid level and give advanced warning in case of anomalies.

3.1.3.6 Control rack and monitoring

The control rack displayed the pressure readings, status of flow-meter flow alarm relays and contained buttons to control the operation of the circuit. The safety interlocks for the system were generated by hard-wired logic due to the simplicity of the system.

Ten pressure probe signals (4–20 mA) were fed into individual digital display multimeters (A puissance 3 -VUP391) possessing two alarm-level relay outputs (hi =AL1 and lo =AL2) and an independent analogue output (4–20 mA).

The multimeters provided the visual display and the alarm relays used in the interlock logic. The analogue output was used to feed a monitoring PC card and a slave display panel fixed on the distribution rack. The signals passed via a LABPC+ card into a PC running LABview system which displayed and stored data. Programmable software alarm levels on the monitored pressures generated alarms and Mobile phone messages to the operator.

3.1.3.7 Operational experience

Tests were carried out in September 1997 using a prototype liquid radiator made from Neoceram. The full system was then transported to the SPS ALICE test beam and installed for the end of September.

The system was first filled and circulated with 10 litres of raw liquid and then emptied to remove particles and impurities leached from the wetted surfaces. Table 3.7 contains an abridged summary of the October 1997 run.

Raw liquid was added at the start-up of each run to allow the maximum cleaning time before data taking started. No further liquid was then added. At the end of data taking the radiators were emptied and the circuit closed down to prevent needless evaporation losses. Isolation valves (V26, V29, V40, V44) were added to facilitate this operation. After close down, the reservoir was pressurized to 100 mbar with

nitrogen. The safety bubbler on the distribution rack was then used as the operational bubbler for the continuing purge of this rack.

Table 3.7: October 1997 run summary

Radiator 2 only	
01/10/97	System purged, molecular sieve #1 (MS#1) installed Add 18 litres drum 85 Start closed circuit circulation Nitrogen purge flow 20 l/h
03/10/97	Fill return line
04/10/97	Fill and circulate the radiator
05/10/97	Measure T% drum 91 ECD test – no measurable trace C_6F_{14} in HMPID
06/10/97	Add 18 litres drum 91
07/10/97	Measure T% Add MS# 2
09/10/97	Measure T%
10/10/97	Measure T% Start recovery system $-5^\circ C$ Add MS# 3
11/10/97	Recovery at $-20^\circ C$ Start data taking
17/10/97	Empty radiator Fill radiator
18/10/97	Measure T%
19/10/97	Measure T%
22/10/97	Measure T%
25/10/97	Empty radiator End data taking Measure T%
30/10/97	ECD test – empty radiator – no measurable trace of C_6F_{14} in HMPID
30/10/97	ECD test – full radiator – no measurable trace of C_6F_{14} in HMPID Empty radiator, continue closed-circuit circulation
13/11/97	Disconnect liquid filling lines and liquid return line from mini-rack Disconnect aerial reference line. Purge mini-rack 15 l/h (safety bubbler) Purge liquid in return line back to reservoir N_2 20 l/h
27/11/97	Measure T% Drain 0.45 l sample from system
16/12/97	Measure T% Close down and seal off system

The system ran stably and safely during the three data taking runs. However, there were some aspects of the operation which were not wholly satisfactory and need attention in the final design. For instance:

- The reference pressure was found to vary when the large external doors to the experimental hall were opened. In cold weather, the sharp drop in ambient temperature caused a drop in the pressure due to condensation of C_6F_{14} vapour. The purge nitrogen flow was maintained at a relatively high value of 20 l/h for the first two runs in order to prevent air from sucking back through the operational bubbler. Insulation or regulation of the temperature of the liquid system in non-regulated environments may be necessary.

- A transient surge in gas flow through the operational bubbler was observed each time liquid fell into the radiator outlet tank when empty ('dry'). Since the pressure of the operational bubbler was slightly flow-dependent, the reference pressure rose several millibars until equilibrium was reached. It would be advisable to trap a larger volume of liquid at the bottom of each large tank to avoid this effect. Links between all large volumes and the operational bubbler should be in large diameter to prevent pressure build-up due to line impedance in such an event.
- The exchange of filter cartridges was a significant perturbation on the system. A freshly regenerated cartridge of molecular sieve is normally pressurized with 1 bar argon. This excess pressure must be purged before opening the cartridge towards the system. The entry of liquid into the molecular sieve generates heat and gas, which must also be purged beforehand. Valve V24 (Fig. 3.12) was used to bleed off the excess gas. Nevertheless, circulation to the radiators had to be stopped (V11) during this operation.
- Each change of cartridge resulted in a loss of about 1 litre of liquid. The cartridge was positioned above the reservoir to allow draining the liquid back into the reservoir before changing it. However, vapour was lost when filling the cartridge and the liquid absorbed in the molecular sieve pellets was also not recovered. A method to recuperate this loss would be useful.
- The final system will require a pre-cleaning unit to inject clean liquid into the purified bulk liquid, instead of filling new raw liquid directly into the reservoir, as was the case so far.

3.1.3.8 Cleaning and liquid transparency

The liquid used in the HMPID prototype tests originated from the same batch of PF-5060DL (30097). Prior to introducing raw liquid into the system, the sample cell was filled and the transparency measured. The transmission of several raw samples is shown in Fig. 3.14a.

The samples from the batch 30097 are similar, as expected. There is a strong absorption band around 185 nm which later proved difficult to remove. This band is not apparent in the sample from batch 30184. A simulation of the transmission over 1 cm of a gas volume containing 120 mbar oxygen and 10 mbar water vapour is shown for comparison.

The molecular sieve (13X-1001 UETIKON) preferentially removes water vapour but has also a capacity to trap many different impurity molecules. It is the only filter now in use in the fluid systems of the DELPHI RICH. After use in the system, the 13X pellets are discarded and new pellets added to prevent possible reactions when a 'wet' filter is regenerated. The new pellets are regenerated at 200 °C for 24 hours under constant argon purge.

Dissolved oxygen in the raw liquid is most efficiently removed with an active filter such as Oxisorb (MESSER GRIESHEIM) or cartridges of activated copper (highly dispersed copper, know also as catalyst copper – EST/SM CERN). The latter produced a dramatic improvement in the transparency of small samples from batch 30097, removing oxygen and the source of the band around 185 nm (Fig. 3.14b). However, problems have been encountered with these filters in the past. DELPHI had problems with batches of PF-5060DL containing non fully fluorinated impurities [7]. These impurities underwent chemical reaction in the filters that degraded the UV transparency of the bulk liquid.

Another method to remove dissolved oxygen is by intensive bubbling of nitrogen through the liquid thereby replacing the dissolved oxygen with nitrogen [4]. However, an efficient recovery system (−40 °C) is required to avoid heavy liquid vapour losses. The provisional system operated at −20 °C so that this technique was not tested. The 20 l/h nitrogen purge of the system produced a slow purging of the out-gassed oxygen.

The cleaning strategy for the first runs was conservative: use only molecular sieve cartridges and nitrogen purging to remove the impurities present in the raw material.

The evolution of the liquid transparency (after filters) for the initial run with one radiator in October 1997 (Table 3.7) is shown in Fig. 3.14c. The cleaning system had to remove impurities in the raw liquid plus those from the newly operational system. The liquid was exposed to only two new cartridges

but reached an acceptable level of transparency by the start of data taking. The absorption band around 185 nm was reduced but still significant. The system was then left to run on for a further two months. A significant improvement was observed despite no further change of cartridges.

In preparation for the April 1998 run, the bulk liquid was exposed to three new cartridges since 12 litres of raw liquid were added. The evolution of the liquid transparency (after filters) is shown in Fig. 3.14d. The liquid quality was found to be good throughout the run and better than in October 1997.

After modifications and the introduction of the second radiator into the HMPID before the July 1998 run, a short-term degradation in the liquid quality might have been expected. In addition, 16 litres of raw liquid were added to the system. Again the liquid was exposed to three new cartridges before data taking. The evolution of the liquid transparency (after filters) is shown in Fig. 3.14e. The transparency measured was an improvement on the earlier runs and approached the excellent results obtained with small samples using an activated copper filter.

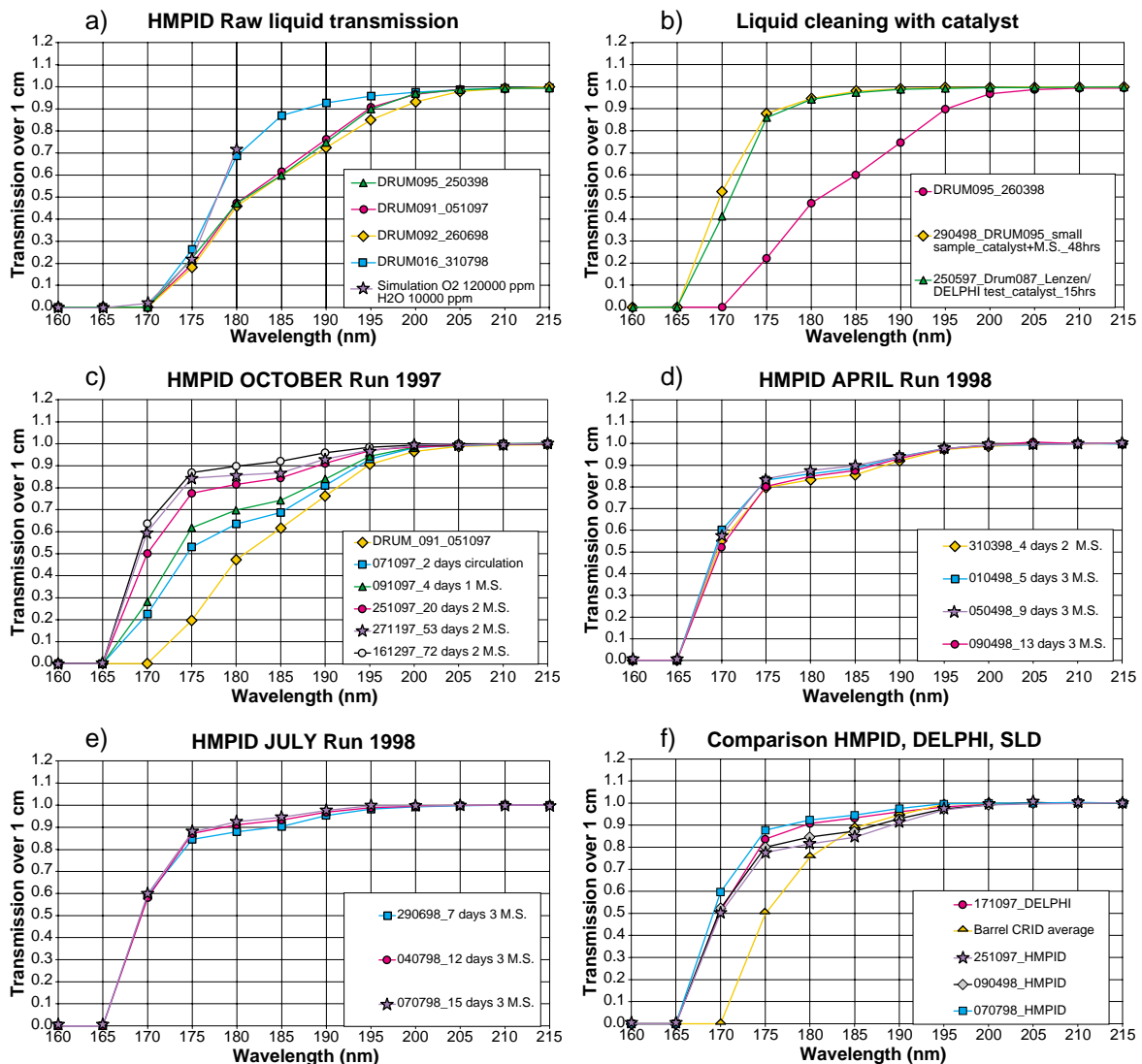


Figure 3.14: Transparency curves for different samples. For details see text.

In summary, the results obtained in the first runs of the prototype liquid system were encouraging. Good-quality transparencies were obtained using safe, passive cleaning methods. The gravity flow distribution system proved safe and stable.

The quantities of liquid involved (35 l) were, however, still small compared with the order of 250 litres required in a large system. In addition, liquid from a single batch had been used while in a large system, mixing of different batches is inevitable.

A comparison of the transparency at the end of each data-taking period is shown together with data from the DELPHI and SLD systems [8] (see Fig. 3.14f). It can be surmised that it will be difficult but not impossible to routinely maintain the quality achieved in the HMPID prototype when the size and complexity of the system increases. Some contingency on the performance side (e.g. number of emitted photons) should, however, be included to allow for a decrease in the average liquid quality in the final system.

3.1.3.9 Future developments

A systematic study of the chemical composition through analysis (GC, IR, etc.) in parallel with cleaning and UV transparency measurements seems essential to improve understanding and predictability in the cleaning process. A multi-cell, automated, on-line UV transparency measurement system is being adapted for use with the prototype and is now near completion.

The future development of diagnostics such as on-line liquid phase measurements of water vapour and oxygen traces would improve the ability to monitor the evolution of the liquid during cleaning. An on-line UV liquid refractometer would complement these instruments.

It is planned to investigate as additional filter materials: silica gel, activated copper catalyst and OX-ISORB. Passive methods such as using zeolite membranes and liquid out-gassing methods [9] seem promising techniques and merit further study.

3.1.4 The electronics chain

As discussed in Chapter 2, the low interaction rate at ALICE allows an electronics scheme with the following specific features:

- a charge-sensitive preamplifier with a long integrating time > 800 ns,
- analog charge measurement,
- multiplexed operation (MPX),

to achieve optimal single-electron detection efficiency and sub-millimetric localization from the readout of MWPC cathode pad signals.

The HMPID readout electronics is designed to satisfy the system requirements specific to ALICE operational modes:

- maximum trigger interaction rates of $1 \div 10$ kHz and 100 kHz in ion and proton collider modes, respectively,
- a system size of 160 k channels with an occupancy of hit channels expected to be less than 15% per event,
- an implementation on the detectors with a surface density of 16 kchannel/m².

The adopted multiplexed analog schematic is composed of two parts:

- an analog part based on the CMOS VLSI front-end chip GASSIPLEX [10], providing 16 analog multiplexed channels,
- a digital part performing the digitization and synchronized zero suppression.

Longer analog sequences can be treated by connecting several GASSIPLEX chips in a ‘daisy chain’ mode.

The development of this system was firstly devoted to the analog part, the chip GASSIPLEX. Most of the R&D work on the detectors was carried out using the first version of GASSIPLEX, referred to

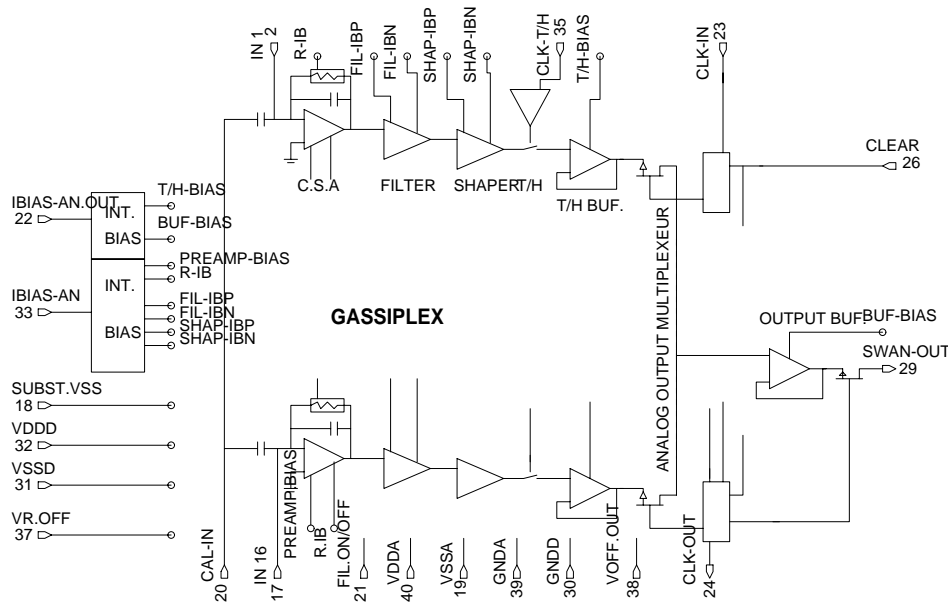
as GASSI-1.5, designed in $1.5\ \mu\text{m}$ MIETEC technology. A second version, GASSI-0.7-1, the first chip developed in 1995 at the prototype level using the new $0.7\ \mu\text{m}$ technology from MIETEC, demonstrates a very good noise performance and improved layout features such as a reduced sensitivity to latch-up. The third and final version, GASSI-0.7-2, is presently under completion, the last specifications requested by ALICE, not only from the HMPID but also from the Muon Arm spectrometer being inserted. The basic architecture of this chip is identical and its characteristics and performance will be described later.

During the detector test period, the system aspect of this FEE was investigated using standard readout elements such as the VME modules C-RAMS. In fact, for test-beam purposes, it was possible to operate the system using up to 960 MPX steps — a number much larger than the one foreseen for ALICE operation (48–64) — chosen to minimize the size of the test readout system.

In parallel, the components of the final digital part were designed as ASIC chips to constitute a modular Multi-Chip Module (MCM) based on 48-64 MPX steps needed to keep the MPX dead time compatible with the ALICE trigger rate. The main digital component is a chip referred to as DILOGIC which performs the zero suppression after the digitization effected by a commercial ADC chip.

3.1.4.1 Front-end chip: GASSIPLEX and its operation

The 16-channel GASSIPLEX chip is composed of several functional blocks per channel (Fig. 3.15): a charge-sensitive amplifier (CSA), a switchable filter (SF), a shaping amplifier (SH) and a Track/Hold stage (T/H).



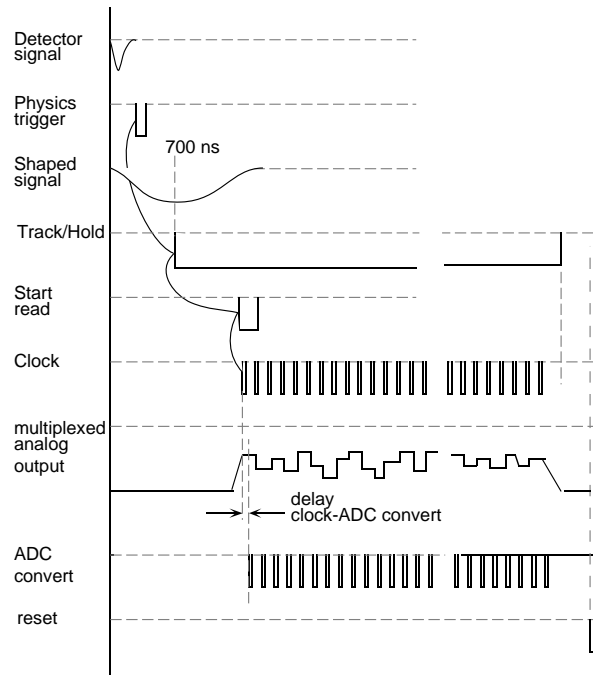


Figure 3.16: Time sequence of the control signals operating the multiplexed readout of GASSIPLEX-1.5.

Test pulses can be sent to all channel inputs through a calibrated capacitance via a common test input line in the $1.5 \mu\text{m}$ version, whilst sequential channel-to-channel calibration is performed in the $0.7 \mu\text{m}$ version.

Charge-sensitive amplifier (CSA)

This low-noise amplifier is characterized by a long decay time constant of $30 \mu\text{s}$ which makes it sensitive to the largest amount of the detector current. This feature and a very good noise figure of the full analog channel, provide an exceptional performance for detecting very low-level signals in MWPC down to a threshold of 0.3 fC . The linear output range of the CSA can be symmetrized.

Switchable filter and shaper amplifier SF,SH

GASSIPLEX is designed to be connected to wire chambers as well as to silicon strip detectors. A switchable filtering stage is necessary to match the different input current shapes of these two kinds of detectors. With solid-state detectors which provide a fast input current ($< 100 \text{ ns}$), the filter is by-passed. The input current per channel should not exceed 1 nA . With wire detectors (MWPC), it is known that the slow drift of ions towards the cathode is responsible for a hyperbolic long-tailed current, which lasts for tens of microseconds and consequently disturbs the output baseline as fast differentiation is used. The filter was designed to extract, in several hundreds of nanoseconds, the greatest part of the charge delivered by the detector and to transform the long integrating time of the charge signal into a step function (Fig. 3.17a,b). After the filter, a shaping circuit made of a low-pass followed by a band-pass filter transforms this step function into a semi-Gaussian shape where one-third of the time is taken to reach the peaking time and two-thirds to return to the baseline (Fig. 3.17a,b). A pole-zero cancellation circuit compensates the decay time constant of the CSA, resulting in a very precise return to the baseline in a short time: $\pm 0.5\%$ of the peaking time amplitude in $3 \mu\text{s}$ and $6 \mu\text{s}$ for the $1.5 \mu\text{m}$ and $0.7 \mu\text{m}$ versions, respectively (Fig. 3.18).

This essential feature sets the front-end occupation time at less than 3 or $6 \mu\text{s}$, without analog overlapping of events for versions $1.5 \mu\text{m}$ and $0.7 \mu\text{m}$, respectively. An external bias resistor permits a slight adjustment ($\pm 100 \text{ ns}$) of the peaking time. This time is 700 and 1200 ns for the $1.5 \mu\text{m}$ and $0.7 \mu\text{m}$ versions, respectively. It provides a natural built-in delay used to wait for the external trigger decision.

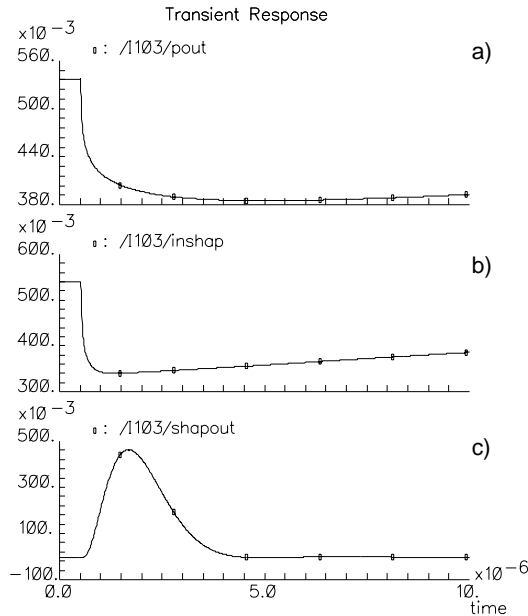


Figure 3.17: Simulated wave forms of the Filter and Shaper stages: a) input current, b) after the Filter, c) after the Shaper.

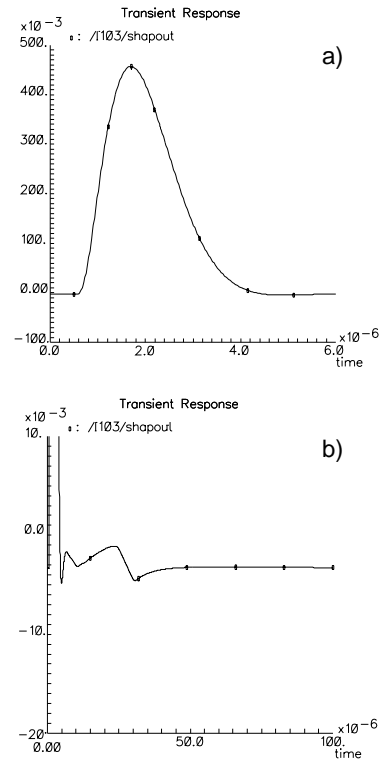


Figure 3.18: a) Shaper waveform (full scale: $6 \mu\text{s}$).
b) Shaper base line recovery (full scale: $100 \mu\text{s}$).

Track and Hold stage (T/H)

In operation mode, all the switches driven by the T/H stage are closed, while those driven by the MPX stage are open in the whole system. When an event occurs, the capacitors associated to hit channels are charged up by the corresponding detector currents. An external trigger signal, synchronous to this event, is used to generate a ‘HOLD’ signal, sent to the whole system, in order to open all switches at a time corresponding to the peaking time of the shaping amplifier (Fig. 3.16). Therefore, the maximum charge signals are stored for those channels with a real signal (hit). Charges corresponding to their pedestal values are stored for those not having been hit.

As long as the HOLD signal is maintained ‘on’, the switches are open and the charges are kept frozen in the capacitors. Charges have a very low leakage rate -1 mV/ms . As soon as the HOLD signal is released, the switches are closed and the charges lost. A fast clear can be implemented according to that feature as the recovery time of the circuit is less than 200 ns .

Multiplexing

The decision to read out an event (charges stored in the capacitors) is independent of the T/H operation. For this purpose, a ‘START READ’ signal is generated from the event trigger logic with any delay convenient to the user. This signal starts a train of MPX clock pulses, issued from an external device, which allows the number and frequency of the clock pulses to be adjusted.

The clock train is also synchronously sent to the readout module where the digitization is performed. The digital conversion and the zero suppression of each analog step is carried out between two clock pulses. The sequencer should make it possible to adjust the delay between the two trains in order for the ADC conversion to be carried out during the flat part of each analog step (see Fig. 3.16).

However, although the two clock trains are issued from the same source, the MPX clock train is propagated through all the GASSIPLEX chips to operate the MPX function. Therefore, this train accumulates some delay (32 ns per chip) with respect to the ADC convert train. If the time between two clock pulses is too narrow, the synchronism is no longer satisfied after a certain number of clock pulses. So, for a large number of MPX steps (> 300), a module has been developed which compensates these delays on the ADC convert train.

CLEAR/BUSY

As soon as the clock train is over and the digitization performed, a CLEAR signal is sent to the GASSIPLEX, repositioning all switches to their initial positions. This signal can be sent after the HOLD signal is released.

Usually, as soon as a HOLD signal has been generated, the trigger logic is vetoed by a BUSY signal to protect the whole system from new events. This protection is released by the computer (via an output register) when all tasks are terminated.

3.1.4.2 GASSIPLEX intrinsic performance

In Fig. 3.19 the linearity and noise figure curves of the two GASSIPLEX versions are shown, respectively. In Table 3.8 the main electronic features of the two GASSIPLEX chips are summarized.

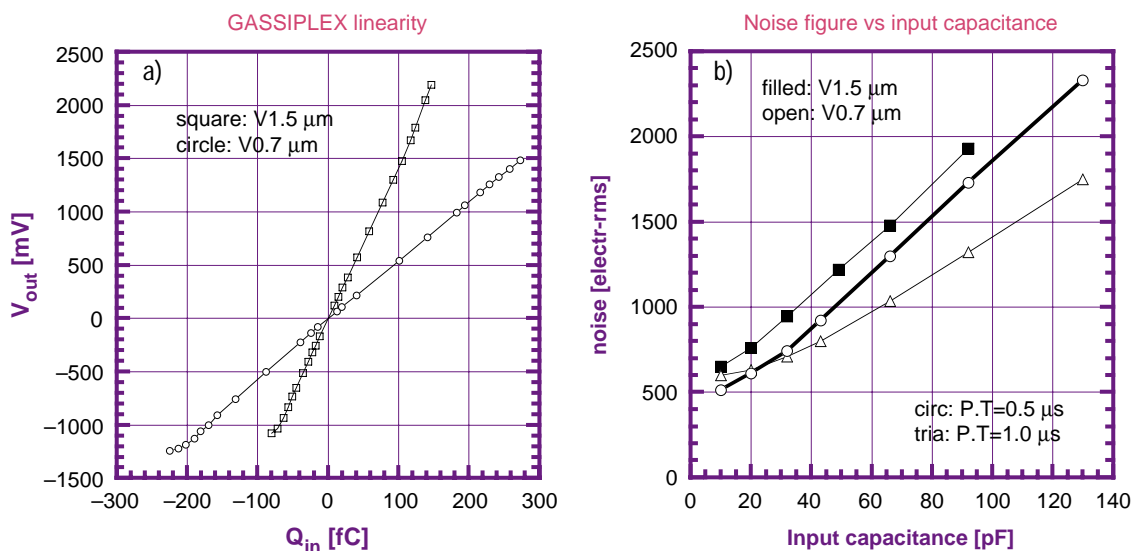


Figure 3.19: GASSIPLEX-1.5: linearity and noise curves.

3.1.4.3 GASSIPLEX system aspect

Pedestal, noise level and threshold definition

GASSIPLEX is an ungated, asynchronous device, which means that its inputs/outputs are always sensitive. Therefore, when the T/H signal is set, each output is raised at a constant DC level in the absence of input signal. This baseline, called 'pedestal' is channel-dependent within the chip. Measuring the fluctuation of the pedestal level gives the noise figure of this channel (in practice, as the r.m.s. of a pedestal distribution). Calling $PED(i)$ and $SIG(i)$ the average and r.m.s. values of a pedestal distribution, the operating threshold of the channel (i) is defined as: $TH(i) = PED(i) + N \cdot SIG(i)$, where N is a selectable constant, usually ≥ 3 .

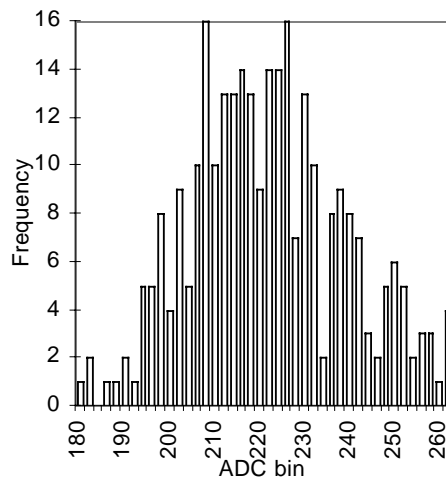
This procedure has the essential advantage of attributing the correct threshold value to every channel, regardless of the gain, noise figure and pedestal spreads among the channels and is, in fact, the prime reason to have chosen analog-based operation.

Table 3.8: Measured performances of the GASSIPLEX 1.5 and 0.7 μm versions

		GASSIPLEX V. 1.5 μm	GASSIPLEX V. 0.7 μm
Silicon area	mm^2	$4.2 \times 4.6 = 19.3$	$3.46 \times 4 = 13.8$
VDD/VSS	V	± 3.5	± 2.5
Noise at P.T.* = 500 ns	r.m.s. e	630 at 0 pF	485 at 0 pF
Noise slope at P.T. = 500 ns	e r.m.s./pF	16	15.8
			12.0 at P.T. = 1 μs
Noise at P.T. = 1 μs	r.m.s. e		585
Linear dynamic range	fC	-75 to 150**	-250 to 300
Conversion gain	mV/fC	12.3	4.9
Base line recovery		< 0.5% μs after 3	< 0.5% after 3 μs
Range peaking time	ns	400 to 650	400 to 1000
Power consumption	mW/chan	6	6
Analog readout speed	MHz	10	10 max

* P.T. = Peaking Time.

** X 2 when operated in silicon mode.

**Figure 3.20:** Distribution of the mean pedestal value per GASSIPLEX chip taken over a batch of 300 chips.

Usually, the PED(i) have little fluctuation within a chip ($\leq 2\%$). However, a significant spread can be found among chips as can be seen in Fig. 3.20, where a distribution of average values of pedestals per chip is shown. The average of such distributions depends, in fact, on the production batch of the chips. This feature has to be taken into account when a large number of chips are associated in long daisy chains. In order to benefit from the largest dynamical range in a chain, all pedestals should be set at a value as close as possible to the zero-DC level and should have the smallest dispersion. It was therefore necessary to sort out the chips in order to associate them in daisy chains by increasing the mean PED/chip values. The overall adjustment of the mean pedestal value of a chain was then performed independently by the buffer amplifier, at a positive or negative level, depending on the working range of the ADC device in use. As described in Section 3.2.4, that inconvenience will be solved in the final FEE version.

Operation of the system

The schematic of a GASSIPLEX-based operation system is shown in Fig. 3.21. It is composed of the following elements:

1. a trigger/control signal generator used to:
 - set the trigger modes: generator mode for pedestal and calibration measurements, or physics mode to record data from any experimental triggering array;
 - send the T/H and CLEAR signals to the GASSIPLEX chains using level shifters adapting the logic signal levels to those requested in the chip;
 - start the MPX readout sequence.

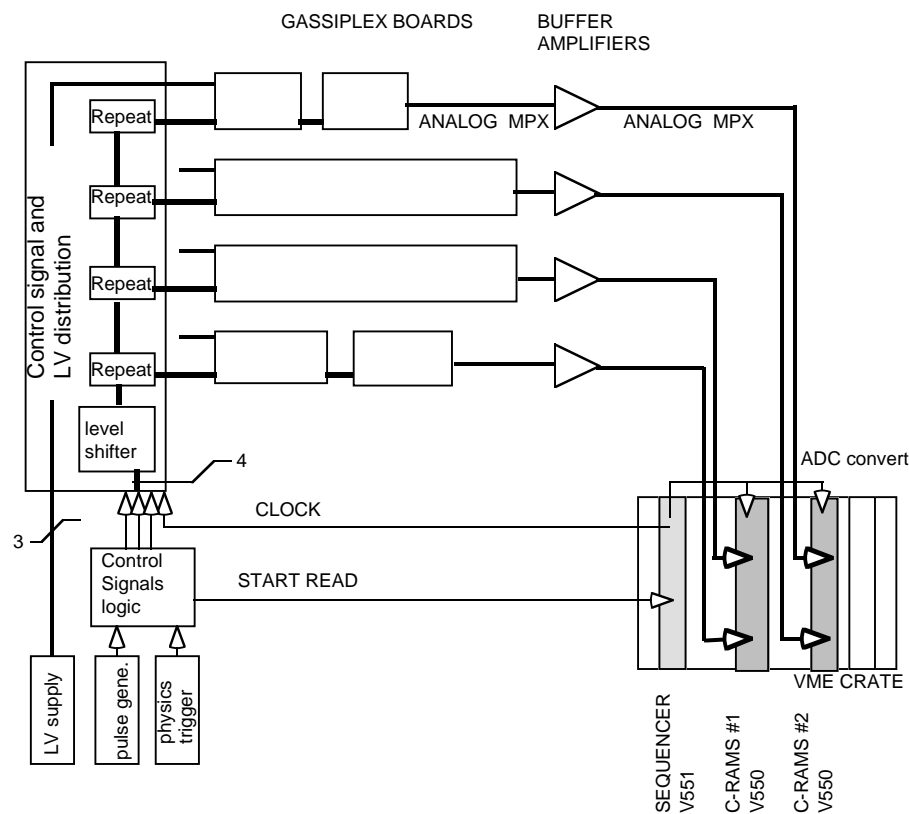


Figure 3.21: Schematic of a GASSIPLEX-based operation system.

2. a multiplexing sequencer used to:
 - send the CLOCK train to the GASSIPLEX chains and the digitizing units;
 - adjust the frequency, the number of CLOCK signals and the delay between the CLOCK trains.
3. digitizer and zero suppressor modules.

During the R&D and test phase, the GASSIPLEX chips were implemented on boards with 3, 6, or 15 chips, easily daisy-chained, using flat cables between the boards. As seen in Fig. 2.26 on page 37, these boards were plugged on the back of the pad panels to form chains of up to 960 channels on proto-2. Each chain was followed by a buffer amplifier driving a low impedance cable transporting the analog MPX signal to the counting room where the digitizers and data acquisition are located.

Element 1 is a specific NIM module designed at Subatech, Nantes [11]. For a large system operating many chains in parallel, a single-level shifter was used, followed by repetitor cards to regenerate the control signals at each chain. Elements 2 and 3 are the CAEN-VME modules V551 and V550, respectively. The maximum rate of digitization/zero suppression is 5 MHz.

In the HMPID system, all these elements will be mounted on the detectors, necessitating the new more integrated versions described in Section 3.2.4.

3.1.4.4 System performance

In order to correctly exploit physics data, the basic state of the system, i.e. the pedestal and noise tables of all channels, must be known and their stability must be under control. This operation is referred to as a ‘pedestal run’ providing the necessary pedestal and threshold tables which are stored in the memories of the digitizer/zero suppressor modules, e.g. V550. At every event, all digitizations, $A(i)$, are compared with the corresponding threshold values $TH(i)$. Only if $A(i) \geq TH(i)$, are the values $[A(i)-PED(i)]$ and their addresses stored in a FIFO memory to be read out by the DAQ system. The pedestal distributions are recorded with a pulse generator as the trigger, in the absence of any other detector signal. This condition can easily be fulfilled under test beam conditions by taking pedestal measurements between particle bursts.

At ALICE, the detectors are irradiated in a DC-mode for periods lasting a few tens of hours without beam interruption. At low interaction rates, pedestal runs could be taken in interaction mode but as few times as possible, implying a good stability of the pedestal values between measurements. In fact, the stability is governed by the level of the input gain temperature coefficient. In Fig. 3.22, we show a set of measurements characterizing the basic state of the FEE equipping proto-2, measured under operation at the SPS test beam. It corresponds to 15 360 pad channels (960 GASSIPLEX chips) readout by eight CRAMS modules. 960 channels were multiplexed per CRAMS input at a clock rate of 1 MHz. One ADC channel corresponds to 0.17 fC. In plot (a) we show the distribution of pedestal values, reflecting the spread discussed before. Plot (b) shows the distribution of sigma values corresponding to an r.m.s. noise figure of 1120 ± 155 electrons; (c) and (d) show the pedestal and sigma channel maps corresponding to 1920 channels. In (e) to (g) are shown the distributions of the differences between pedestal values measured at different time intervals, demonstrating a good stability over an 18-hour period. Linearity curves obtained by pulsing all channel inputs are shown in (h) for 240 channels, (i) indicating an r.m.s. of the electronic gain of 2%.

3.1.4.5 Preliminary developments of the HMPID electronics

The MultiChip Module (MCM)

In order to satisfy the trigger and data flow rates expected in pp and Pb–Pb operational modes at ALICE, the final electronic system will be organized in a serial/parallel architecture based on a modular array composed of three GASSIPLEX chips (48 channels) and a MCM composed of one ADC and one zero-suppressor chip, referred to as DILOGIC, as shown in Fig. 3.23. The analog part will be still implemented at the back of the pad panels, while the multiplexed analog signals will be now propagated in parallel on a bus PCB to the frame of the module where the MCMs are concentrated on a motherboard. The data transfer to the DAQ is achieved by a serial optical link.

In this section, we shall only describe the R&D made on the first prototype version of the ASIC DILOGIC-1 and the operation of a MCM prototype. The complete system is described in Section 3.2.4.

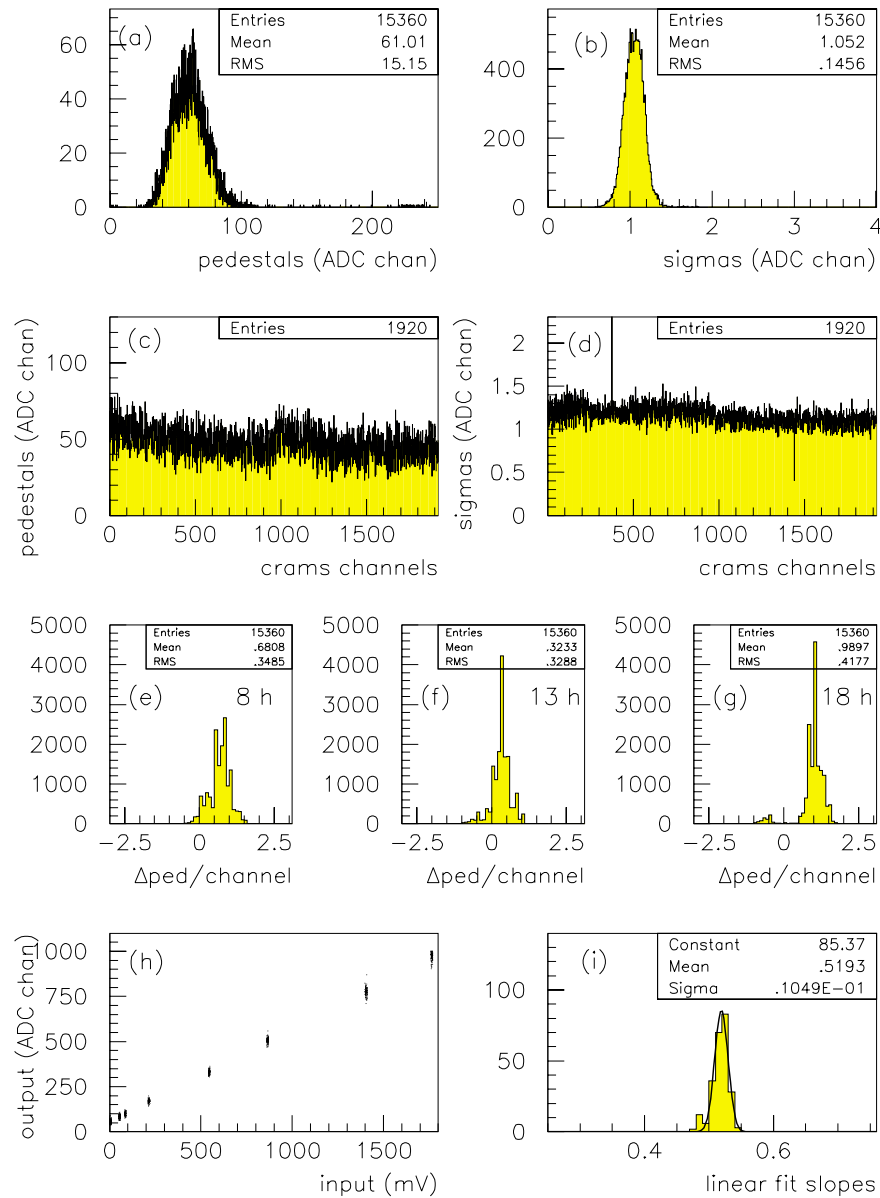


Figure 3.22: Pedestal and noise measurements, pedestal stability and gain calibration of a system of 15 360 GAS-SIPLEX channels. Measurements taken with proto-2 during a test beam period.

DILOGIC-1

The schematics of the first version, designed with the MIETEC $0.7 \mu\text{m}$ technology, is shown in Fig. 3.24. It works in pipeline mode with the ADC and channels (16, 32 or 64) read out sequentially. Each ADC conversion is fed into the DILOGIC-1 with the corresponding address to be processed in order to eliminate the empty channels, to subtract the pedestals, to fill the memories with a bit-map of the event and the digitized information of the hit channels, and finally to make an Input/Output connection with the outside world through a dedicated link.

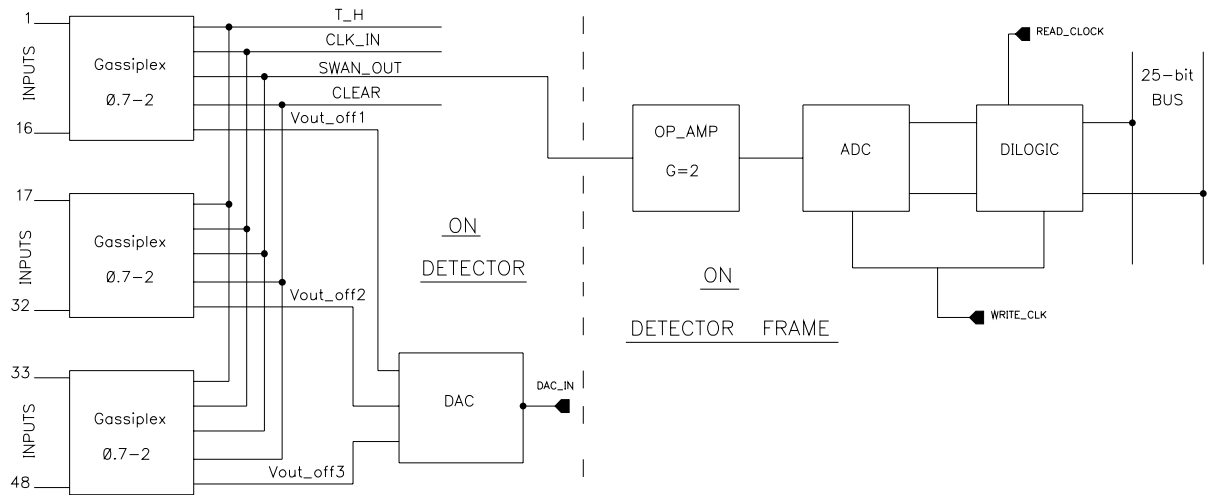


Figure 3.23: Schematics of the Multi Chip Module (MCM) constituting the basic readout cell of the module. It is based on a 48-channel multiplexed operation (3 GASSIPLEX chips). On the right side of the hatched line are the MCM elements implemented on the chamber frames.

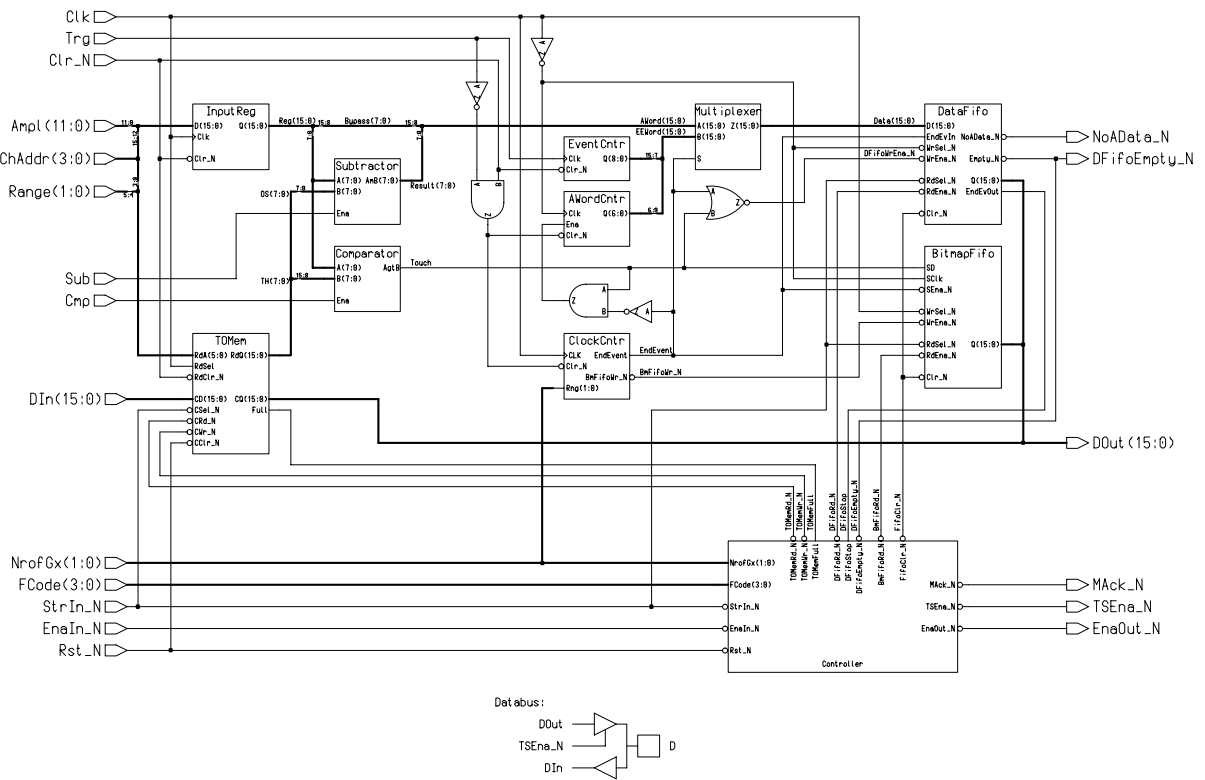


Figure 3.24: Schematics of the DILOGIC-1 performing the zero-suppression in the MCM.

The sparse data scan section is made up of a digital comparator and a subtractor, with an 8-bit range; each one is fed on one side by the analog information and on the other side by the contents of two separate memories filled respectively for each channel by the chosen level of comparison (pedestal + $N_{\sigma_{noise}}$) and the pedestal value. At present, DILOGIC-1 can process up to 64 channels with a single range 8-bit ADC and 16 channels with the 4-range CRIAD- ADC0u7. The BIT-MAP memory (64 words \times 16-bits) is filled with ones for channels above threshold or zeros for channels below the threshold; the analog data memory (512 words \times 16-bits) is filled with the amplitude information and the address of the selected channels. An End-Event word turns off the event readout sequence; it contains the number of the hit channels (7-bits) and the number of the events (9-bits). In this way, DILOGIC-1 needs one more clock compared to the GASSIPLEX multiplexer clock; it can process 16, 32, or 64 channels. Figure 3.25a gives the timing diagram of the write operation and Fig. 3.25b shows the timing diagram of the read sequence.

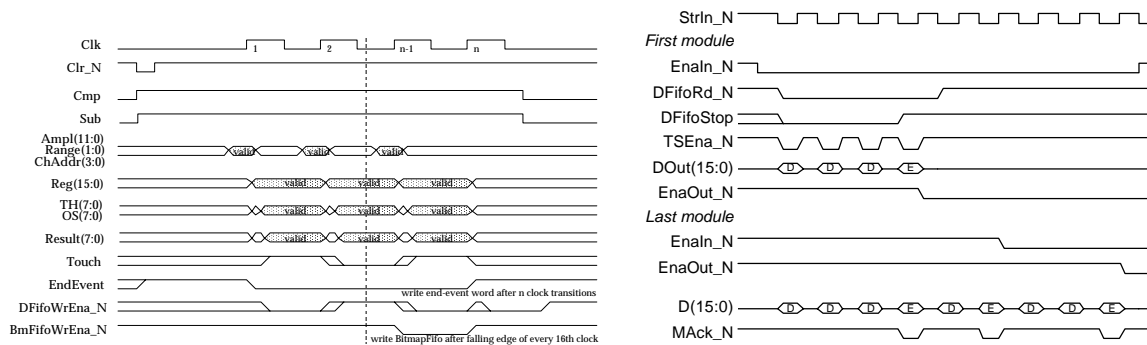


Figure 3.25: Operation of the DILOGIC: timing diagram of the analog write operation (a) and of the analog read sequence (b).

The output of DILOGIC-1 is made of a bi-directional 16-bit bus and a few control lines which allow the number of channels to process and the storage mode (with or without zero suppression) to be selected; on the output side, a function code of 4 bits allows the mode of operation shown in Table 3.9 to be chosen. Two flags give, respectively, the content of the data FIFO and the kind of data it contains: analog information + End-Event words or just End-Event words (event empty). A Mack signal comes out in phase with the End-Event word and a Token-in allows the readout of the chip, whilst a Token-out performs the Daisy-Chain to the next DILOGIC. A separate clocking permits an asynchronous operation, write during read.

Table 3.9: Readout controller code

F-code	Function
1000	Pattern readout
1001	Pattern delete
1010	Analog readout
1011	Analog delete
1100	Reset FIFO pointer
1101	Reset daisy chain
1110	Write Th. and Ped. Memory
1111	Read Th. and Ped. Memory
0xxx	Disable Dilogic

DILOGIC-1 was designed for a maximum write clock of 10 MHz and a maximum read clock of 20 MHz with a capacitive load of 50 pF, at a power consumption of 80 mW.

DILOGIC-1 was implemented on an MCM-Digitplex card. The first card was made with four GASSIPLEX (64 channels) and a second card was developed with four GASSIPLEX to fit the HMPID standard which is 48 channels. The results of the tests will be presented in the next section. A new DILOGIC-2 is under development to fit the HMPID requirements and to allow choices in ADC precision up to 12 bits and channel numbers up to 256. It will be described in Section 3.2.4.

MCM-Digitplex

The MCM-Digitplex [12] is a compact on-detector analog-to-digital processor for the readout of particle detectors. Each MCM has on board, a set of GASSIPLEX readout chips, a fast digitizer, digital pre-processing and data buffering. In this way, the MCM-Digitplex is able to select triggered events and provide the addresses and amplitudes of hit channels. A 64-channel prototype was developed, as shown in Fig. 3.26, and the first results obtained from electrical tests. Directly mounted on a custom-made VME digital I/O board and operated at a conversion rate of 5 MHz (limited by the present set-up), the noise level is kept at 700 e r.m.s. at zero pF additional input capacitance with a slope of 15 e /pF.

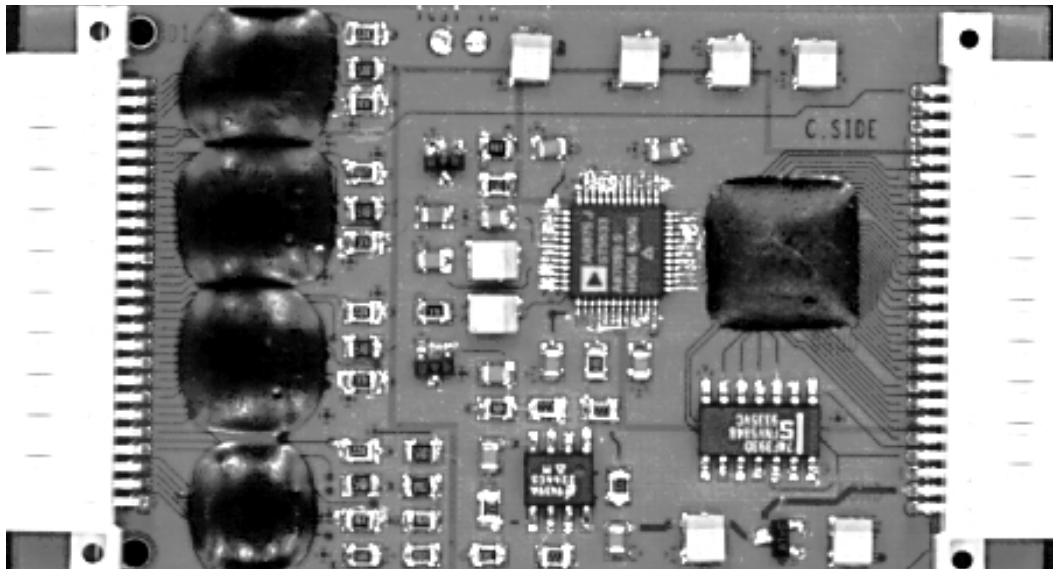


Figure 3.26: Photograph of a MCM-Digitplex board. The GASSIPLEX and DILOGIC-1 are implemented as dies, wire-bounded on the PCB and protected with plastic glue.

A set of 48-channel modules interfacing an 8-module readout bus was prepared and will be tested with the prototype of the HMPID detectors of the ALICE experiment. In the following the functionality of the full set was verified and the performance of a single card is presented.

Performance

In spite of the VME environment, the performance of the analog section was similar to that obtained with a single, shielded GASSIPLEX (Table 3.8): 700 e r.m.s. compared with 650 e r.m.s. The other characteristics are unchanged, particularly the inter-channel crosstalk which is lower than -60 db. The total power consumption of the 64-channel MCM-Digitplex is 1080 mW, which is 16.8 mW/channel; 300 mW are consumed by the discrete components: ADC, address counter and analog buffer.

Figure 3.27 show the measured pedestal spread, noise and data selection obtained on a MCM chip.

The idea to use an on-detector analog-to-digital processor was abandoned in favour of a simple 48-channel analog-multiplexed card. The digitization, the data processing and the memorization were moved out to the frame of the detector and are described in Section 3.2.4.

GASSIPLEX-0.7

The new version (Fig. 3.28) in 0.7 μm technology has a peaking time adjustable from 1.0 to 1.3 μs compatible with the trigger L0 latency. If this value is marginal due to a longer latency time imposed, an earlier fast multiplicity trigger instrumented in the zone generating a pre-T/H of 2 μs duration and sent to the HMPID in a time shorter than the L0 trigger latency might be envisaged. This pre-T/H, if validated by T_0 , maintains the Hold on for normal readout; if not validated, the pre-T/H is released and the system is ready to accept the next trigger after 100 ns.

The time for baseline recovery at 1% of the peak amplitude was increased to about 5–6 μs . That value of the occupation time corresponds to a 1% probability of overlapping consecutive events with very dense central Pb collisions. For higher rates in pp mode, the event density is so low that a higher probability of overlapping consecutive events should not create problems in the pattern recognition.

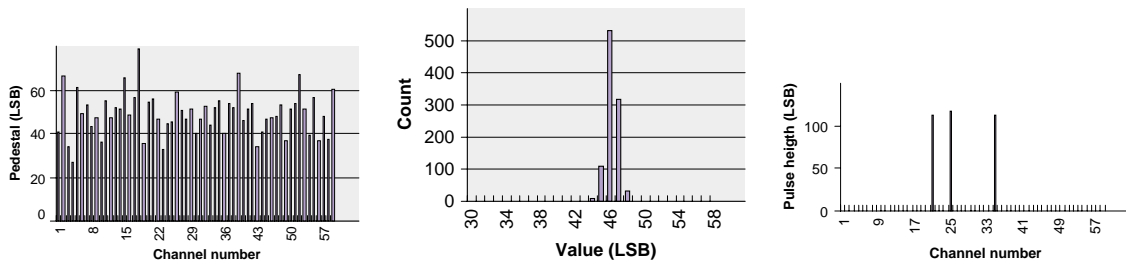


Figure 3.27: (a) Test of the MCM-Digitplex showing the spread of 64 pedestals. (b) Test of the MCM-Digitplex showing a channel noise performance equals to 0.73 LSB (least significant bit). (c) Test of the MCM-Digitplex showing a 3-channel hit configuration obtained with data selection.

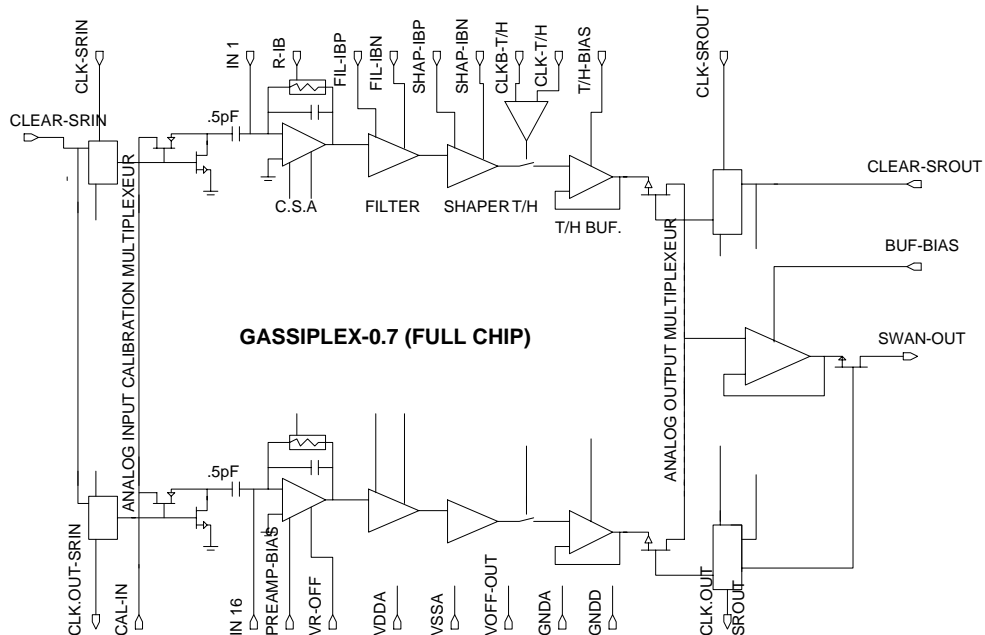


Figure 3.28: Schematics of the functional blocks composing GASSIPLEX-0.7. The calibration block is different from the 1.5 μm version (Fig. 3.15).

3.1.5 The CsI evaporation system

The basic properties of the CsI film were described in Section 2.1.1 and the main procedures to achieve films of high QE performance discussed. The CsI evaporation facility described now was used to process

all the PCs studied up to now and will be the one in use for the final production of the HMPID PCs. The station is being extended with another vessel in which the PC freshly evaporated can be translated under vacuum and scanned for local evaluation of its QE.

3.1.5.1 CsI evaporation facility

The CsI evaporation facility is shown schematically in Fig. 3.29 and in colour Figs. 3.iii and 3.iv. The main body is a cylindrical vessel, made of stainless steel, of 0.8 m diameter, 1 m long, lying horizontally on a support and closed by rotatable doors to allow easy access from both ends. All around the vessel, a large number of ports are implemented, equipped with Conflat metallic sealed flanges used to install auxillary equipment such as pumps, pressure probes, electrical and motion feedthroughs, etc.

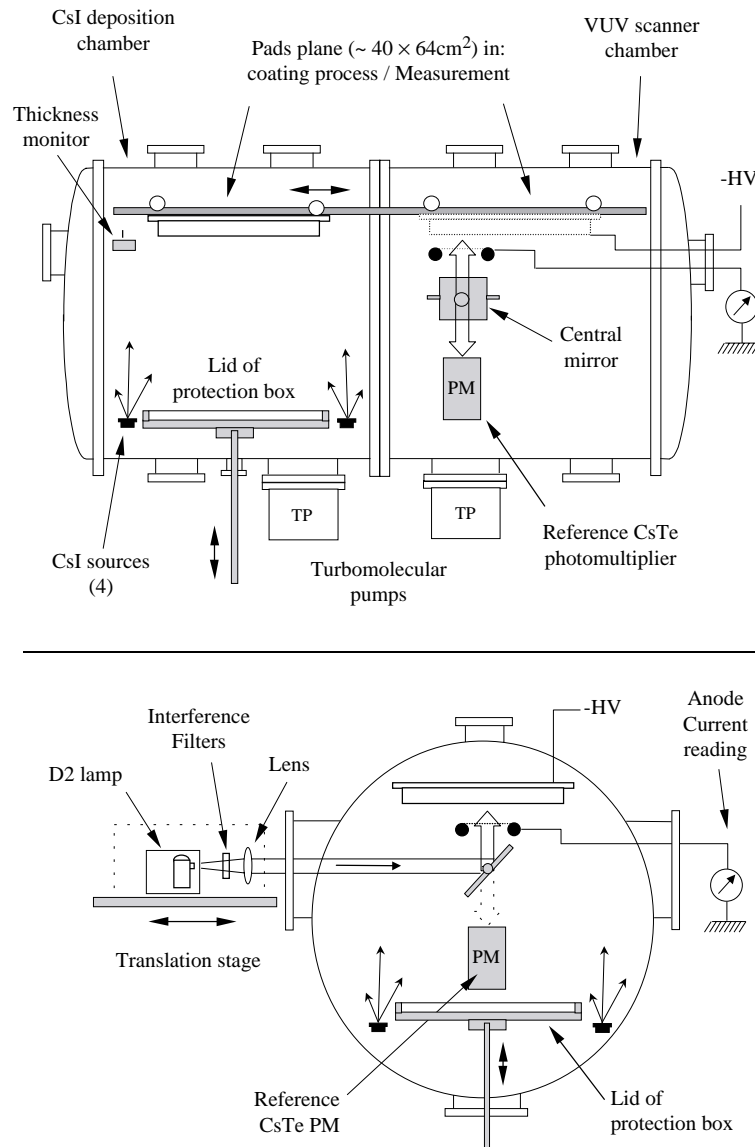


Figure 3.29: Schematic side- and cross-views of the CsI evaporation system. On the top: the evaporation and the QE measurement parts are on the left and on the right side, respectively. At the bottom: principle of the QE evaluation based on the measurement of the photocurrent produced by local irradiation of the CsI PC by a monochromatic UV beam, the intensity of which is obtained from a calibrated PM.

The primary and secondary vacuum are obtained from a 120 m³/h Alcatel rotary pump and two Leybold Turbovac pumps, for a total evacuation speed of 2500 l/s, respectively, separated by a URB040 Balzers catalyser trap. Resistive heating bands are wound around the cylindrical vessel allowing the system to be heated up to about 100 °C, for outgassing and temperature conditioning.

A pressure ionization gauge SVT AL310 and Pirani/Penning Palzers TPG300 gauges are used to monitor the residual pressure. A Quadrupole Mass Spectrometer Balzers QMS200 is now available to analyse partial pressures of residual gases. The total residual pressure reached after outgassing is 2×10^{-7} Torr and 5×10^{-7} Torr with a pad panel array installed in the vessel.

Manipulation of the pad panel

The side of the pad panel where the FEE connectors are implemented is first enclosed in a box made of a metallic lid tightly fixed to the back of the pad panel. When installed inside the evaporator, a primary vacuum is independently made in this box as the full vessel is evacuated. In this way, we avoid an over-long outgassing time expected from the FEE-instrumented side, and balance the pressure on both sides of the pad panel. Then, although only the clean pad face is exposed to vacuum, a long outgassing time is necessary to reach a total residual pressure of 5×10^{-7} Torr indicating that moisture is still present at the surface of the pad PCB. Further improvement, such as increasing the outgassing temperature, should be investigated in order to reach a lower pressure.

A second metallic lid is installed at the bottom of the evaporator, fixed on a motorized system enabling it to be moved vertically up and down inside the evaporator. This lid is designed in such a way that it constitutes, when put in contact with the pad panel, a tight box to protect the CsI film. After the CsI film has been deposited and the vessel filled with argon at atmospheric pressure, the lid is lifted and kept firmly pressed against the pad panel frame in order to compress the O-ring and ensure a good tightness in the absence of screws.

Then, the so-constituted box is flushed with argon at atmospheric pressure and the evaporator vented at the same time. After opening the evaporator the necessary screws are inserted to tighten the lid on the pad panel definitively, the pressure exerted by the lifting device is released and the CsI pad panel removed from the evaporator under inert gas protection, having never been in contact with air.

CsI evaporation system

Given the diameter of the evaporator, the distance available from the boats to the substrate is reduced to about 50 cm. In order to ensure a uniform thickness of the CsI film over the large area of PCs, four evaporation boats are used. Their locations with respect to the PC are optimized such as to ensure a variation of the film thickness of about 10% over an area of 65×50 cm², as seen in Fig. 3.30.

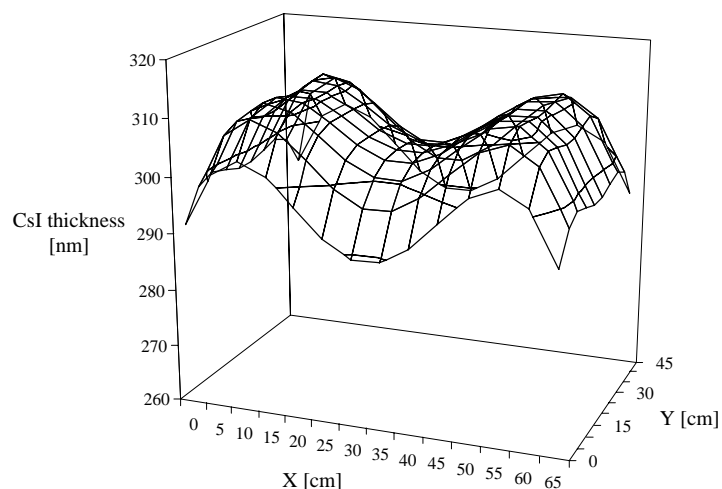


Figure 3.30: Thickness mapping of a CsI film of 60×40 cm² area obtained by evaporation from four boats.

The boats are made of molybdenum and heated independently by Joule effect. The CsI loads are calculated such as to ensure the desired film thickness after the complete evaporation of the content of the four boats. The CsI loads are pre-molten in the boats under vacuum in order to have a good thermal contact between the CsI and the boat, and avoid local overheating.

The four boats are evaporated simultaneously under the control of a quartz balance Edwards FTM5 monitoring the evaporation rate and the thickness. During a few seconds, a shutter masks the source in order to collect the beginning of the evaporation, possibly polluted, and is then removed. A slight drop in pressure of about 25% of the initial pressure is usually observed at the beginning of the evaporation, probably as a consequence of the reduced outgassing of the vessel and the pad panel caused by the freshly deposited CsI layer.

Conditioning

After the installation of the pad panel and the boats in the evaporator, the sequence of operations is as follows:

- pumping and outgassing during 2–3 days at 60 °C until a residual pressure of 2×10^{-6} Torr is reached,
- CsI evaporation on substrate maintained at 60 °C,
- heat conditioning at 60 °C under vacuum during 8–12 hours at a pressure of 2×10^{-6} Torr,
- stop heating for cooling down to 40 °C,
- venting the protection box and the evaporator with argon,
- lift the lid to form the protection box,
- opening of the evaporator and transfer of the pad panel to storage under argon flow.

The transfer of the CsI pad panel to the detector is described in Section 3.2.3.

3.1.5.2 Purpose and description of the VUV scanning set-up

The primary evaluation of the QE of a large PC using Cherenkov measurements at the test beam becomes impracticable with 42 pad panels as foreseen for the completion of the HMPID. So far, a simpler and faster method has been elaborated for evaluating the PC performance just after processing. As schematized in Fig. 3.29 and Fig. 3.31, it is based on the measurement of the direct photocurrent emitted under a local illumination of the CsI PC by a monochromatic and collimated VUV light beam. A cylindrical vessel the same size as the evaporator is appended to it to create a volume large enough to scan the PC.

The set-up is composed of the following elements.

- A motorized linear motion, parallel to the cylinder axis (x -coordinate), which performs first the transfer of the pad panel from the evaporation to the measurement vessel and then moves the panel by steps for the scan.
- Perpendicular to the evaporator axis (y -coordinate), a mechanical structure supports another stage providing the motion of the measurement arm in the y -direction. An expandable and tight connection is made between the stage and the measurement vessel by a tombac of 110 mm diameter, allowing a scan over 50 cm in the y direction.
- The VUV source, a D₂ lamp, its housing and the necessary CaF₂ optics delivering the VUV collimated beam are located on the y -moving stage. The UV beam is propagated through a tube up to a mirror fixed at the other extremity of the measuring arm, reflecting the beam up or down thanks to a remotely controlled action. At the same end of the arm, a wired electrode is fixed which collects the photoelectrons emitted when the mirror is positioned in such a way that the beam is directed towards the PC. Rotating the mirror by 90 degrees directs the beam to a reference phototube allowing the intensity of the incident photon flux to be calibrated. The phototube is a Hamamatsu R1460, 1 inch diameter, MgF₂ window. The CsTe photocathode response was calibrated against a NIST

photodiode in the 150–220 nm range. This array keeps the length of the UV beam and electrical connections fixed while the stage is moved for scanning purposes.

- In addition to the control of the parameters during the CsI film processing phase (pressure, temperature, rate, etc.), the aim of the VUV system is to perform automatic QE measurements by scanning large-area PCs. X/Y motions and positions of the measuring arm and the pad panel and relevant physical parameters (voltages, currents, etc.) have to be monitored. A slow-control monitoring task has been written for that purpose.

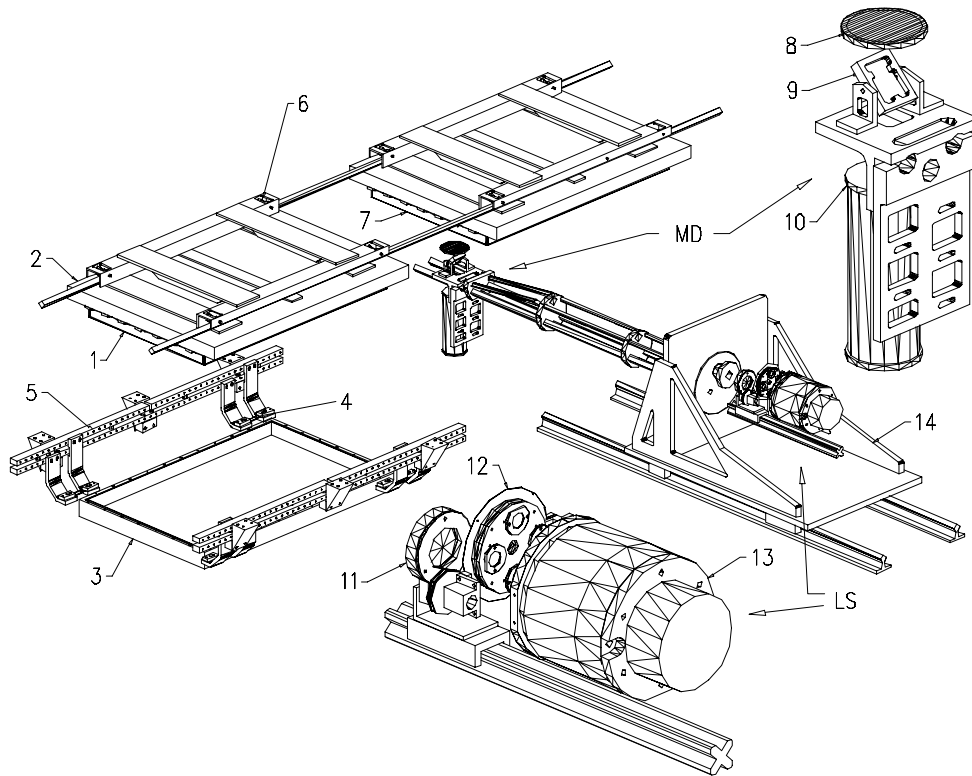


Figure 3.31: Axonometric view of the system used for the linear transport of the pad plane, and the UV-optical arm inside the vacuum vessel. Detailed: LS: The UV-source with interference filter wheel and MD: the photocurrent measuring device.

3.2 HMPID system description

3.2.1 Introduction

In Section 3.1, all the essential elements constituting a CsI RICH module and some auxiliary devices have been described in terms of functionality and performance. For the most critical ones, detailed discussions about their production and assembly procedures were presented and proofs of principle established, showing that they can be used in a large system. The successful test of a full ‘essential size’ prototype described in Section 2.3 has confirmed these remarks. In this chapter, the system aspect of the HMPID detector will be discussed by describing all the sub-systems composing the HMPID detector, at least at the level of a schematic. Next, the production and assembly schemes of each sub-system will be given.

The HMPID detector system is composed of seven modules having in common a number of auxiliary systems. The main sub-systems described are listed in Table 3.10.

Table 3.10: Main sub-systems constituting the HMPID detector

MODULES	
7	CsI RICH chamber with radiator
7	System instrumenting 23 040 pad channels for analog multiplexed readout, digitization and zero suppression
AUXILIARY	
1	Evaporation plant for production of CsI photocathodes
1	Storage plant for CsI photocathodes
1	Test and monitoring system
1	High-Voltage supply system
1	Control signal and trigger electronics system
1	Low-Voltage supply system
1	Data transfer system
1	Data acquisition system
1	Main gas mixture supply with purification and contaminant control systems
1	Main C ₆ F ₁₄ supply and system for circulating the liquid through the 7 modules according to gravity flow scheme
1	Slow-control and monitoring system

The production of the HMPID can be split into four main parts — the radiator array, the chamber modules, the pad panels, the electronics — and two auxiliary systems, the gas and liquid supplies. The production of these items could be carried out independently over a period of time comparable for each of them, ranging from 12 to 15 months if effected in a continuous way. In fact, for more effective sharing of the institute manpower resources, production and testing activities will frequently be interleaved. We present these time schedules in a general diagram shown in Chapter 5.

3.2.2 The CsI RICH modules

The prototype that has been built can be considered as a final version of a HMPID module, even though its size will be increased by one-third. In the framework of a test period spreading over two years under test beam irradiations close to the ones expected at ALICE, all the major components fulfilled both the requirements of stable operation and satisfactory performance. In addition, it has been demonstrated that the numerous operations associated with the production of the module, e.g. the assembly of quartz radiator trays or the processing and mounting of the CsI photocathodes, can be performed reliably using simple procedures and tools. Lastly, over the available lifetime of the detector the performance was found to be stable. Possible improvements that would affect the present design could be oriented towards reducing the material budget of some elements, e.g. the radiator trays.

Therefore, we summarize the main components and assembly procedures of a HMPID CsI RICH module.

3.2.2.1 Components

A module consists of three main frames requiring conventional machining of Peral plates with tolerances of $\pm 50 \mu\text{m}$ at several locations. A flatness tolerance of $\pm 100 \mu\text{m}$ over the whole frame is required. The elements constituting the detector, the MWPC and the radiator array are associated to each frame and are listed in Table 3.11. Their design is made such that the assembly, mounting and dismounting opera-

tions cause no difficulties and ensure the necessary tolerances for reproducible operation, as discussed in Sections 3.1.1 and 3.1.2.

Table 3.11: Main elements constituting a module

No.	Frame	Main elements associated with the frame	Function	Ref.
1	Frame-1		Hold the 6 CsI pad panels Hold the anode plane Hold the digital electronics	3.1.1.2
6		Pad panel	CsI photocathode hold the FEE	3.1.1.1
6		Anode wire PCB	To solder 20 μ m anode wires	3.1.1.2
1		Anode support line	To stabilize the anode wires	3.1.1.2
1	Frame-2		Hold the wired cathode MWPC Hold the collection electrode	3.1.1.3
6		Bars for crimping cath. wires		3.1.1.3
1		Collection electrode frame		3.1.1.3
1		Distance frame	To adjust the gap of the MWPC	3.1.1.3
1	Frame-3		Hold the Cherenkov radiators	3.1.1.4
3		Radiator tray	Contains the C_6F_{14} liquid	3.1.2.3
1		Piping array	Connect tray to the C_6F_{14} supply	3.1.2.3

3.2.2.2 Assembly and production test

We summarize the main steps for assembling a module according to the procedures detailed in Section 3.1.1 and 3.1.2. These operations are split into five parts which can be carried out independently (in parallel) and are expected to be performed in comparable periods of time.

Module: Radiator array

- production (external firm) of the quartz plates,
- production (external firm) of the Neoceram parts,
- production (external firm) of the mechanical parts: back plane and spare parts,
- quality control of the back plane and leak test,
- control and transparency test of the quartz plate,
- assembly of the Neoceram elements,
- assembly of the radiator tray with quartz,
- mounting of the trays in the back plane with piping.

Production test of a radiator tray: TEST-RAD-1

Each radiator tray is installed in the back plane which is closed by a panel allowing a tight box to be formed which is flushed with argon. The radiator tray is filled with C_6F_{14} in the vertical position in order to apply the same hydrostatic pressure expected at ALICE. Then, the circulated gas is passed through an analyser allowing traces of electronegative gas with high sensitivity to be measured. A tray is accepted when the trace level is maintained below 0.5 ppm during a fixed period.

The necessary equipment, C_6F_{14} circulation, analysers, etc. are those used during the beam test of proto-2.

Module: Frames and MWPC

- production (external firms) of all mechanical parts and PCBs,
- quality control, final polishing, cleaning of all frames and mechanical components,
- installation on Frame-1 of the PCBs holding the anode wires and frame thickness adjustment by machining,
- installation of support lines and soldering of the anode wires (20 μm),
- test of anode wire tension,
- weaving of the cathode and of the collection electrode using crimped pins,
- distance frame machining for thickness adjustment,
- test of the cathode wire tension.

Module: Pad panels

- production (external firm) of the pad PCBs,
- production (external firm) of all mechanical parts, frames, protective boxes,
- quality control, final polishing, cleaning of all frames,
- soldering of the signal Kapton circuits on the back of the pad PCBs,
- preparation of the sandwich panel elements (foam, 2d PCB, etc.),
- final assembly of the pad panel,
- assembly of the protection box for CsI PC,
- electrical and leak tests.

Production test of a module: TEST-MOD-1

Once all the parts are available, a module is preassembled with the pad panels not yet coated with CsI. The aim of this operation is to certify that the wire electrodes and the pad cathodes satisfy the conditions for stable operation at the maximum voltage. For this purpose, the measurement of the chamber current is a convenient tool as any defective part of the chamber driving a too high current can easily be located by disconnecting a group of eight, or even a single anode wire from the HV supply. In addition, it is foreseen to equip one-third of the anode wire plane with FEE (96 channels) in order to have a better characterization of the behaviour of the chamber in terms of rates and pulse shapes.

The sequence of tests is foreseen as follows:

- After leak test, the module is flushed with CH_4 . The radiator trays are filled with C_6F_{14} .
- Traces of contaminants, O_2 , H_2O and electronegative gas are measured and monitored for a fixed period.
- Having shortened all pads to ground, the module is put under high voltage. The chamber current, the rates and pulse-height spectra of anode wires signals are recorded as background and under local irradiation by a Ru^{106} or Sr^{90} source.
- Eventual repairs or replacements are performed if a part of the chamber does not satisfy the specifications listed below.

The specifications to be achieved for the acceptance of a module are:

- The fractions, in volume, of contaminating species must be less than 5 ppm for oxygen and moisture, and < 1 ppm for electronegative gas at a CH_4 flux of 30 l/h;
- a total dark current at maximum voltage (2250 V in CH_4) less than 1 nA for a third of a module;
- a uniform wire rate map corresponding to the expected local cosmic irradiation;
- a uniform map of the most probable pulse height corresponding to the expected local cosmic irradiation.

Once these specifications have been maintained for a fixed period of time, the module is accepted and the pad panels are ready for CsI evaporation. The next sequence of tests are discussed in Section 3.2.5.

3.2.3 The evaporation system for CsI photocathodes

It is planned to use the evaporation system described in Section 3.1.5 to perform the production of the 42 CsI PCs equipping the seven HMPID modules. That system will be composed of two parts: the one used for the evaporation of the CsI film and the other one, the VUV scanner, in which the CsI PC is translated for evaluation of the QE performance by an automated two-dimensional scanner².

The scanning part of the system will be available at the end of 1998. Before launching the PC production, it is foreseen to complete an experimental programme defining and testing the final choices still pending in order that the bulk production is undertaken with a guarantee of achieving the highest yield of optimally performing PCs.

The preliminary programme will be devoted to fixing the following points:

- scan existing PCs for comparison between the Cherenkov and the VUV beam QE evaluations,
- quantify the QE improvement by heat treatment in case of large-area PCs and optimize the post-treatment parameters (see Sections 2.1.1.3 and 3.1.5.1)
- choose the final pad PCB technology (see Section 3.1.1.1),
- optimize the outgassing operation,
- validate the possibility to re-evaporate further CsI films on the same substrate after removal of a non-satisfactory one.

As discussed before, these studies necessitate a statistical analysis from several samples to be conclusive. For time- and cost-based arguments, it is unrealistic to perform these tests using the Cherenkov photon counting technique at a test beam. On the contrary, the VUV scanner is well adapted since the evaporations will be made on the PCB samples only, without assembling the entire pad panel structure needed for FEE implementation. Also, smaller sample sizes will be used, allowing for examination of several samples at a time. At the end of the preliminary programme, expected to last about a year, the evaporation system will be fully completed and the slow-control system ready and checked to operate safely in automated mode for a long production period.

3.2.3.1 Procedures for the final production of the CsI PCs

The final production of the 42 CsI PCs can be launched as soon as the production and test programs, TEST-MOD-1 and TEST-MOD-2 (see Section 3.2.5), of the pad panels and the modules have been completed. The completion of the PC production has to be scheduled as close as possible to the start of the experiment in order to minimize the storage period.

For the time being, the sequence of operations foreseen for the production of a CsI PC repeats the one which was used during the R&D period described in Section 3.1.5.1. Variations in some parameters are expected to result from the preliminary programme but are not expected to affect seriously the main sequence described below.

Evaporation sequence

- premelting of the CsI boats,
- preliminary heating of the pad panel under neutral gas flow to eliminate moisture,
- installation of the pad panel and the boats in the evaporator,
- pumping and outgassing the evaporation system for 2–3 days at 60 °C until a residual pressure of 2×10^{-6} Torr is reached,
- CsI evaporation on substrate held at 60 °C,
- heat conditioning at 60 °C under vacuum for 8–12 hours at a pressure of 2×10^{-6} Torr,
- stop heating for cooling down.

²The system has been built and operated in close collaboration with the TA1/EP-CERN group. It might be considered as a facility possibly used by other groups, e.g. COMPASS/NA58, also aiming at the production of a large number of CsI PCs.

QE evaluation sequence

- transfer of the CsI PC into the measuring part of the system,
- two-dimensional scan based on 24 measurements, (6×4 X/Y locations) according to the parameters defined by the preliminary programme: wavelengths, photon flux, duration, etc.

Storage sequence

- venting the protection box and the evaporator with argon,
- lifting the lid to form the protection box,
- opening of the evaporator and transfer of the pad panel to the storage under argon flow system (see next section).

The transfer of the CsI pad panel onto the detector is detailed in Section 3.2.2.3.

3.2.3.2 Components

A large part of the evaporation system has already been built (see colour Figs. 3.iii and 3.iv) and will be completed by the end of 1999.

In addition, one has to build a system for storing the PCs, keeping them in their individual protective boxes under constant argon flow. That facility (the CsI-PC storage system) will be of transient or complementary utilization since the PCs will usually be mounted on a module and also kept under argon flow for storage.

The storage facility is composed of a primary argon source with input and output manifold systems to supply each box and to control the contaminant fraction.

3.2.3.3 Assembly and test

As mentioned in Section 2.3.2.3, the mounting of the CsI PC panels was performed on proto-2 by using a large glove box mounted at the back of the module and allowing the transfer of a PC from its protection box to the module under controlled argon environment. To allow for some parallel installation, two glove boxes will be built of the size of a final module. A perspective view is shown in Fig. 3.32, illustrating the sequence of operation for mounting PCs on a module:

- The HMPID module, equipped with blank panels in place of the pad ones, is circulated with argon.
- The glove box is fixed to the module without its closing lid.
- Two CsI PC panels protected by their boxes are hung vertically close to the blanks with the back sides facing the operator and kept under argon flow.
- The glove box is closed with the lid holding the gloves and flushed with argon.
- When the oxygen and moisture fractions are below a fixed value (100 ppm), a blank panel is removed from the module and stored aside, and then a CsI PC panel is removed from its protective box and fixed in place of the blank panel. There is room enough in the glove box to fix two CsI PCs in a single sequence, meaning that three sequences are needed per module, i.e. about 6–8 days.

An equivalent procedure is used to remove CsI PCs from a module in case of opening of a chamber.

3.2.3.4 Production schedule

The production of PCs is segmented in batches of six PCs with an interruption of 15 days for maintenance of the evaporation system. As soon as a batch of six PCs is available, they are installed on a module and ready for test for a period of 1.5 months (see TEST-MOD-3 in Section 3.2.5). The total duration amounts to 16 months, assuming a continuous activity. It is advisable to carry on this programme without interruption in order to minimize the storage period (aging) before the start of the experiment (Section 2.3.2.3).

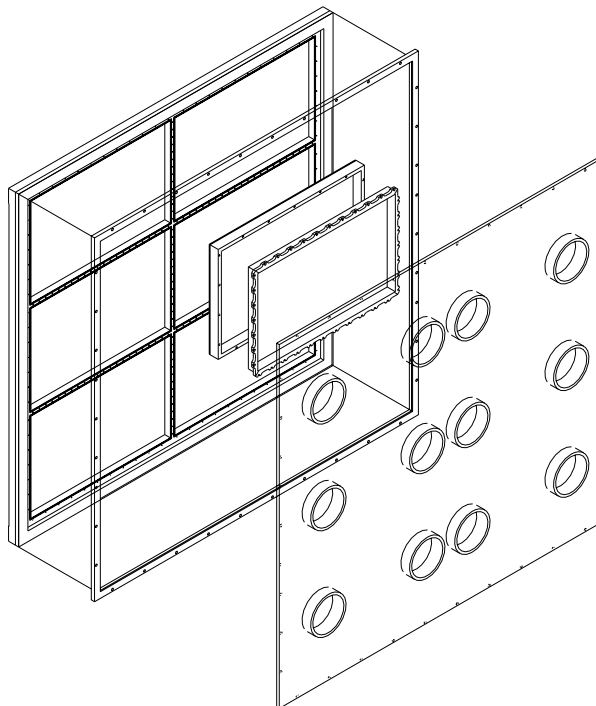


Figure 3.32: Axonometric view of the glove box array used to transfer under controlled argon atmosphere a CsI photocathode from its protective box to the detector.

3.2.4 The readout electronic system

Several modes of operation are expected to be exploited for the physics at ALICE since the LHC collider will be run with protons and with different species of ion beams, i.e. calcium and lead.

The main experimental parameters are shown [13] for three running modes in Table 3.12. Two extreme situations have to be treated by the readout system: a data flow corresponding to a high rate of events of low charged multiplicity in pp mode, changing to a low rate of very high charged multiplicity in Pb–Pb mode.

Table 3.12: Main experimental parameters at ALICE

Collider mode	Unit	pp	Pb–Pb	Ca–Ca
Bunch interval	ns	25	125	125
L0-trigger latency	μs	1.2	1.2	1.2
Max. interaction rate, mini. bias	kHz	100	10	10–100
Max. interaction rate, central	kHz	100	1	1–10
Charged multiplicity in 1 rapidity unit central collision		8	8000	1200
Hit occupancy, mini. bias	%	$3\text{--}4 \cdot 10^{-3}$	3–4	0.45–0.6
Hit occupancy, central	%	$1.5\text{--}2 \cdot 10^{-2}$	15–20	2.2–3
DAQ rate central/mini. bias	Hz	1000	40	150
Luminosity half-life time	h	10	10	> 50

The first-level trigger latency (L0) originates from considerations described by the Trigger Group in Ref. [14] and has been fixed to $1.2 \mu\text{s}$. As stated in Chapter 1, the evaluation of the hit occupancy is based on the highest expectation of the charged-particle multiplicity, actually model-dependent. The DAQ rate

is in fact driven by the large tracking systems, ITS and TPC [13], producing very large event sizes. In case of operation of the TPC, one has to consider a dead time imposed by the $200 \mu\text{s}$ drift time necessary to collect the primary ionization deposited by an event.

3.2.4.1 Final version: system schematics

Referring to Section 3.1.4.5, the final electronic system is based on a modular array composed of three GASSIPLEX chips (48 channels) and an MCM composed of one ADC and one zero-suppressor chip, referred to as DILOGIC. It has been shown that the modular array and the associated ASICs are operational at the prototype level. Final ASIC versions, described below, are being completed. The final readout system is presented at the schematic phase and the final design is still in progress.

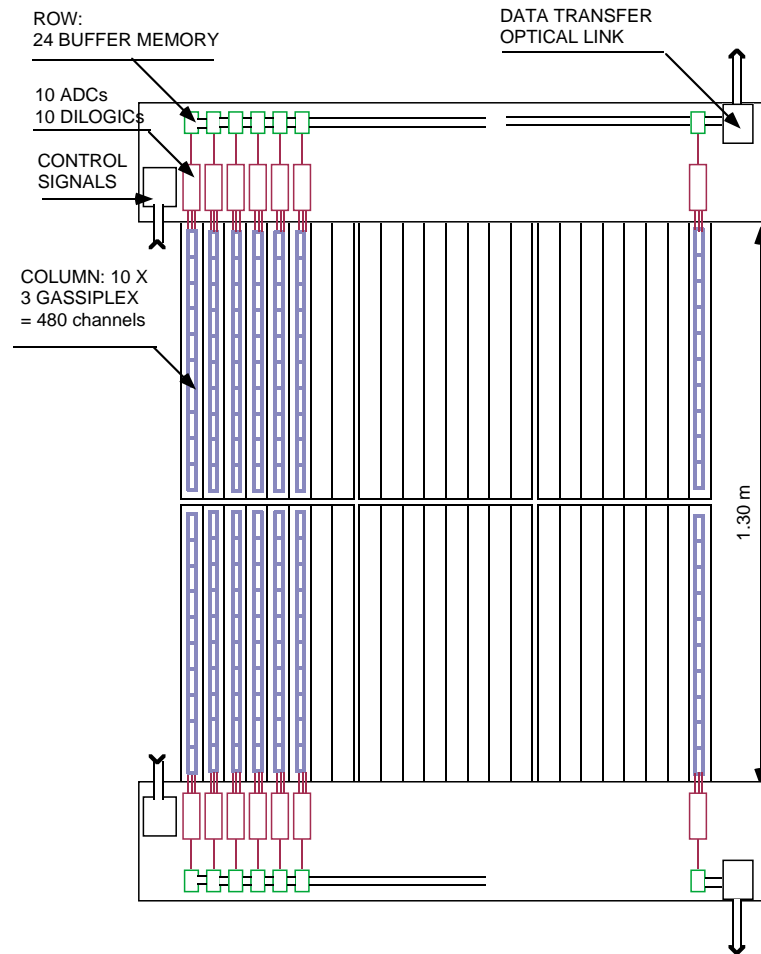


Figure 3.33: Schematics of the implementation of the FE and readout electronics on a HMPID module.

The implementation of the modular arrays to read out the HMPID modules is organized according to a parallel/serial architecture as shown in Fig. 3.33. The module is first subdivided into two halves, each of them in turn partitioned into 24 columns. A column is composed of 10 modular arrays, i.e. 480 pad channels. Each column is connected to a buffer memory with a capacity to store data from 480 channels needed for pedestal measurements. Finally, the 24 memories are bussed in a row linked to the DDL sender card. The readout sequence of one-half of a module is done as follows:

- parallel multiplexing of all the modular arrays ending with data stored in the DILOGIC FIFOs,
- serial transfer of the data from the 10 DILOGICs into the buffer memory performed in parallel on the 24 columns,

- serial transfer from the row of 24 buffer memories into the DDL sender card,
- transfer from the DDL to the DAQ buffer cards.

Given the specifications of the two final ASICs, the time necessary to read out an event is evaluated in Table 3.13 for two modes of physics and pedestal operation, according to the detector occupancy and conservative readout clock frequencies.

In case of Pb–Pb mode, the total readout time is significantly smaller than the corresponding L0-trigger periods, implying small dead-time loss even in case of event rejection. That is not the case in pp mode where the two durations are comparable in time. However, since the second-level trigger (L1) is available after 2.4 μs [14] and has a much longer period, one could apply a fast clear on the data after 2.4 μs each time there is no L1 signal associated with the L0 one. The pedestal/calibration mode is discussed in the next section.

Table 3.13: Readout time of the HMPID system for various operating modes at ALICE

Operation mode	Unit	pp	Pb–Pb central	Pb–Pb mini. bias	Pedestal
Occupancy	%	0.2	15	3	100
Word/column (480 chan. max)	No.	1	72	15	480/2 = 240
Word/row (24 buf. mem.)	No.	24	1728	350	5760
		freq.	dur. [μs]	dur. [μs]	dur. [μs]
MPX, 48 chan.	MHz	7.5	6.4	6.4	6.4
Transfer colum	MHz	10	0.1	7.2	1.5
Transfer row	MHz	20	1.2	86	18
Transfer DDL	MHz	25	1	69	14
Total	μs		8.7	169	40
L0-trig. period	μs		10	1000	100
L1-trig. period	μs		1000	20 000	4000

3.2.4.2 Components

1. Final version: GASSIPLEX-0.7-2

This chip has the same architecture as the GASSIPLEX-0.7-1, described and characterized in Section 3.1.4.1. It has been modified as follows:

- i) the peaking time can be adjusted between 1.1 and 1.3 μs , to satisfy the ALICE L0-trigger latency,
- ii) the test/calibration pulse can be sent channel by channel in a sequential mode,
- iii) the dynamic range has been increased by decreasing the sensitivity, to fit the requirements of three ALICE detectors aiming to use the chip in different operational modes: HMPID CsI RICH for single electron detection, Veto-PHOS and DI-MUONS pad chambers for MIP localization. The sensitivity can be adjusted according to the needs, by changing the gain on the internal output buffer or on the external buffer (always necessary by groups of 3–4 chips). Its new characteristics are shown in Table 3.14.

The prototype of the GASSIPLEX-0.7-2 was developed at CERN [15] and submitted in August 1998 to IMEC for prototype fabrication to be delivered in autumn 1998.

2. Final version: DILOGIC-2

This chip has the same architecture as the first version, DILOGIC-1, described in Section 3.1.4.5.

Table 3.14: GASSIPLEX- 0.7-2 performance

Technology	MIETEC- 0.7 μm
Peaking time	1.2 μs
Peaking time adjust.	1.1 to 1.3 μs
Noise at 0 pF	600 <i>er.m.s.</i>
Noise slope	11 <i>er.m.s./pF</i>
Absolute dynamic range	2 V
Dynamic range at 4 mV/fC	500 fC
Minimum sensitivity	4 mV/fC
Baseline recovery	< $\pm 0.5\%$ after 6 μs
Analog readout speed	10 MHz max.
Silicon area	$3.63 \times 4 = 14.5 \text{ mm}^2$
Power consumption	8 mW/channel at 10 MHz

Its capacity has been increased in order to handle more input steps and larger digitization sizes. Its main features are:

- Zero suppression and pedestal subtraction.
- Selectable number of units of 16 channels to be read: 1, 3, 4, 8 4-bit readout protocol.
- 19 bit \times 512 words DATA memory.
- 16 bit \times 256 words bit-map memory.
- 16 bit \times 256 words threshold and subtraction memory.
- 19 bit bi-directional bus.
- 15 MHz max. writing speed.
- 20 MHz max. readout speed.
- Full testability.
- Silicon area: 47 mm^2 I/O connections: 60 pads.
- Power consumption: 100 mW.

Given the maximum capacity of the memories, the chip can be configured by matching the number of inputs and the digitization size of the ADC, e.g. as in Table 3.15.

Table 3.15: DILOGIC-2 configurations

Config.	No. of inputs	ADC	No. of ADC bits
1	64	CRIAD [x]	4 ranges
2	64	linear	12
3	256	linear	10
HMPID	48	linear	12

The DILOGIC-2 has 55 000 equivalent gates, memories not included. The prototype fabrication, using 0.7 μm technology, will be done at IMEC from a block diagram and specifications written at CERN [16]. Delivery of prototypes is expected in February 1999.

3. Cards and motherboards

Figure 3.34a shows a perspective view of the hardware implementation of the readout electronics on half of a module and Fig. 3.34b shows the way it is attached to the module. All the components are described below.

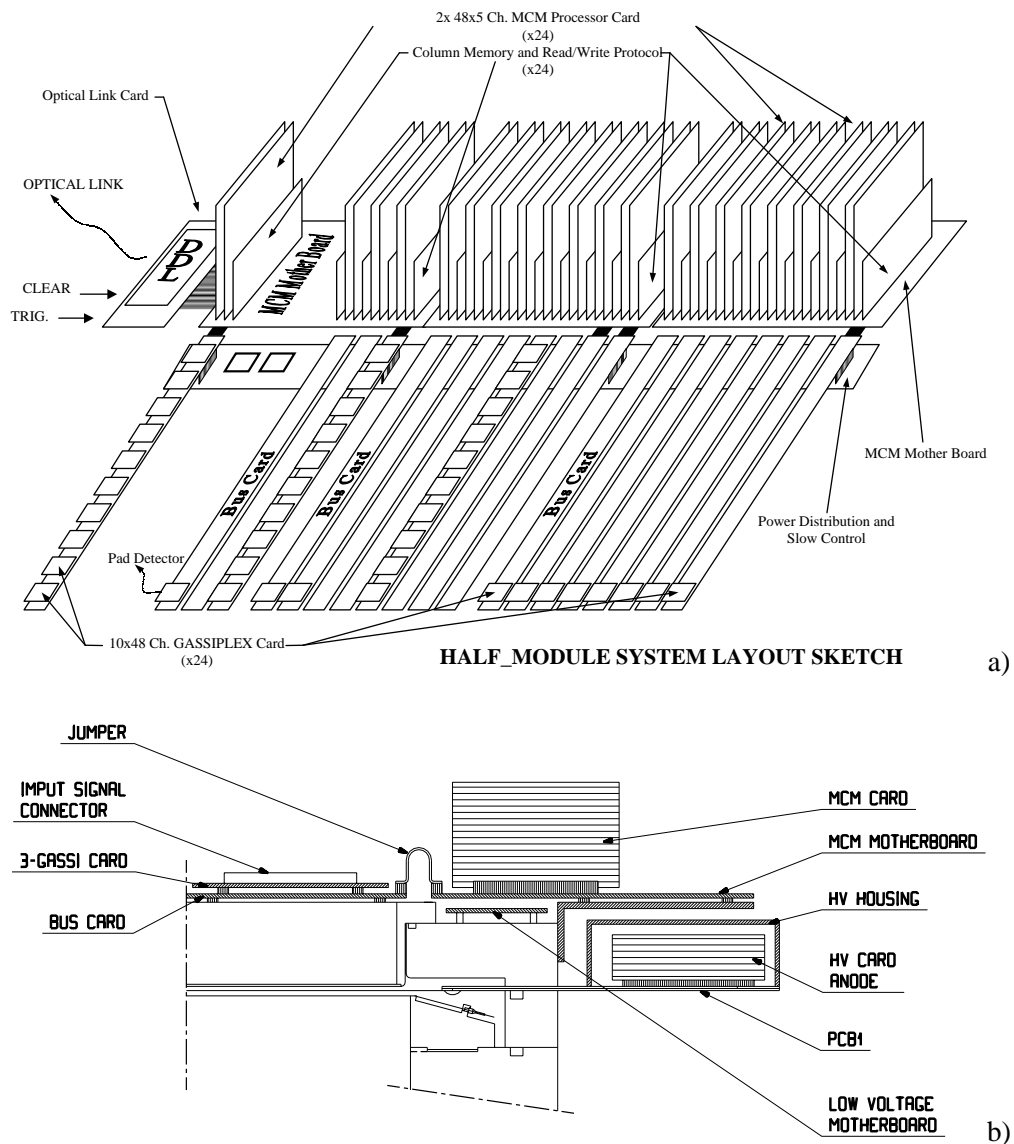


Figure 3.34: (a) Axonometric view of the electronics boards on the HMPID module. (b) mechanical fixation of the electronics boards on the module.

i) 3-GASSIPLEX card:

Ten of these cards are mounted on a motherboard directly attached to the pad-panel back plane, to perform the readout of 10×48 channels in a row. The components of the card 3-GASSIPLEX are, as seen in Fig. 3.35:

- 3-GASSIPLEX chips and the necessary SMD components to make the biasing and the decoupling of the DC pins,
- a multiple DAC to equalize the DC level of the mean value of the pedestals of each chip, avoiding the GASSIPLEX chips sorting as described in Section 3.1.4.3,
- a set of logic buffers to separate each card from the others to avoid the spoliation of a common logic line by a damaged chip,
- a small HV protection card put near the input connector to protect the channels from HV spark.

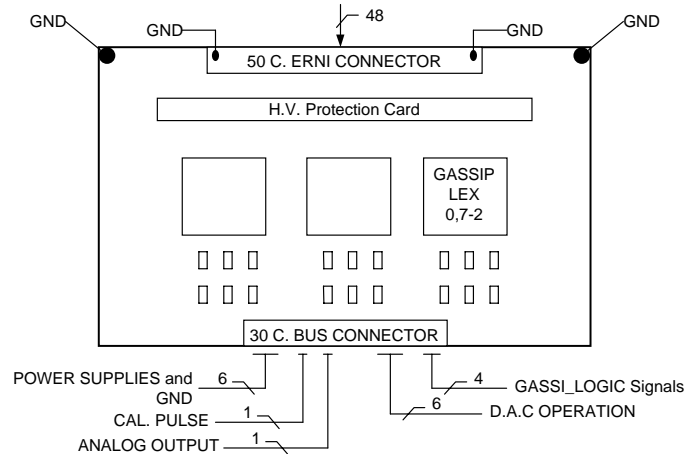


Figure 3.35: Schematic of a 3-GASSIPLEX card.

Finally, two connectors make the connections on one side to the detector pads using the Kapton circuits and on the other side to the column bus card. The connections to the column bus card are done through a standard 2×15 contact connector. The ± 2.75 V supplies and the ground will use six contacts, the GASSIPLEX logic signals and the DAC operation will need respectively four and six contacts, while the calibration pulse as well as the 48-channel multiplexed output will use one each. The other contacts are reserved.

ii) Column bus card:

As seen in Fig. 3.34a, this multilayer board supports ten 3-GASSIPLEX cards and distributes the common functions: LV supplies, grounding, DAC operation, GASSIPLEX logic signals and calibration. The analog multiplexed outputs are separated to be processed individually on the MCM processor cards. This bus card has two separated connections: one to the MCM motherboard and the other to the power and slow control board.

iii) MCM processor card:

The MCM processor cards, shown schematically in Fig. 3.36, are mounted on the MCM motherboard attached to the frame of the detector. One card processes 240 channels using five groups, each composed of an analog buffer which adjusts the front-end sensitivity at the operating value, a fast 10-bit ADC (or 12-bit), a DILOGIC-2 and some active components. Two connectors make the connections on one side to five 3-GASSIPLEX cards and on the other to the Column Memory and Read/Write protocol card (CMRW). Two MCM processor cards are connected to the CMRW card which stores data from one column; 24 of these cards collect the data corresponding to a half-module.

There are three main operations: reading–writing pedestals, data acquisition and testing.

The pedestals have first to be measured when the detector is not active.

Collected for each column in the CMRW card, they are sent to the control room to be processed and sent back to the threshold and subtraction memory of each DILOGIC-2. Each channel will need one DILOGIC clock cycle to read or write a pedestal because 16 bits are needed per channel.

The data acquisition is performed as follows.

When a trigger occurs, all the necessary clocks are generated by the clock generator fed by a common half-module oscillator. The sequence is: GASSIPLEX multiplexing clock, ADC clock, address-generator clock, DILOGIC-2 write-clock. The DILOGIC-2 processes the data given by the ADC and stores the good data in its FIFO memory.

The write sequence takes $6.4 \mu\text{s}$. After that time, the DILOGIC memory of each column is emptied in the CMRW card, during this process the empty end-of-event word, which closes the reading of each event in a DILOGIC-2, is discarded. The CMRW card will be filled only with good data.

Then the data are ready to be sent to the control room by the DDL.

The testing can be divided in three parts: the front-end electronics, the digitization and the DILOGIC-2.

The front-end electronics can be tested by the calibration signal and the DAC by its effect on the output DC level of the 3-GASSIPLEX.

The injection of a calibrated signal also allows the digitization to be tested. The DILOGIC-2 can be tested in a separate mode. After having been put in test mode, its bi-directional output bus allows a sequence of data to be injected to test the threshold and subtraction circuit, the write protocol, the read protocol and the different memories.

iv) Column memory and read–write protocol card:

This card, as seen in Fig. 3.34a, collects the data coming from each column and makes the connections with the DDL through a 32-bit bus. Its memory capacity is at least 512 words of 32 bits, which is the necessary number of words to read/write the pedestals and the necessary number of bits to process all the operations.

Around the memories, a few components will take care of the read/write protocol of the three main operations.

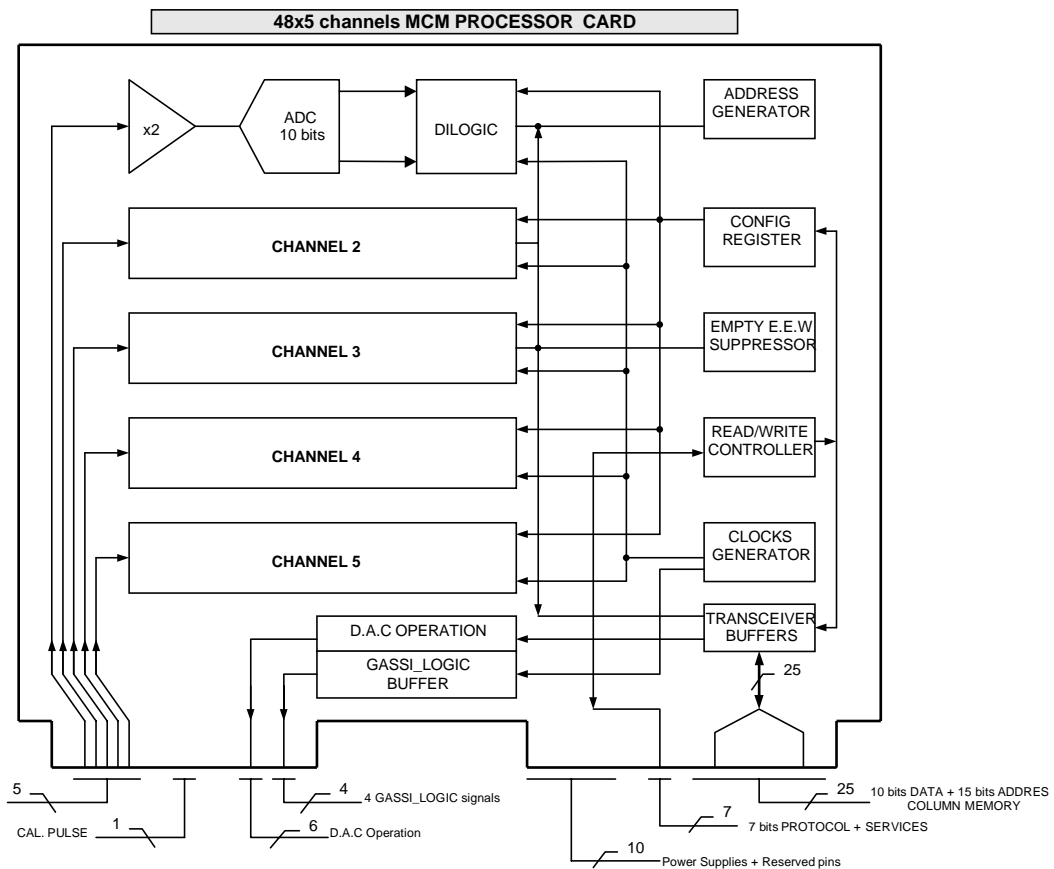


Figure 3.36: Schematics of the functional blocks of a MCM-processor card performing digitization and zero suppression of 5×48 channels.

3.2.4.3 Assembly and tests

The only components that are not available on the market are the two ASICs, GASSIPLEX-0.7-2 and DILOGIC-2. It is foreseen for them to be produced in the same foundry, MIETEC.

GASSIPLEX-0.7-2

After some prototyping production, it has been decided to mount the GASSIPLEX die in a plastic package without previous testing on wafer. This kind of package, of a very low price (1.2 CHF/chip), is actually well controlled and has a performance comparable to a more expensive ceramic one.

After delivery, two operations have to be done: the chip acceptance and the burn-in tests. The first one could be done in an automatic way by the same firm that makes the packaging, provided the firm gets material and procedures from us. The second one is foreseen to be done by the collaboration, using two specialized boards on which 256 chips are mounted on sockets. Burn-in and chip characterization are done on the same batch.

It is possible also to give this work to a specialized firm which will make the tests on a specification basis.

DILOGIC-2

This will be encapsulated in a plastic package and tested by a specialized firm.

FEE card assembly

The assembly of all cards and boards is sub-contracted as industrial support to firms that are specialized in surface-mounting components.

The tests of all cards is done in the collaboration, using a dedicated test set-up. The acceptance test is finalized on the module.

Table 3.16 summarizes the main elements constituting the FEE readout system. The data transfer and DAQ systems are described separately in Section 3.2.8.

Table 3.16: Components of the readout electronics

ASIC chips	No.
GASSIPLEX-0.7-2	10 080
DILOGIC-2	3360
CARDS and BOARDS	
3-GASSIPLEX card	3360
Column bus card	336
Power/slow control board	42
MCM processor card	672
MCM motherboard	42
CMRW protocol card	336
TEST BOARDS	
Burn-in	2
Digital test	2

3.2.5 The test and monitoring systems

Several tests have been performed during the production period, meant essentially to provide green lights for pursuing the construction of the modules:

- the radiator trays are declared leak-tight but the UV transparency must be evaluated,

- the photodetector chambers are leak-tight and stable at the operating voltage but the single-electron detection efficiency and gain homogeneity must be measured,
- the QE of the CsI PCs have been previously evaluated in vacuum but the response must be checked for single-photon counting in the gaseous MWPC,
- the FEE components are individually checked but the system behaviour must be evaluated when mounted on a module.

Therefore, to answer these questions, an intermediate test is still needed to ensure that the response to single electrons is adequate over the whole module before starting the CsI evaporation programme. In fact, this request is similar to the one related to the need of a monitoring facility aimed at following the evolution with time of the QEs in a module when the CsI PCs are installed.

The method that was routinely used for single-electron studies with the prototypes was to illuminate the pad cathode, coated with CsI or not, with a pencil beam of UV light generated by an ORIEL deuterium lamp, a quartz optical fibre and a collimating device. The trigger signal needed to read out the pad FEE is given by the anode wire signal provided a sensitive enough amplifier is selected.

Two systems are under development to provide means to test the response of a module to single electrons and to monitor in a simple way the QE in a module.

Test of the response of a module to single electrons: TEST-MOD-2

Two methods are being investigated to generate a low enough rate of single electrons into a large module. The first is to use a Neodym YAG laser emitting at 266 nm, creating along the beam path in the gas primary ionization essentially composed of single electrons given the low energy transfers. Adjusting the energy of the light pulse at a low enough value allows a density of primaries to be created such that they are well separated along the path of the beam. The laser provides the trigger needed to read out the pad FEE. The geometry of the light beam propagating into the chamber has to be optimized in such a way that an optimum scan of the whole chamber can be performed per laser shot.

The second method is to install a set of quartz tubes traversing the proximity gap. A small UV lamp is moved inside these tubes, illuminating the pad plane and generating single electrons by photoelectric effect at the pad surface. This equipment can be easily removed since the pad panels are as yet uncoated with CsI.

The goals of the test are:

- having implemented all the FEE elements previously tested on a module, to evaluate in a real operational mode the FEE system response, i.e. noise figure, preamp gain calibration, pedestal stability, readout protocols, etc.;
- by using one of the methods to generate single electrons, to record at various chamber gains PH spectra corresponding to delimited pad zones in order to produce a map of the chamber gain (i.e. the mean value, A_0 , of each PH spectrum) per pad panel (see Sections 2.1.2.4 and 2.3.2.4).

In case of too large a gain discrepancy between panels, the distance pad-plane-to-anode wires could still be readjusted by proper machining of the pad-panel frame. In case of satisfactory results, the module and the FEE are ready for the last operation, that is the CsI evaporation on the pad panels.

Monitoring of the QE

The system under development consists of a feedthrough allowing to transmit a quasi-monochromatic UV pencil beam to illuminate a CsI-coated pad and to count the single-photoelectron rates at several adjacent anode wires. A part of the UV beam is deviated on a calibrated solar-blind photomultiplier (Hamamatsu R1460) ensuring the normalization of the incident photon flux and therefore of the single-electron rate. PH spectra will be recorded as well in order to make the measurements at the same chamber gain. Laboratory tests will be performed to check the relation of the QE to the counting rate and the reproducibility and stability of the method.

If the method is found relevant, several devices could be installed along the frames of the module.

Final test: TEST-MOD-3

Following the production schedule of the CsI PCs (see Table 5.1), we are planning to perform a final test of every module fully equipped, possibly at the ALICE test beam line, T10 at the PS East Hall. As described in Chapter 2, such a test provides in one go all the information listed at the beginning in real operational conditions. In addition, it provides an essential characterization of the performance of the whole detector, QEs, gain, transparencies, photoelectron yield, that is of prime importance as input parameters for the pattern recognition and simulation programs as discussed in Chapter 4. Last, we have experienced while testing proto-2 at the SPS that a full scan of a module using single-particle events can be performed in 4–5 days, not including the filling and purification of the radiators. All elements necessary for the development phase are available in our laboratory, including the expensive Neodym YAG laser.

3.2.6 Control signal and trigger electronics

The control signals needed to operate the FEE will be generated on board by the MCM processor card at arrival of the TRIGGER signal. They are:

- 1) TRACK & HOLD
- 2) CLOCKS train (multiplexing)
- 3) CONVERTS train
- 4) CLEAR to the Gassiplex chips

When operating in pedestal mode, the signal sequence stays exactly the same but the trigger signal is supplied by a pulse generator driven by computer.

During the MPX sequence, a signal will be available to the trigger logic of the experiment to participate in the generation of the BUSY.

A RESET signal, driven by the trigger logic and/or by computer will reset the full system (FEE + MCM processor) forcing it to a defined state.

It will also be used to initialize the system (e.g. when switching on power supplies).

Finally the same signal can be used, after the occurrence of a trigger, to abort the readout sequence.

3.2.7 Low-voltage system/high-voltage system**3.2.7.1 Final schematics****Low-voltage supply**

The operating low voltages of GASSIPLEX are ± 2.75 V. Each column of 30 chips is supplied separately by voltage regulators (24 couples in total) mounted on the power and slow-control board, fed in turn by a main double power supply corresponding to a half-module board. The choice of a double supply is needed to ensure that both polarities are fed at the same time when the system is powered on.

The voltage regulators on each column have to be able to sustain 3 W each; a protection circuit has to be implemented to detect the over-current in case of latch-up and switch off the supplies of the column concerned by this latch-up. Two other power supplies are needed for the digital electronics (see Table 3.17). The LV supply units have to be located outside the L3 magnet.

Table 3.17: Elements of the low-voltage system

	Voltage (V)	Current (A)		No. of units	Power W/2.5 m ²
Analog part: GASSIPLEX					
Column: 10 3-GASSI cards	± 2.75	0.8	switch.		
Half-module	± 2.75	20	switch.	14	220
Digital part (half-module)					
MCMs, memories, etc.	+ 5	20	switch.	14	200
ADCs, buffers	± 5	4	linear	14	80

High-voltage supply

At the moment, it is foreseen to supply one-third of a module with one HV channel in order to keep some flexibility in adjusting the operating voltages. Also, it allows parts of the module to be operated in case of malfunctioning of a sector. A more elaborate system (see Section 3.1.1.2) is under study allowing for a finer segmentation (by groups of 16 wires) of the HV distribution, which is attractive but necessitates cost evaluation.

The CAEN 2 channels NIM HV-unit N471A is currently under consideration, providing all remote control facilities (ramping, limits, etc.) and allowing for direct monitoring of very small current down to the nanoampere level. The specifications of the LV units are listed in Table 3.18

Table 3.18: LV units

	Unit supplying		
	GASSIPLEX	DIGITAL	ADCs, buffers
Regulation	Switching	Switching	Linear
Voltage [V]	± 5	+5	± 5
Adjustment [%]	± 10	± 5	± 5
Current, max. [A]	25	25	5
Noise ripple [mV, pp]	< 20	< 30	< 5
Overtoltage protection	y	y	y
Overcurrent protection	y	y	y

3.2.8 The data-transfer system and data-acquisition systems

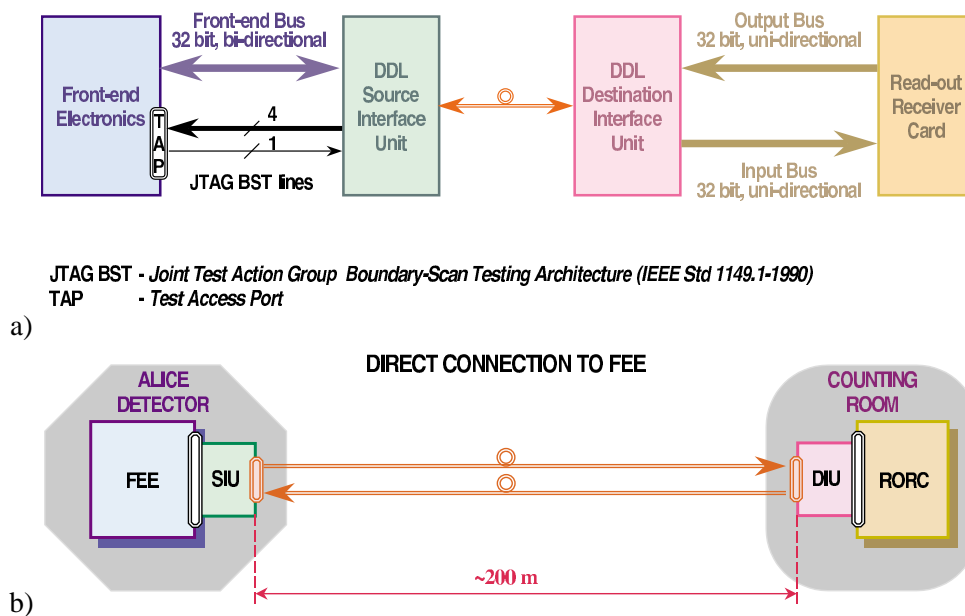
3.2.8.1 The data-transfer system

The trigger level 0 provides the track and hold signal to the GASSIPLEX readout system at a rate of 1200 Hz maximum (see Table 3.19) and with a fixed delay of $1.2 \mu\text{s}$. The trigger level 1 can then either dispose of the event or confirm it. In the first case, the readout system is reset. The trigger level 1 has a fixed delay of $2.7 \mu\text{s}$ and the readout system reset takes $\leq 0.3 \mu\text{s}$. This reset will therefore not introduce any additional dead time to the detector dead time of $5 \mu\text{s}$.

In the latter case the readout is initiated in parallel in the 14 half-modules of the detector. The data are then transferred to the DAQ system by several standard ALICE Detector Data Links (DDL) [17]. The logical interface of the DDL can be seen in Fig. 3.37a. There is one DDL dedicated to each half-module. The data are transferred from the row of 24 buffers of the half-module to the DDL Source Interface Unit (SIU) at a speed of up to 25 MHz. The SIU will be mounted directly on the readout card on the detector as shown in Fig. 3.37b. It is the same clock which will drive the transfer from the buffers and the DDL SIU.

Table 3.19: Expected rates for different modes of operation

Collision mode	Pb–Pb	Ca–Ca	pp
Luminosity	10^{27}	2.7×10^{27}	10^{29}
Interaction rate (Hz)	8000	8000	3×10^5
L0 rate (Hz)	1000	1000	1200
L1 rate (Hz)	800	800	1000
L2 rates			
TPC $\mu\mu$	40	~ 3	–
TPC MB	40	40	–
NO TPC low p_T	660	–	650
NO TPC high p_T	165	–	30

**Figure 3.37:** (a) DDL logical interface. (b) Direct connection between the front-end electronics on the detector and the DDL.

The DDL is also used to load pedestals and thresholds from the DAQ system to the memories of the DILOGIC chips and to set up and to control the DILOGIC chips.

The physics data transferred by the DDL are buffered in the ALICE readout receiver board (RORC) [18]. The RORC has several functions:

- to be the mothercard for four DDL Destination Interface Units (DIU)
- to act as the transmitting memory for the commands and the data transferred by the DDL to the readout system;
- to act as a remote master for the front-end control and test;
- to act as the receiving memory for the physics data transferred by the DDL to the DAQ;
- to detect the end of the data blocks and manage the data blocks received through the DDL;
- to interface with the trigger system (clear the BUSY status data when a complete data block has been received from one detector).

Once the data have been transferred in the RORCs, they are under the control of the DAQ system. The RORC includes enough buffering to store several tens of events from the HMPID. From this point in the acquisition chain, the data are processed completely asynchronously from the trigger levels 0 and 1.

A prototype of the DDL DIU and of the RORC have been developed and are working properly. A prototype of the DDL SIU is currently under design and will be ready by the end of 1998. Its main characteristics correspond to the needs of the HMPID. A test of integration of the HMPID readout system and of the DDL will be done in 1999. The specifications of the DDL will be frozen after a successful integration test has been done with the HMPID and the other major ALICE detectors. The production will be started one year before the assembly of the HMPID.

The data-transfer system of the HMPID will consist of a single Front-End Digital Crate (FEDC) including four RORCs and one Local Data Concentrator (LDC) (see Fig. 3.38). This crate will also contain the RORCs of the CPVeto detector. A standard computer (workstation or PC) is also included in the system. It makes it possible to work independently during the integration and installation phases and to run interactive programs to perform local test or debugging after the installation.

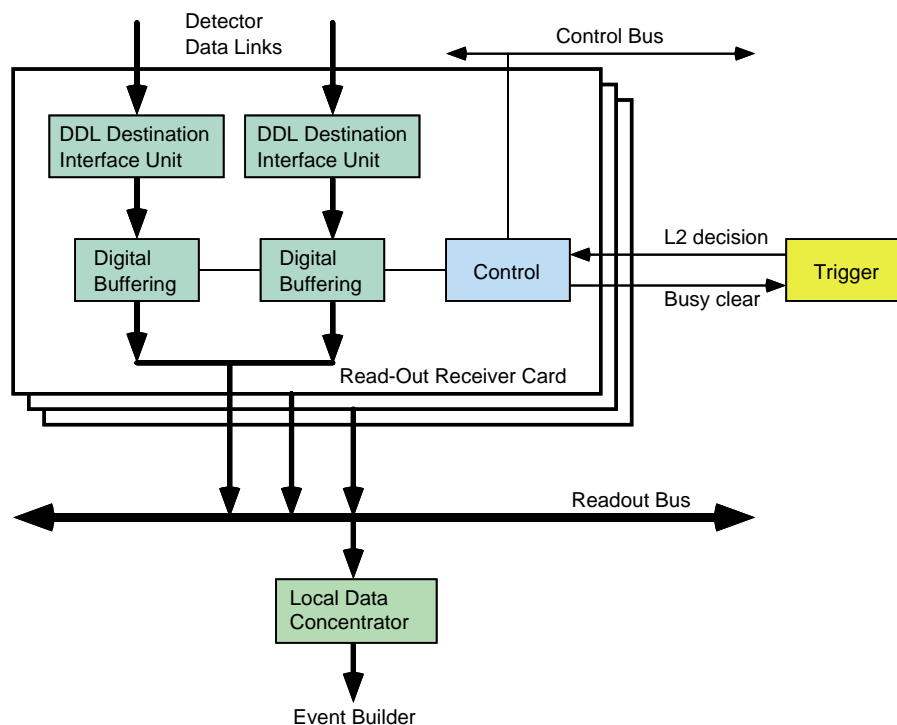


Figure 3.38: Front-end digital crate architecture.

The current prototypes of the data transfer system use VME crates and the LDC is implemented as a single-board computer running the UNIX operating system. The implementation will most probably evolve with the technology but the main functionalities will remain.

3.2.8.2 Data-acquisition system

The main functions of the data-acquisition system when it takes part in a global run with the other ALICE detectors are [14]:

- to validate or discard the event fragments depending on the trigger level 2 decision;
- to read out the data fragments from several RORCs and assemble them into one sub-event;
- to send the sub-event to the computer designated by the event-building and distribution system as event builder to build the complete ALICE event.

The data-acquisition system allows data to be taken in stand-alone mode as well. In this case, the LDC records the data locally instead of sending them to the event-builder computer. This facility can be used for the tests during the preparation and the installation phases of the experiment. During the production phase, it will also allow calibration runs to be made independently of the other detectors and acquire the pedestals needed for the readout electronics. In this case the DAQ will acquire data from all the channels and will prepare pedestal tables which will be loaded at the beginning of the runs.

A prototype of the DAQ system is currently in use for the test beams. It includes a first version of the DAQ software.

3.2.8.3 Components

The modules needed for the data transfer are listed in Table 3.20.

Table 3.20: Data transfer units

Data transfer units	Quantity
DDL	14
RORC	4
FEDC	1
LDC	1
Work station	1

3.2.9 Gas mixture distribution system

3.2.9.1 Design parameters and final layout

The HMPID detector comprises a total gas volume of 1.4 m^3 and operates with 100% methane as nominal gas. This volume is split into seven chamber modules of $1400 \times 1400 \times 100 \text{ mm}^3$, i.e. 0.2 m^3 , each of them supplied individually with gas. In order to protect the very sensitive CsI PC plates there are three basic requirements that need to be met by the gas system:

- The modules must be protected against oxygen and water vapour at all times both during construction and operation, thus giving the requirement that all circuits be purged before the initial module connections are made. Particular attention must be paid to oxygen and moisture analysis of the incoming gas.
- Possible leak of the radiator trays filled with C_6F_{14} and enclosed in the chamber volume must be detected as electronegative contaminant.
- The modules must be permanently supplied with either the operating gas, or, purged with an inert gas (e.g. clean nitrogen or argon), a manually operated supply must ensure the purging of the system during unattended operator closures.

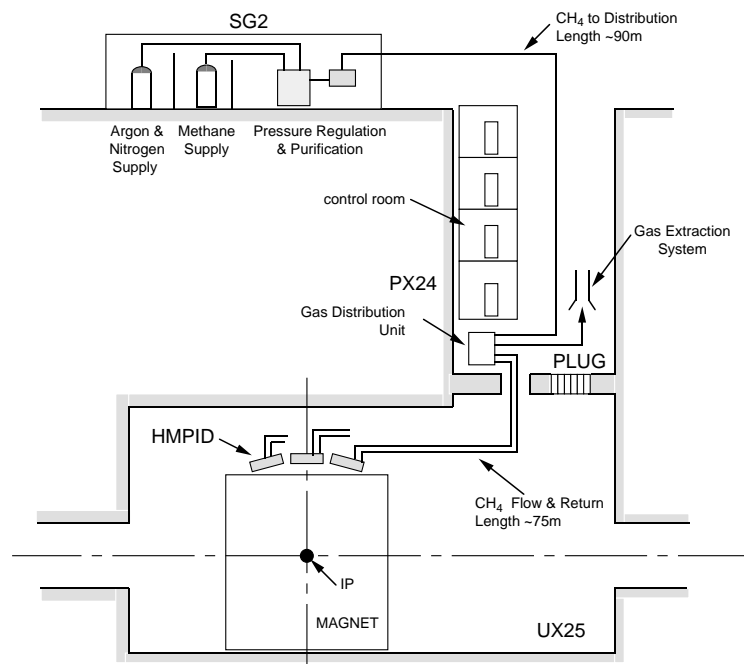
The proposed design consists of a single-pass gas system that distributes the gas to each module at a flow rate of 30 l/h (four volume changes per day) and at a pressure of 7 mbar (above atmosphere). The design parameters are given in Table 3.21.

The primary pressure regulation, purifier and system purge will be located in the surface gas building (SG). The final distribution and flow control to the individual modules will take place on the shielding plug area in the access shaft (PX24), which is accessible during LHC machine operation. Return gas will be exhausted into the dedicated gas extraction system located in the shielding plug area. An overview of the system can be seen in Fig. 3.39.

Table 3.21: Design parameters of the gas system

Total volume	1.3 m ³
Number of modules	7
Module volume	0.185 m ³
Gas mixture*	100% CH ₄
Volume exchanges/day	4
Total flow rate	210 l/h
Working pressure	7 mbar

* The system has a provision to supply binary mixtures.

**Figure 3.39:** Schematic of the gas distribution system.

3.2.9.2 Components

Gas supplies

The methane gas is supplied from standard batteries, each battery having a capacity of approximately 108 m³; two batteries will be installed in parallel, in the gas storage room of the surface gas building. Automatic changeover and primary pressure regulation will ensure an interruption-free supply of gas to the panel in the mixing room, at a nominal pressure of 5 bar.

Argon gas for purging and inerting is supplied from a liquefied argon storage dewar, with reserve batteries which will ensure an interruption-free supply at a nominal pressure of 5 bar.

Pressure regulation and mixing unit

Although the module gas at the present time is 100% methane, a standard LHC gas mixing unit is proposed which will allow a second gas component to be added if required. An argon supply is also incorporated which is used to keep the system purged during stand-by. A three-way valve is incorporated into each supply line which will allow a small volume of gas to flow via the exhaust keeping the lines clean (see Fig. 3.40).

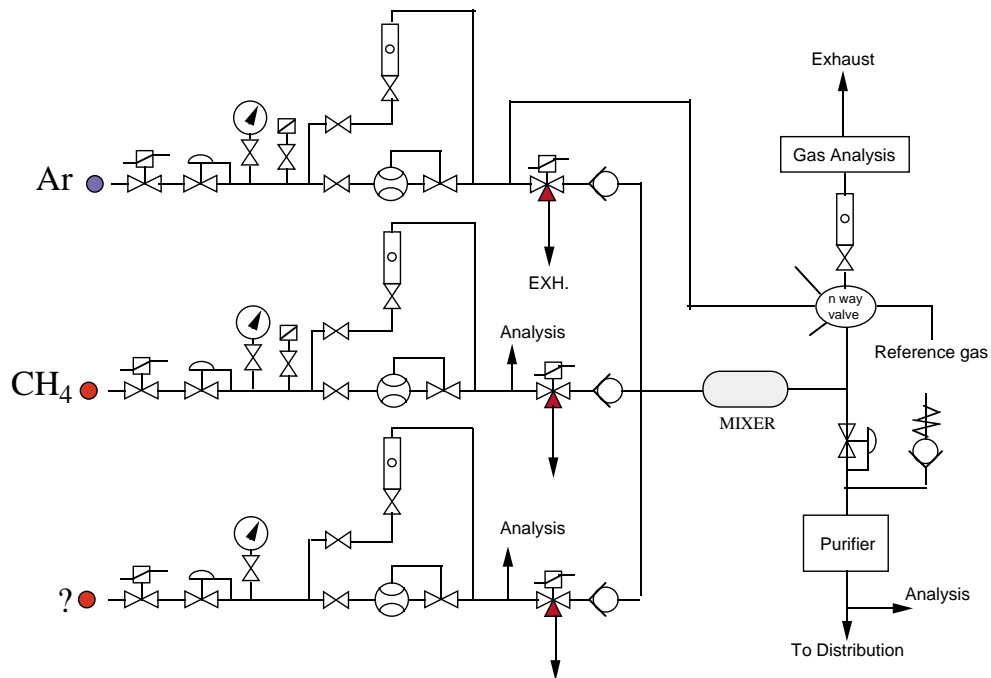


Figure 3.40: Gas mixer unit located at the surface level.

The flow of component gases is metered by mass flow controllers, which have an absolute precision of 0.3% in constant conditions. Flows are monitored by a process control computer. In the event of a second component being added the mixing unit can either work in a constant ratio mode, or alternatively may be derived from comparison of the running mixture with a reference gas mixture in an analysis instrument. The medium-term stability in constant flow conditions is better than 0.1%: absolute stability will depend on the absolute precision of the analysing instrument.

Normal flow rates are typically about 30% of full-scale flow. Detector filling and purging would generally be at maximum flow rate, resulting in a volume exchange time of 0.6 hours.

Gas analysis & purification

The quality of methane 35 as supplied from the CERN stores is considered adequate as far as impurities are concerned. However, since the risk associated with the connection of a gas cylinder having impurities above the limit is non-negligible, inline purifier cartridges for the removal of oxygen and moisture will be installed. The size of the cartridges will be such that a one-year operating cycle can be achieved without change. A 0.4 micron filter is installed in the purifier outlet to trap dust.

Sampling points will be incorporated into the downstream side of each of the component gases of the pressure regulating/mixing unit, for the online measurement of oxygen and moisture in the incoming gases.

On the distribution rack, sampling points on the return gas flow from each of the seven modules will monitor gas for impurities of oxygen and moisture along with monitoring for traces of C_6F_{14} .

Flow distribution

Final pressure regulation and flow distribution to the seven modules will take place in the shielding plug area. Gas arriving from the surface building will pass through a pressure regulator, before being distributed and passing through individual throttle valves, Fig. 3.41. A safety relief device is incorporated into the manifold to prevent over-pressure of the modules, this device will either be a simple relief valve or a rupture disc depending on the pressure limits.

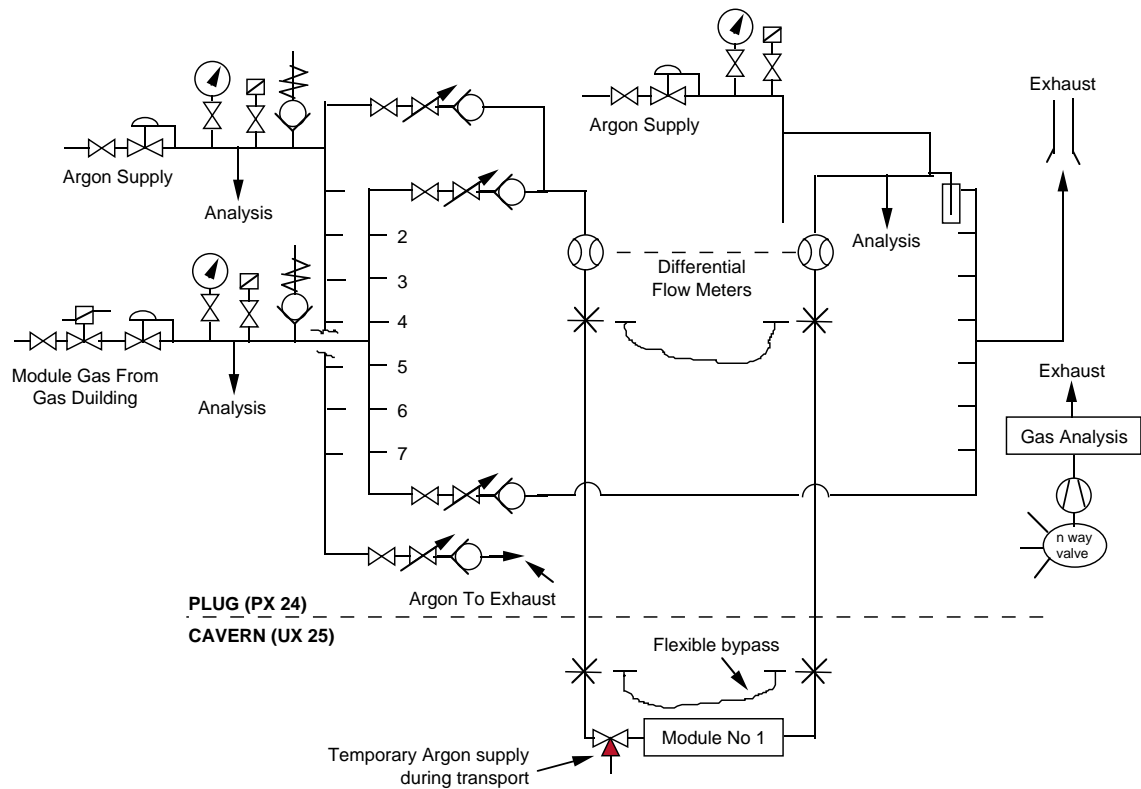


Figure 3.41: Schematics of the gas distribution system.

Differential flow monitors are incorporated into the flow and return lines, which will allow easy adjustment of individual channel flows using the throttle valves, and will allow the detection of leaks by comparing flow-rate changes.

The return gas from the modules will pass through bubblers, to allow visual control of flow, before venting into the dedicated flammable-gas extraction system.

To prevent excess stressing of the modules due to fluctuations in atmospheric pressure in case of a loss of the primary gas supply, a system of back-filling with argon gas is proposed. This allows one to fill or ballast with gas to keep the modules at a slightly positive over-pressure. Since gas is fed in near to the exhaust outlet no dilution of the module gas will occur.

Sampling points are installed in both gas flow and return lines for the detection of oxygen and moisture and the return gas will also be monitored for traces of C_6F_{14} .

Purging

A flexible bypass will be provided to allow purging with argon of each gas circuit before the modules are installed. In case of a major methane leak any individual module may be isolated and purged. Quick connectors will be provided on a patch panel located on the HMPID support structure to allow removal of individual modules. A three-way valve will be incorporated to allow an argon gas cylinder to be connected to maintain purging during transport.

Distribution pipework

All tubes, valves and fittings within the system will be made of stainless steel. The tubes will be butt-welded together to reduce the possibility of contamination and leaks to a minimum. Existing gas pipes at point 2 will be re-used as far as possible. Table 3.22 shows an overall view of the main piping parameters. At the shielding-plug end they will be modified to link up with the new position of the distribution rack. In the experimental area (UX25) they will be extended into the L3 solenoid magnet and onto the HMPID

frame. A patch panel, equipped with self-sealing quick connectors will allow disconnection for removal of the modules.

Table 3.22: Main piping parameters

	No.	Diam.	Length	Velocity	Re	Dp
SG2-distribution	1	22/20	90 m	0.371	220	0.154
Distribution-module	7	10/8	75 m	0.132	80	0.710
Module-exhaust	7	16/14	75 m	0.075	45	0.076

Reserve pipes will be installed, to avoid re-opening of the magnet doors in the future.

Power supply purging

The high-tension connectors located on each side of the module must be purged with a neutral gas to eliminate any risk of methane chamber gas coming into contact with the components. For economic reasons nitrogen will be used for this operation: the gas will be supplied from a manifold in the shielding-plug area (PX25). In case of breakdown of the nitrogen flow, automatic shut-down of the chamber gas system will be put into action.

Safety

The gas return from each module will be monitored for traces of water vapour, oxygen and C_6F_{14} , which will give a good indication of leaks. In the event of abnormality the chamber gas supply will be shut off and the module will be purged with argon; in addition, the corresponding liquid radiator will be isolated and purged with nitrogen at a higher pressure than the module gas volume. In case of failure of the module gas supply, or any other reason why the supply of gas is interrupted, argon will be fed into the outlet side of each module to maintain a positive pressure with respect to atmosphere.

The internal volume of the ALICE solenoid magnet will be continuously monitored for traces of flammable gases; in the event of an alarm resulting from a leak of flammable gas, all primary supplies of flammable gases will be shut off at the primary supply level.

3.2.10 The C_6F_{14} circulation system

3.2.10.1 Introduction

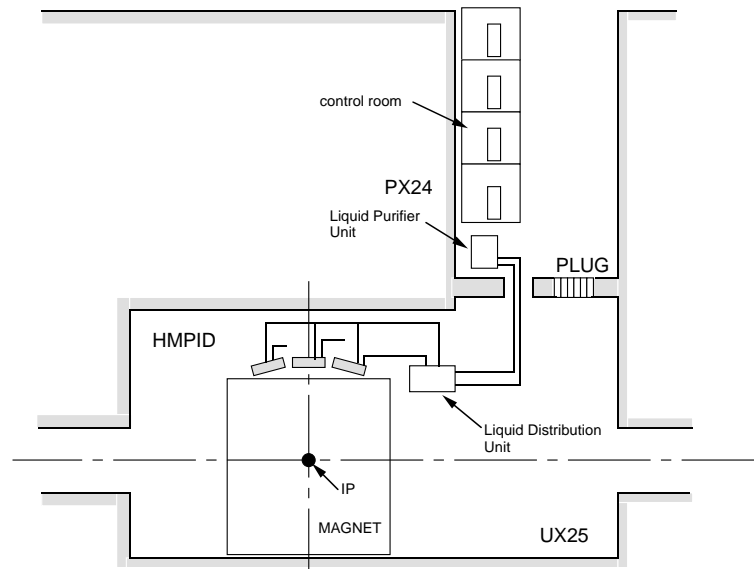
The distribution system is designed to supply Perfluorohexane (C_6F_{14}) liquid to each of the twenty-one radiator modules at a constant flow of up to 3 l/hr. The maximum working pressure of 120 mbar above atmospheric pressure, for each radiator must not be exceeded (see Table 3.23). A circulation scheme is proposed which will eliminate any possibility of over-pressure taking into account the various geometrical positions of the radiator modules. A gravity feed system was constructed and successfully tested for the HMPID prototype, and has been described in Section 3.1.3. The circuit was designed such that priority was given at all times to the supply of liquid to the radiator modules. The full-sized system will follow very closely that design. An overall layout of the system is shown in Fig. 3.42.

The system can be split into three distinct units:

1. The tank and purifier unit will be installed in an area which will be accessible at all times during LHC operation, and will be located in the Pit PX24 on the radiation shielding plug.
2. The distribution rack will be located in the experimental hall on the platform at 3.32 metres above beam height, close to the ALICE solenoid magnet. This rack will house the intermediate tank, header tubes and lower tank. The pumps that return the liquid to the top tank will be installed below this rack.

Table 3.23: Maximum Radiator working pressure

Maximum Radiator height	98 mbar
Outlet tube height	8 mbar
Vapour column to exhaust	12 mbar
Bubble	2 mbar
TOTAL	120 mbar

**Figure 3.42:** Overall view of the liquid system.

3. The pipe distribution to the modules proper, which is located on the HMPID support frame, within the ALICE solenoid magnet.

3.2.10.2 Design

Principle of operation

The liquid distribution system has been designed to have as few active components as possible, especially in areas which will not be accessible during LHC operation. The system is designed using a gravity flow principle with the priority flow given to the radiator modules, excess flow cascades to the lower tank. In case of power or other system failure, all liquid in the circuit, except for the radiators, will drain automatically into the lower tank. Manual valves will allow the radiator units to be drained and sealed-off if required. The lower tank has a capacity capable of holding the entire contents of the system, including operational losses during one year of operation. The liquid volume in the circuit is calculated to be of the order of 250 litres. A schematic diagram of the liquid distribution system can be seen in Fig. 3.43.

From the lower tank the liquid is pumped to the upper tank at a constant flow rate of 210 l/h, against a calculated pressure head of 6 bar. The constant flow is achieved by the use of a mass-flow-meter controlling a bypass valve on the pump; a safety relief bypass valve is also mounted in parallel to protect the pump from overpressure. A filter installed at the inlet protects the pump. Perfluorohexane is a high-density, low-viscosity liquid and not recommended for applications where a high degree of lubrication is required, therefore, special care is required in the choice of pumps. Two pumps, which are of the well proven magnetically coupled gear type, are mounted in parallel to provide redundancy.

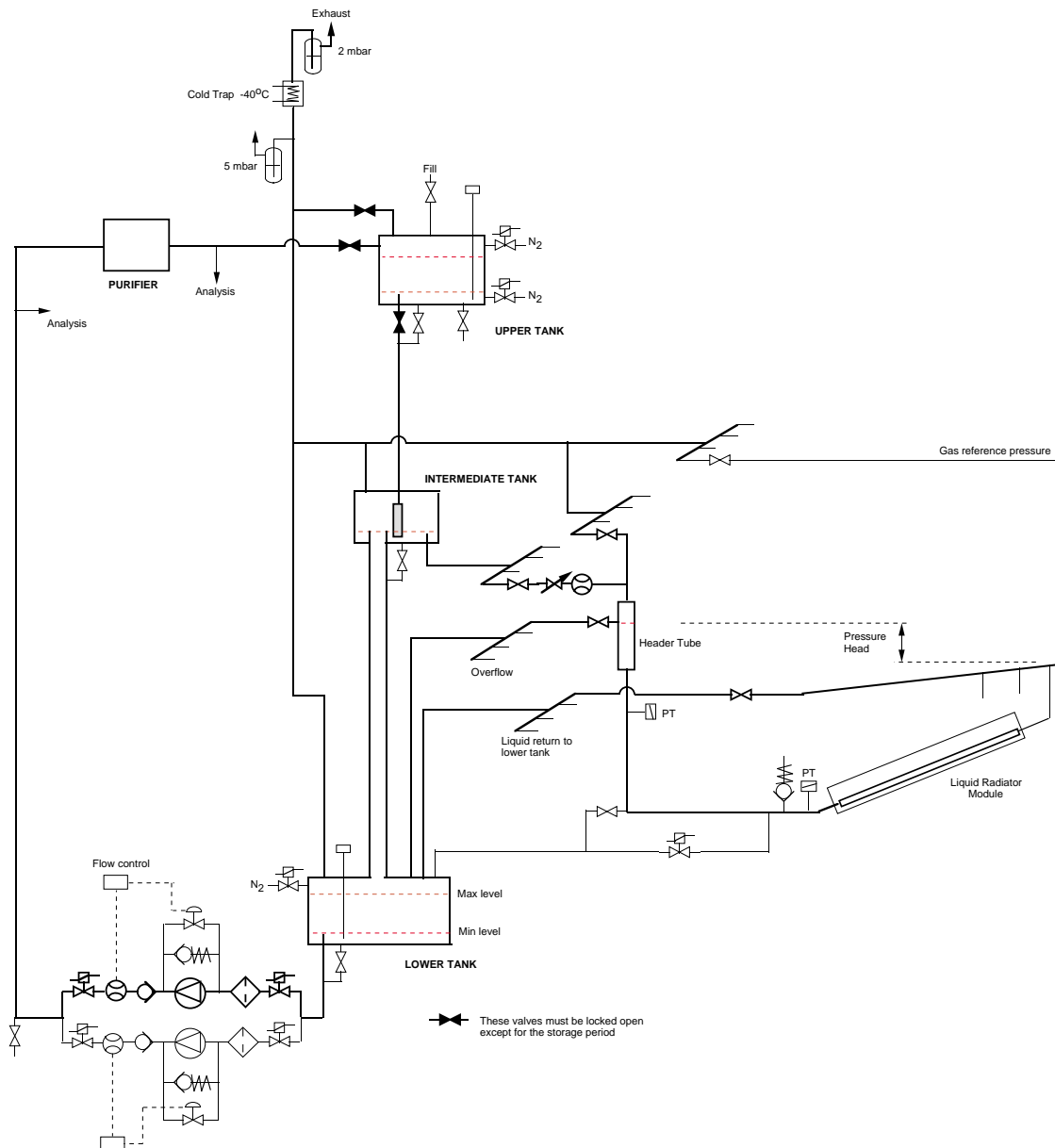


Figure 3.43: Liquid distribution system.

Liquid flows from the upper tank, by gravity, into the intermediate tank. A phase separator is installed in the outlet of the line, and sufficient depth of liquid is allowed for in the bottom of the tank to allow outgassing of the liquid. From this tank the liquid is distributed to the twenty-one header tubes, at a total flow rate of 130 l/h. The excess flow leaves the intermediate tank via the overflow to the lower tank.

The flow of liquid from the intermediate tank via a distribution manifold to each header tube is regulated by a flow meter and manual throttle valve at 6 l/h. The height of each header tube is a function of the orientation and height of its respective Radiator and of the pressure losses in the inlet pipes.

Owing to the hydraulic pressure in the individual header tubes the liquid flows to the radiator module. The flow rate is controlled in the range of 1–3 l/h, by the pressure drop in the entrance tube. The radiators are filled from the bottom thus displacing the nitrogen purge gas through the outlet situated in the upper part of each Radiator. Excess liquid from the header tubes leaves via the overflow to the lower tank. A solenoid valve is installed in the circuit which will allow individual radiators to be shut off if required. A general view, showing the pipe layout on the HMPID support frame, can be seen in Fig. 3.44.

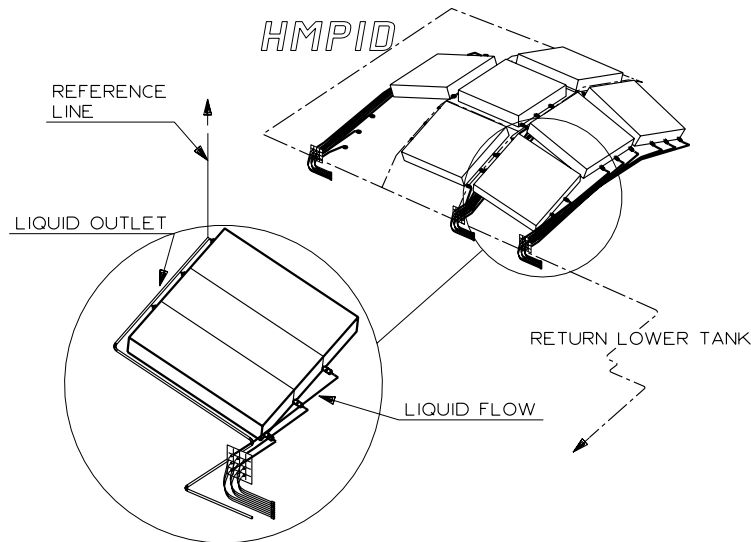


Figure 3.44: Pipe layout on support frame.

A manifold has been designed to collect the liquid as it exits from each group of three radiators. As a means of ensuring that liquid does not back flow into a radiator, the outlet from each radiator will enter the manifold above the liquid level.

The collector tube diameter is such that the liquid occupies only a small section of the tube. Each outlet manifold has also a gas reference pressure line connected to the main exhaust line which avoids pressure oscillations in the output pipes. The geometry of all return pipes is such that they have a constant slope back to the lower tank.

Each radiator may be isolated and drained if required by the bypass valve. Large-diameter valves are installed in the output lines so that each set of three radiator modules may be isolated in case of a component failure.

Setting-up and purging

After the installation of the liquid circulating system and before the radiator modules are connected to the system, all circuits and tanks are to be purged with nitrogen to remove oxygen and moisture. The system will be designed to allow vacuum pump-out and back-filling with nitrogen. For this operation the safety bubblers will temporarily be removed.

Once purging has been completed the system will be put into operation to thoroughly rinse and outgas the circuit. Only liquid from the same batch that has been pre-cleaned will be transvased into the system, in quantities for one year of operation.

3.2.10.3 Components

Materials

Stainless steel will be used for all tubes, valves and fittings within the system to reduce the possibility of contamination and leaks to a minimum; as far as possible only welded joints will be used. In places where it is necessary to dismount parts for maintenance, compression fittings will be used. The tubes and fittings will be supplied from the manufacturer degreased and passivated since cleaning will be difficult after installation.

All parts of valves and other instruments which have contact with the liquid must be of stainless steel to avoid contamination of the liquid.

'O' ring type joints will be avoided as much as possible; where they are found to be necessary, elastomers made of Viton will be used.

Purifier

On-line purification will be carried out on the full liquid flow as it is pumped from the lower to the upper tank. Two purifier columns are installed in parallel such that in the event of one becoming saturated or blocked, the flow of liquid will be diverted through the second column, see Fig. 3.45.

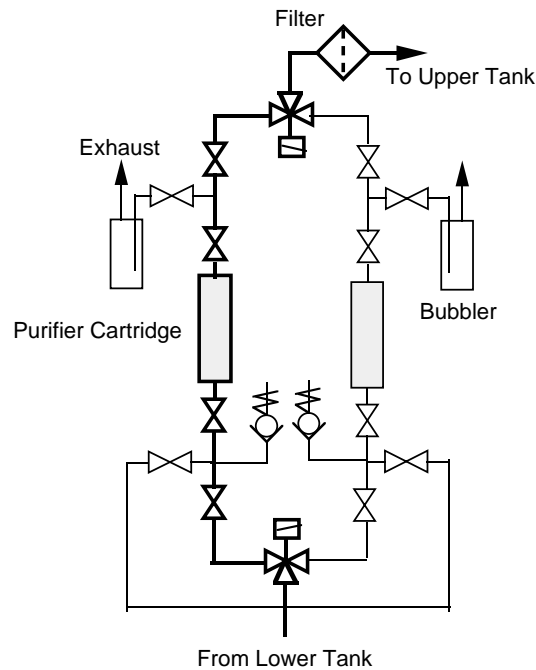


Figure 3.45: Purifier unit.

Zeolite 13X has been found to be satisfactory for removing water vapour and other impurities in the liquid. After filling, the columns are purged and filled with clean nitrogen at a pressure of 1 bar. Precautions are required when changing columns since an exothermic reaction takes place when replacing the nitrogen purge gas with the process liquid, resulting in formation of important quantities of gas. Only when there is a steady flow of liquid leaving the column and the temperature has returned to ambient can the purge liquid be shut off and the column isolated. Safety relief valves are installed to protect from overpressure.

Quality monitoring

The liquid quality will be continuously monitored. Sampling lines before and after the purifier will send liquid to an array of diagnostic devices. It is intended to measure the UV transparency, refractive index, oxygen and moisture content in the liquid phase on-line.

On-line monitoring of the oxygen and moisture content of the reference gas is also planned. The moisture level will be used to interlock the cold trap in the exhaust line. The dew point temperature of -40°C corresponds only to a moisture content of about 100 ppm, if values above this are detected the cold trap will be heated to avoid freezing.

Liquid recovery

In the event that all the liquid in the system must be changed or recovered, drain valves are installed below all low points which allows the liquid to be drained to the lower tank.

To keep the oxygen and moisture to a minimum due to the effects of outgassing or air trapped when modifications are carried out, the system is continuously purged with nitrogen at a flow rate of 60 l/h, which is exhausted to the atmosphere. At the present time there are no restrictions to exhausting this product to the atmosphere, however, since this product has a known greenhouse effect, long-term legislation

may require it to be recovered. For economic reasons this liquid must be recovered, since, at normal operating temperatures the vapour has a saturation of approximately 25% volume in nitrogen, which would result in the loss of 3.6 litres per day.

To recover the liquid, we propose to install a cold trap in the exhaust line, which will have a working temperature of $-40\text{ }^{\circ}\text{C}$. This will reduce the vapour content in the exhaust outlet to less than 1% resulting in a maximum loss of 0.15 litres per day.

Safety

The pressure in the radiator, even when empty, will be 13 mbar due to the vapour column of 23 metres, In the case of a leak in a radiator, vapour will migrate into the gas volume which will have a maximum working pressure of 7 mbar. If traces of C_6F_{14} are found in the methane gas outlet the entire module will be closed down and sealed off. The gas volume will be purged with argon. Since there are three radiator units in each module, which are interconnected by the gas reference line, all three units in the Module must be isolated and drained to the lower tank. In the event of a blockage of the radiator output line, the maximum pressure in the most inclined radiator will rise from 120 to 140 mbar.

3.2.11 The slow control system

The ALICE detector control system (DCS) is characterised in Ref. [14] and will be described in detail later in the ALICE Computing Technical Proposal. The signals to be measured for the HMPID are listed in Table 3.24.

Table 3.24: Main parameters of the detector control system for the HMPID

Systems Subsystems	Location	Controlled parameters	Number	Type	Parameters	Control
Gas supply	PX24	Primary flows	20	Analog	Flow	Read
	PX24	Primary pressures	10	Analog	Pressure	Read
	Detector	Temperatures	20	Analog	Temperature	Read
	PX24		5	Serial IF	Complex	Read
	PX24	Safety switch	1	Binary	Voltage	On,, Off
	PX24	Purity control	2	Serial IF	Complex	Read
	UX25	Gas pressure MWPC	14	Analog	Pressure	Read
	Detector	Temperatures	80	Analog	Temperature	Read
Radiator	UX25	Gas flow MWPC	7	Analog	Flow	Read
	UX25	Circulator valves	80	Binary	Voltage	ReadWrite
	PX24	Pumps & circulators	32	Binary	Voltage	On,, Off
	PX24	Liquid flow	64	Analog	Flow	Read
	PX24	Pressure	10	Analog	Pressure	Read
	Detector	Temperature	80	Analog	Temperature	Read
	PX24	VUV transp. Syst.	1	Serial IF	Complex	Read
PX24	Safety system	1	Binary	Voltage	On,, Off	
Other system	PX24	VUV transp. Syst.	1	Serial IF	Complex	Read
HV	PX24	Chamber voltage	12	Analog	Voltage	ReadWrite
	PX24	Chamber current	14	Analog	Current	Read
	PX24	Current limits	14	Analog	Thresholds	ReadWrite
LV	PX24	Readout electronics	42	Analog	Voltage	ReadWrite
	PX24	RO sign. Cntrl	42	Binary	Voltage	On,, Off
	PX24	FEE	42	Binary	Voltage	On,, Off
	PX24	MWPC FEE supply	28	Analog	Voltage	ReadWrite
	PX24	FEE current monitoring	28	Analog	Current	Read
	PX24	Current limits	28	Analog	Thresholds	ReadWrite
	PX24	chamber	42	Analog	Voltage	ReadWrite
	PX24	chamber	42	Analog	Current	Read

The validation of design choices for the overall ALICE DCS will be performed for a liquid circulator system of the HMPID but an adaptation to other applications is envisaged.

For this purpose a small test and evaluation station is being set. The system is entirely based on standard industrial components following the recommendations of the relevant working groups. The realisation of this first stand-alone system for the control of a detector sub-system will cover all layers of the proposed DCS architecture:

Supervisory Software: LabView/BridgeView

Control Software: Siemens Step7, equivalent to IEC1131

PLC programming libraries

Controller station: Siemens S7 + TCP/IP

Field instrumentation: Temperature sensors, Switches, Valves

figure 3.i
figure 3.ii

figure 3.iii
figure 3.iv